RADIATION DETECTION AND MEASUREMENT 2nd ED.
GLENN F. KNOLL (1989)

CHAPTER · 14

Slow Neutron Detection Methods

Neutrons are detected through nuclear reactions which result in energetic charged particles such as protons, alpha particles, and so on. Virtually every type of neutron detector involves the combination of a target material designed to carry out this conversion together with one of the conventional radiation detectors discussed in earlier chapters. Because the cross section for neutron interactions in most materials is a strong function of neutron energy, rather different techniques have been developed for neutron detection in different energy regions. In this chapter, we discuss those methods that are of primary importance for the detection of neutrons whose energy is below the *cadmium cutoff* of about 0.5 eV. This is conventionally called the slow neutron region and is distinguished from intermediate and fast neutrons with energies above this value. Slow neutrons are of particular significance in present-day nuclear reactors and much of the instrumentation that has been developed for this energy region is aimed at the measurement of reactor neutron flux. Specific detector types that have evolved for this purpose are discussed at the end of this chapter.

We limit our discussion in this chapter to those methods that are intended to indicate only the detection of a neutron, with no attempt made to measure its kinetic energy. Devices that can measure slow neutron energies such as crystal spectrometers or mechanical monochromators are generally complex research-oriented instrumentation systems and are not covered here. In contrast, rather simple detectors can be used to measure the energy of neutrons of higher energy and these are discussed in the next chapter.

We also postpone discussion of *passive* neutron detectors, including activation foils, until Chapter 19. In this chapter we discuss only *active* detectors in which a pulse or current signal is produced by each neutron as it interacts in the device. General reviews of slow neutron detection devices and techniques may be found in Refs. 1–5. More detailed descriptions of those detectors developed specifically for reactor applications are given in Refs. 6 and 7.

I. NUCLEAR REACTIONS OF INTEREST IN NEUTRON DETECTION

In searching for nuclear reactions that might be useful in neutron detection, several factors must be considered. First, the cross section for the reaction must be as large as possible so that efficient detectors can be built with small dimensions. This is particularly

important for detectors in which the target material is incorporated as a gas, of which we shall see several examples. For the same reason, the target nuclide should either be of high isotopic abundance in the natural element, or alternatively, an economic source of artificially enriched samples should be available for detector fabrication. In many applications, intense fields of gamma rays are also found with neutrons and the choice of reaction bears on the ability to discriminate against these gamma rays in the detection process. Of principal importance here is the Q-value of the reaction which determines the energy liberated in the reaction following neutron capture. The higher the Q-value, the greater is the energy given to the reaction products, and the easier is the task of discriminating against gamma-ray events using simple amplitude discrimination.

It is important to point out that all the common reactions used to detect slow neutrons result in heavy charged particles.† Possible reaction products are listed below:

$$\text{target nucleus} + \text{neutron} \rightarrow \begin{cases} \text{recoil nucleus} \\ \text{proton} \\ \text{alpha particle} \\ \text{fission fragments} \end{cases}$$

All the conversion reactions are sufficiently exothermic so that the kinetic energy of the reaction products is determined solely by the Q-value of the reaction and does not reflect the very small incoming energy of the slow neutron.

The distance traveled by the reaction products following their formation also has important consequences in detector design. If we are to capture the full kinetic energy of these products, the detector must be designed with an active volume that is large enough to fully stop the particles. If the detection medium is a solid, this requirement is easily achieved because the range of any of the reaction products shown does not exceed a few tenths of a millimeter in any solid material. If the detection medium is a gas, however, ranges of the reaction products (typically several centimeters) can be significant compared with detector dimensions and some may not deposit all their energy. If the detector is large enough so that these losses can be neglected, the response function will be very simple, consisting only of a single full-energy peak as shown in the sketch.

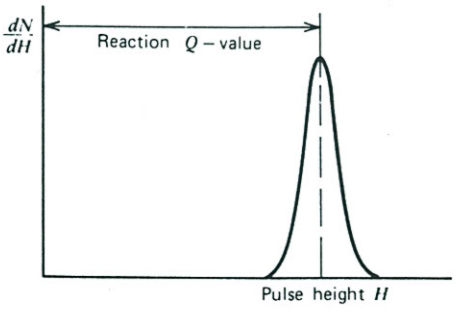

Under these circumstances the detector would exhibit a very flat counting plateau, and the ability to discriminate against low-amplitude events (such as gamma-ray-induced processes) would be maximized. If, on the other hand, a significant number of neutron-induced events do not deposit the full energy, a low-energy continuum is added to the

†Gamma rays produced by neutron capture are used in some specialized detectors, but these applications are relatively rare.

pulse height distribution and the detector performance with respect to these criteria will suffer.

A. The $^{10}B(n, \alpha)$ Reaction

Probably the most popular reaction for the conversion of slow neutrons into directly detectable particles is the $^{10}B(n, \alpha)$ reaction. The reaction may be written

$$^{10}_{5}B + {}^{1}_{0}n \rightarrow \begin{cases} {}^{7}_{3}Li + {}^{4}_{2}\alpha & \text{2.792 MeV (ground state)} \\ {}^{7}_{3}Li^{*} + {}^{4}_{2}\alpha & \text{2.310 MeV (excited state)} \end{cases} \qquad (14\text{-}1)$$

(Q-value)

where the branching indicates that the reaction product ^{7}Li may be left either in its ground state or in its first excited state.† When thermal neutrons (0.025 eV) are used to induce the reaction, about 94% of all reactions lead to the excited state and only 6% directly to the ground state. In either case, the Q-value of the reaction is very large (2.310 or 2.792 MeV) compared with the incoming energy of the slow neutron, so that the energy imparted to the reaction products (^{7}Li and α) is essentially just the Q-value itself. Thus, the incoming kinetic energy of the neutron is submerged in the much larger reaction energy, and it is impossible to extract any information about its original value. Also, because the incoming linear momentum is very small, the reaction products must also show a net momentum of essentially zero. Consequently, the two reaction products must be emitted in exactly opposite directions, and the energy of the reaction will always be shared in the same manner between them. Individual energies of the alpha particle and lithium nucleus can be calculated simply by conservation of energy and momentum as follows:

$$E_{Li} + E_{\alpha} = Q = 2.31 \text{ MeV} \qquad (14\text{-}2)$$

$$m_{Li}v_{Li} = m_{\alpha}v_{\alpha}$$

$$\sqrt{2m_{Li}E_{Li}} = \sqrt{2m_{\alpha}E_{\alpha}} \qquad (14\text{-}3)$$

Solving Eqs. (14-2) and (14-3) simultaneously:

$$E_{Li} = 0.84 \text{ MeV} \quad \text{and} \quad E_{\alpha} = 1.47 \text{ MeV}$$

where the calculation has been carried out for the case of populating the excited state of ^{7}Li. A similar calculation would yield larger values by 21% for reactions leading to the ground state.

Figure 14-1 is a plot of cross sections versus neutron energy for a number of nuclear reactions of interest in neutron detection. The thermal neutron cross section for the $^{10}B(n,\alpha)$ reaction is 3840 barns. The cross-section value drops rapidly with increasing neutron energy and is proportional to $1/v$ (the reciprocal of the neutron velocity) over much of the range. The utility of this reaction stems from its rather large and structureless cross section and from the fact that boron, highly enriched in its ^{10}B concentration, is readily available. The natural isotopic abundance of ^{10}B is 19.8%.

†The excited lithium nucleus quickly returns (half-life of $\sim 10^{-13}$ s) to its ground state with the emission of a 0.48 MeV gamma ray. We assume that this photon always escapes and does not contribute to the response of the detector.

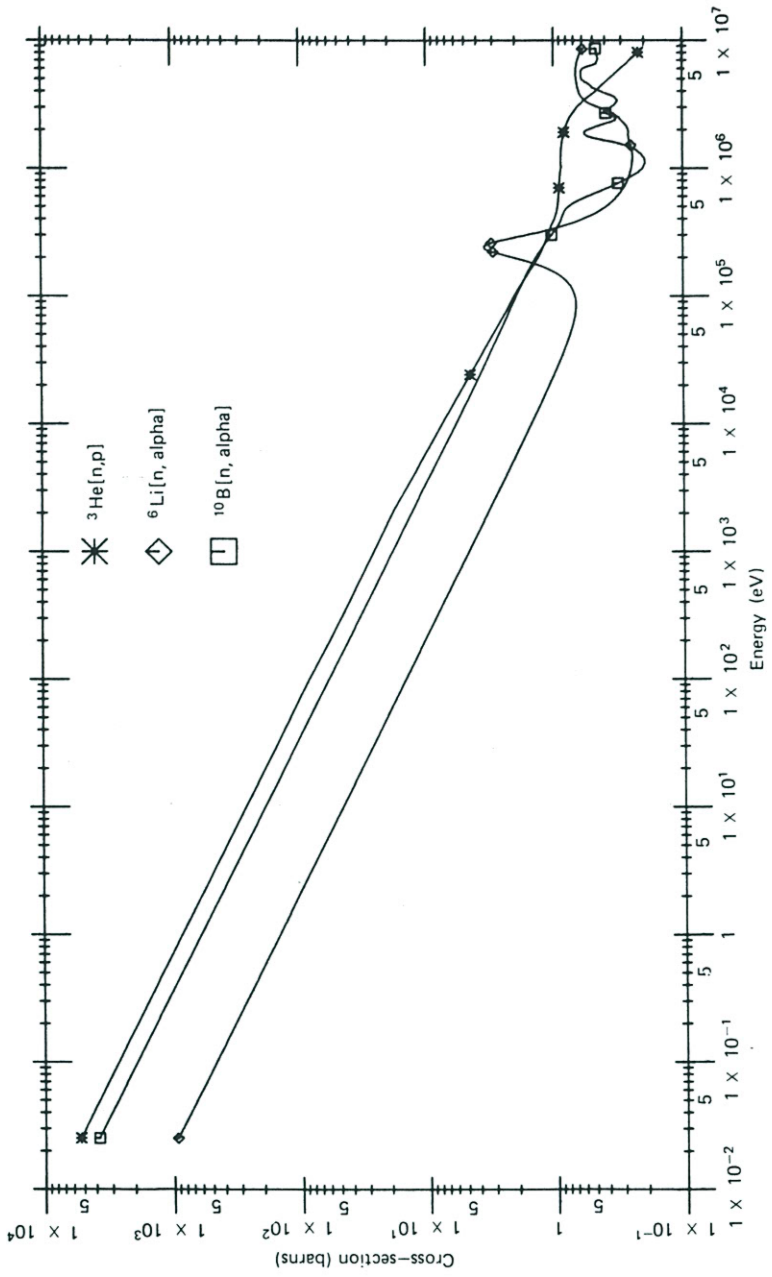

Figure 14-1 Cross section versus neutron energy for some reactions of interest in neutron detection.

B. The ^{6}Li(n, α) Reaction

The next most popular reaction for the detection of slow neutrons is the (n, α) reaction in ^{6}Li. Here the reaction proceeds only to the ground state of the product and is written simply as

$$^{6}_{3}\mathrm{Li} + ^{1}_{0}\mathrm{n} \rightarrow ^{3}_{1}\mathrm{H} + ^{4}_{2}\alpha \qquad \underline{Q\text{-value}}\ 4.78\ \mathrm{MeV}$$

Calculation of the reaction product energies for negligible incoming neutron energy yields the following:

$$E_{^{3}\mathrm{H}} = 2.73\ \mathrm{MeV} \quad \text{and} \quad E_{\alpha} = 2.05\ \mathrm{MeV}$$

The alpha particle and triton produced in the reaction must be oppositely directed when the incoming neutron energy is low.

The thermal neutron cross section for this reaction is 940 barns. Figure 14-1 shows that the cross section remains below that for the ^{10}B reaction until the resonance region (> 100 keV). The lower cross section is generally a disadvantage but is partially offset by the higher Q-value and resulting greater energy given to the reaction products. ^{6}Li occurs with a natural isotopic abundance of 7.40% and is also widely available in separated form.

C. The ^{3}He(n, p) Reaction

The gas ^{3}He is also widely used as a detection medium for neutrons through the reaction

$$^{3}_{2}\mathrm{He} + ^{1}_{0}\mathrm{n} \rightarrow ^{3}_{1}\mathrm{H} + ^{1}_{1}\mathrm{p} \qquad \underline{Q\text{-value}}\ 0.764\ \mathrm{MeV}$$

For reactions induced by slow neutrons, the Q-value of 764 keV leads to oppositely directed reaction products with energies

$$E_{\mathrm{p}} = 0.573\ \mathrm{MeV} \quad \text{and} \quad E_{^{3}\mathrm{H}} = 0.191\ \mathrm{MeV}$$

The thermal neutron cross section for this reaction is 5330 barns, significantly higher than that for the boron reaction, and its value also falls off with a $1/v$ energy dependence (see Fig. 14-1). Although ^{3}He is commercially available, its relatively high cost is a factor in some applications.

D. Neutron-Induced Fission Reactions

The fission cross sections of ^{233}U, ^{235}U, and ^{239}Pu are relatively large at low neutron energies and thus these materials can be used as the basis of slow neutron detectors. One characteristic of the fission reaction is its extremely large Q-value (approximately 200 MeV) compared with the reactions discussed previously. As a result, detectors based on the fission reaction can often give output pulses that are orders of magnitude larger than those induced from competing reactions or incident gamma rays, and very clean discrimination can be accomplished. Figure 14-2 shows a plot of fission cross sections of a variety of fissile nuclides, including some that are of primary use as fast neutron detectors. Almost all fissile nuclides are naturally alpha radioactive and consequently any detector that incorporates these materials will also show a spontaneous output signal due to decay alpha particles. The energy of the decay alpha particles, however, is always many times

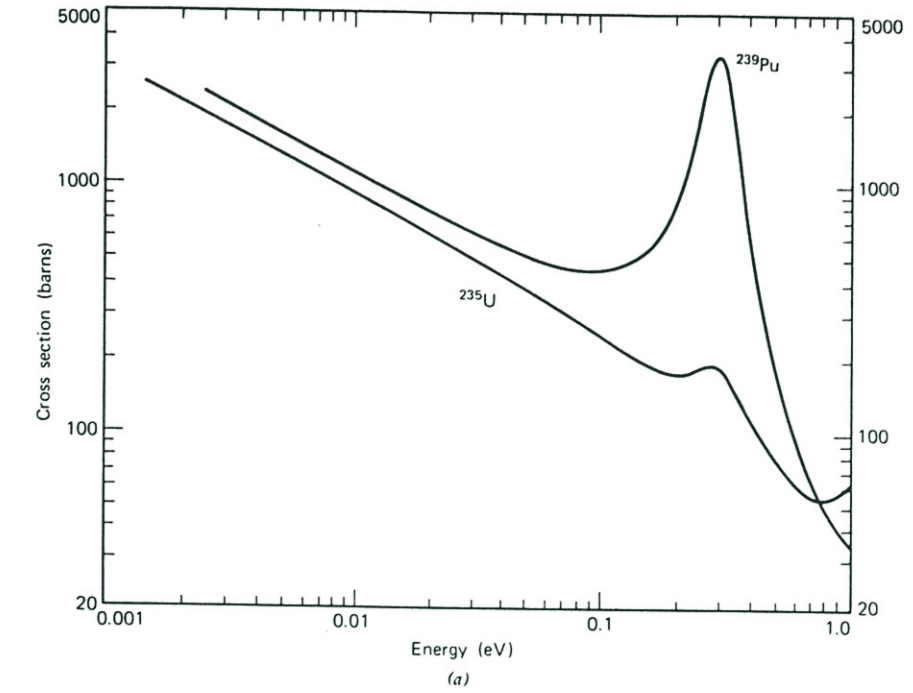

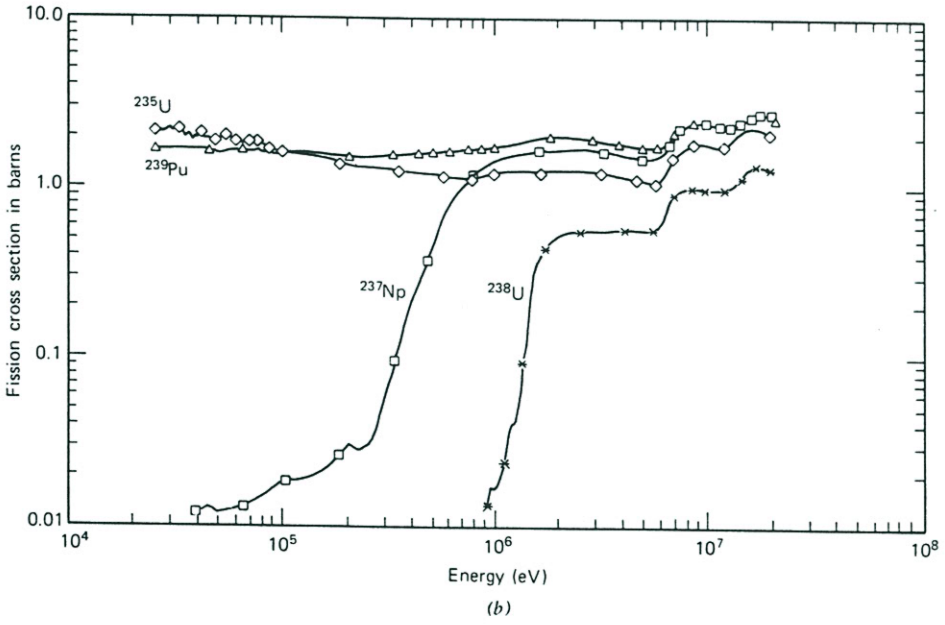

Figure 14-2 Fission cross sections of some common target nuclides used in fission chambers. (a) Slow neutron region where the cross sections shown are relatively large. (b) Fast neutron region. Chambers with ^{237}Np or ^{238}U are used as *threshold detectors* sensitive only to fast neutrons.

less than the energy given off in a fission reaction, and again these events can usually be discriminated easily on a pulse amplitude basis.

II. DETECTORS BASED ON THE BORON REACTION

A widely used detector for slow neutrons is the BF_3 proportional tube. In this device, boron trifluoride serves both as the target for slow neutron conversion into secondary particles as well as a proportional gas. A number of other boron-containing gases have been evaluated, but BF_3 is the near-universal choice because of its superior properties as a proportional gas, as well as its high concentration of boron. In nearly all commercial detectors, the gas is highly enriched in ^{10}B, resulting in an efficiency some five times greater than if the gas contained naturally occurring boron. Because the performance of BF_3 as a proportional gas is poor when operated at higher pressures, its absolute pressure in typical tubes is limited to about 0.5–1.0 atm.

A. BF_3 Tube Pulse Height Spectra — The Wall Effect

Figure 14-3a shows the ideal pulse height spectrum expected from a BF_3 tube of very large dimensions. For a large tube, nearly all the reactions occur sufficiently far from the walls of the detector to deposit the full energy of the products within the proportional gas. In that event, all the energy of the reaction is deposited in the detector and the only variation is a result of the branching of the reaction between the excited state and ground state of the ^7Li product nucleus. The branching ratio for thermal neutrons is such that about 6% of the reactions lead to the ground state and 94% to the first excited state. Therefore, the areas under the peaks shown in Fig. 14-3a should be in the ratio 94 : 6 as illustrated.

Once the size of the tube is no longer large compared with the range of the alpha particle and recoil lithium nucleus produced in the reaction, some events no longer deposit the full reaction energy in the gas. If either particle strikes the chamber wall, a smaller pulse is produced. The cumulative effect of this type of process is known as the *wall effect* in gas counters. Because the range of the alpha particle produced in the reaction is on the order of 1 cm for typical BF_3 gas pressures, almost all practical tubes are small enough in diameter so that the wall effect is significant.

Figure 14-3b shows the differential pulse height spectrum expected from a tube in which the wall effect is important. The primary change from the spectrum shown in Fig. 14-3a is the addition of a continuum to the left of the peaks corresponding to partial energy deposition in the gas of the tube. The two steps or discontinuities in the continuum are an interesting feature of the spectrum and can be explained through the following argument.

Because the incoming neutron carries no appreciable momentum, the two reaction products must be oppositely directed. If the alpha particle strikes the wall, the ^7Li recoil is therefore directed away from the wall and is very likely to deposit its full energy within the gas. Conversely, if the ^7Li recoil strikes a wall, the entire energy of the alpha particle from that same reaction is usually fully absorbed.

Thus, we expect to see wall losses for only one reaction product at a time. There are two possibilities: (1) the alpha particle hits a wall after depositing some fraction of its energy in the fill gas, whereas the ^7Li recoil is fully absorbed in the gas, or (2) the ^7Li recoil hits a wall after depositing part of its energy and the alpha particle is fully absorbed. Under case 1 above, the reaction could occur at a distance from the wall which

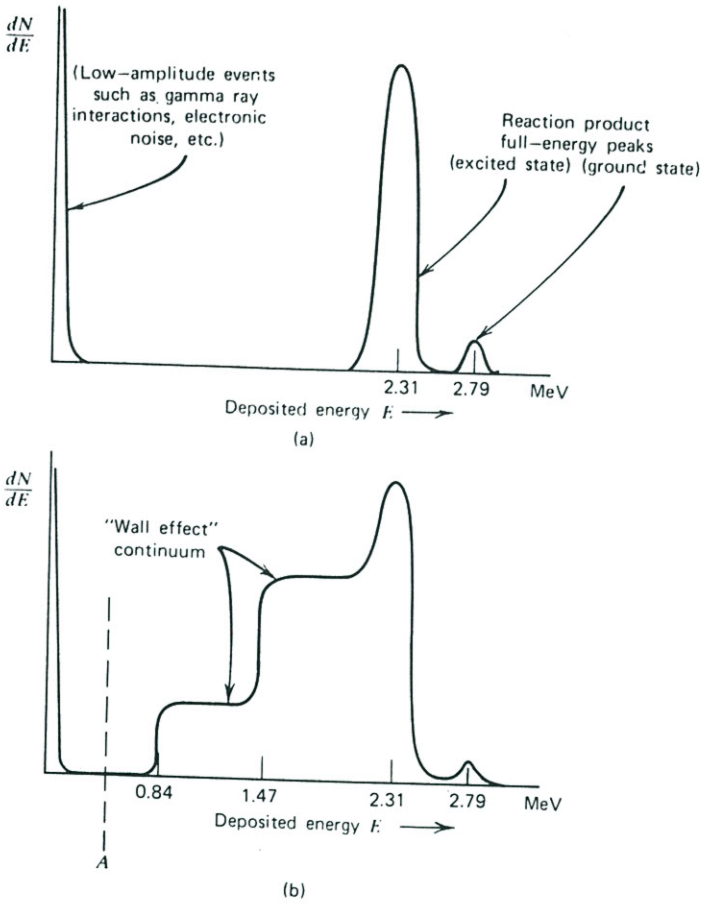

Figure 14-3 Expected pulse height spectra from BF_3 tubes. (a) Spectrum from a large tube in which all reaction products are fully absorbed. (b) Additional continuum due to the wall effect.

might be anywhere between zero and the full alpha particle range. The amount of energy deposited in the gas can correspondingly vary from $(E_{Li} + 0)$ to $(E_{Li} + E_\alpha)$, as illustrated below.

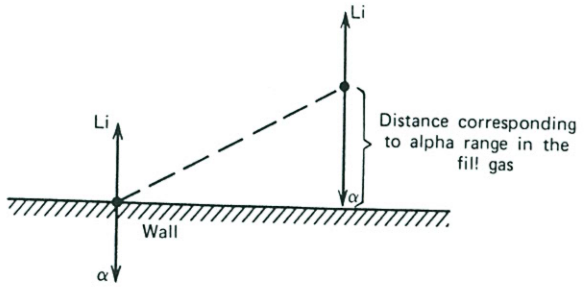

Because all locations of the reaction are more or less equally probable, the distribution of deposited energy will be approximately uniform between these two extremes.

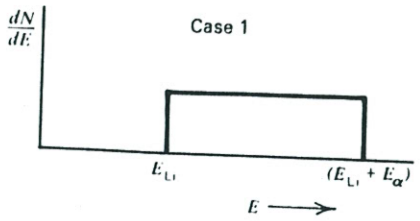

Parallel arguments can be made for case 2 to show that the energy deposited in the gas will vary from $(E_\alpha + 0)$ to $(E_\alpha + E_{\mathrm{Li}})$.

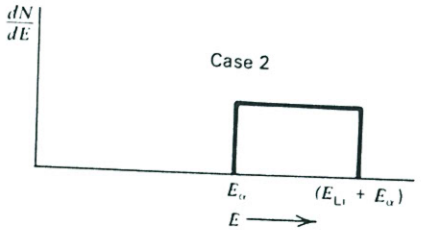

The combined energy deposition distribution of all events in which either reaction product strikes a wall will simply be the sum of the two cases.

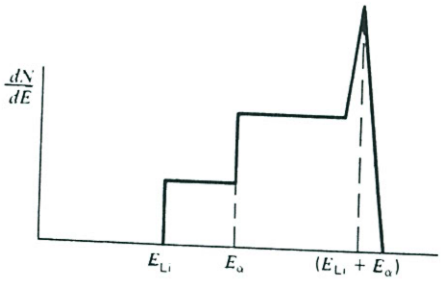

In addition to the wall effect events, the sketch above also shows the location of the full-energy peak that results from all those reactions from which both products are fully absorbed in the gas. The wall effect continuum extends from E_{Li} (0.84 MeV) up to the full-energy peak at $(E_{\mathrm{Li}} + E_\alpha)$ (2.31 MeV). We have considered only those reactions leading to the ^{7}Li excited state because the wall effect continuum associated with the much less probable ground state is normally so small as to be submerged by the remainder of the spectrum.

The BF_3 tube is an example of a detector from which the differential pulse height spectrum tells us nothing about the energy spectrum of the incident radiation but is a function only of the size and geometry of the detector itself. In routine applications, there is consequently no motivation to record the pulse height spectrum from a BF_3 tube other than in an indirect manner. Instead, we are likely to seek a stable operating point or a counting plateau for which small drifts in operating parameters do not significantly affect the neutron sensitivity of the counter. That objective would be met by setting a fixed discriminator level at the point labeled A in Fig. 14-3b. From the arguments given in Chapter 4, we would expect a counting plateau to appear as the high voltage to the tube is

varied, changing the internal gain of the proportional gas multiplication process. The flattest portion of that plateau should occur when the effective discrimination point is at the minimum in the differential pulse height spectrum, or point *A*. Under these conditions, all the neutrons will be counted, whereas low-amplitude events will be rejected. If the wall effect is eliminated or greatly suppressed by making the tube very large, a pulse height spectrum similar to that shown in Fig. 14-3a results. The counting plateau will then extend over a much greater range of applied voltage and thereby extend the useful operating range over which all neutron interactions are counted. A rather complete sample of spectra from a variety of BF_3 tubes is presented by Anderson and Malmskog.[8] A theoretical model has been developed by Cervellati and Kazimierski for the expected pulse height distribution from a BF_3 tube and is compared with experimentally measured distributions.[9]

B. BF_3 Tube Construction

The neutron detection efficiency can be increased and the wall effect suppressed by making the tube larger in dimension. Similar improvements can be achieved by raising the pressure of the BF_3 fill gas. Fowler[10] has reported the successful construction and operation of BF_3 tubes with diameter up to 15 cm and 180 cm long. Filling pressure ranged from 100 to 600 torr (approximately 13–80 kPa). Pressures in the range 200–300 torr (approximately 27–40 kPa) gave the best resolution in this work, whereas the full-energy peaks in the spectrum broadened considerably at higher pressure due to recombination and negative ion formation. In many counting situations, the poorer resolution is of no real consequence, and tubes with the higher gas pressure would be quite acceptable. Small-diameter tubes filled to several atmospheres pressure are commercially available, although pressures in the range 500–600 torr (approximately 67–80 kPa) are much more common.

In common with most proportional counters, BF_3 tubes are universally constructed using cylindrical outer cathodes and small-diameter central wire anodes. Aluminum is often the material of choice for the cathodes because of its low neutron interaction cross section. For low background application, other materials such as stainless steel are preferred because aluminum normally shows a small amount of low-level alpha activity. With typical anode diameters of 0.1 mm or less, operating voltages tend to be about 2000–3000 V. Larger-diameter anode wires and/or higher fill gas pressures require higher applied voltages. Typical gas multiplication at operating voltage is on the order of 100–500.

BF_3 tubes of typical construction are normally limited to operating temperature up to about 100°C, but tubes of special design can extend the operating range to as high as 150°C. However, the pulse amplitude decreases and the pulse height resolution decreases sharply[11] when operated well above room temperature. These changes may be related to the possible desorption of impurities from the counter wall or other components at elevated temperatures.

Because of the relatively high operating voltages, BF_3 tubes share some temperamental qualities with other proportional counters. Spurious pulses of about the same size as signal pulses can sometimes arise from fluctuations in leakage currents through insulators, especially under conditions of high humidity. Spurious counts can also arise in applications in which the counter is subject to vibration or shock.[12] These effects are attributed to detector microphonics and the influence of small particles of lint or dirt within the counter.

C. Gamma-Ray Discrimination

A very important consideration in many applications of BF_3 tubes is their ability to discriminate against gamma rays, which often are found together with the neutron flux to be measured. Gamma rays interact primarily in the wall of the counter and create secondary electrons that may produce ionization in the gas. Because the stopping power for electrons in gases is quite low, a typical electron will deposit only a small fraction of its initial energy within the gas before reaching the opposite wall of the counter. Thus, we should expect that most gamma-ray interactions will result in low-amplitude pulses that will lie in the tail to the left of point A in Fig. 14-3b. Simple amplitude discrimination can then easily eliminate these gamma rays without sacrificing neutron detection efficiency.

If the gamma-ray flux is sufficiently high, however, several complications can reduce the effectiveness of this amplitude discrimination. At high rates, pulse pile-up can result in apparent peak amplitudes for gamma rays which are considerably larger than any individual pulse. Brown[13] discusses the compromise that must then be struck in choosing the pulse-shaping time constant in the detector electronics. Short time constants are desirable to reduce the gamma-ray pile-up but may lead to reduction in the neutron-induced pulse amplitude due to incomplete charge integration. At very high gamma rates, there is evidence that chemical changes occur in the BF_3 gas due to molecular disassociation, leading to degraded pulse height spectra from neutron-induced events.[14] If this degradation is sufficiently severe, it may no longer be possible to separate gamma- and neutron-induced events.[15] In extreme cases, the radiation-induced chemical changes can result in permanent damage to the tube. Verghese et al.[16] report successful discrimination against gamma rays at exposure rates as high as 12 R/h using a conventional BF_3 tube. Developmental tubes that employ activated charcoal within the tube to act as an absorbing agent for contaminants have been reported.[17] These tubes exhibit good operating characteristics in gamma-ray fluxes up to 1000 R/h.

D. Detection Efficiency of a BF_3 Tube

The detection efficiency for neutrons incident along the axis of a BF_3 tube is given approximately by

$$\epsilon(E) = 1 - \exp\left[-\Sigma_a(E)L\right] \tag{14-4}$$

where

$\Sigma_a(E)$ = macroscopic absorption cross section of ^{10}B at energy E

L = active length of the tube

Using Eq. (14-4), we find that the calculated efficiency for a 30 cm long BF_3 tube (96% enriched in ^{10}B) filled to 600 torr (80 kPa) is 91.5% at thermal neutron energies (0.025 eV) but drops to 3.8% at 100 eV. Thus, a BF_3 tube exposed to neutrons with mixed energies will respond principally to the slow neutron component. Equation (14-4) slightly overestimates the neutron counting efficiency because there usually are regions near the end of the tube in which charge collection is inefficient, resulting in reduced neutron response. The influence of these *dead spaces* is most severe for detectors whose length is small and has been the subject of experimental investigations that lead to a more precise prediction of detector efficiency.[18,19] *End window* designs are common in which the dead space and structural materials at one end of the tube are minimized.

Most practical BF_3 counters are filled with pure boron trifluoride enriched to about 96% in ^{10}B. However, because BF_3 is not ideal as a proportional counter gas, counters are

sometimes manufactured using an admixture of BF_3 with a more suitable gas such as argon. This dilution causes a decrease in detection efficiency, but the pulse height spectrum from the tube generally shows sharper peaks and consequently a more stable counting plateau than tubes filled with pure BF_3.

E. Boron-Lined Proportional Counters

An alternate approach is to introduce the boron in the form of a solid coating on the interior walls of an otherwise conventional proportional tube. This configuration has the advantage that a more suitable proportional gas than BF_3 can now be used. Some applications, particularly those in which fast timing is important, are better served by introducing one of the common proportional gases discussed in Chapter 6. Also, the chemical degradation problems in BF_3 when exposed to high gamma ray fluxes can be greatly reduced by using alternative fill gases.

Because the maximum range of the alpha particles from the boron reaction is on the order of 1 mg/cm^2, the efficiency of boron-lined counters will improve only as the coating thickness is increased to about this value. Making the deposit any thicker will simply create layers in the coating which are too far from the filling gas to permit any reaction products to reach the gas, and the efficiency will actually begin to decrease slightly due to the added attenuation of the incident neutrons. Efforts have been made to increase the surface area available for coating by introducing boron-coated plates or baffles within cylindrical tubes, but these configurations have not achieved widespread popularity.

The pulse height spectrum to be expected from a boron-lined proportional chamber with a thick boron layer is sketched in Fig. 14-4. Because the interactions are now taking place in the wall of the chamber and the reaction products are oppositely directed, only

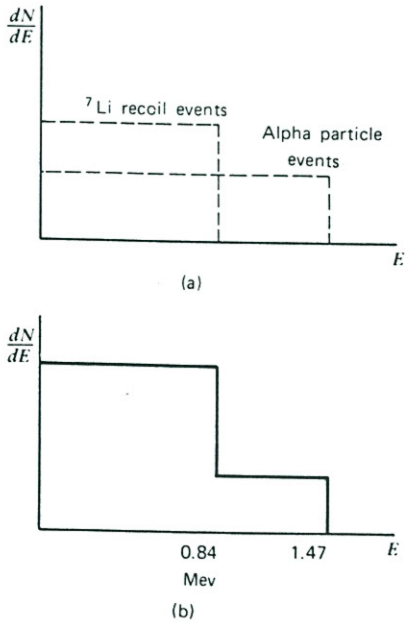

Figure 14-4 Idealized pulse height spectra from a boron-lined proportional tube. (a) Separate contributions of alpha particles and lithium recoil nuclei, which add to give the spectrum shown in plot (b).

one reaction product can be expected per interaction. If the alpha particle is directed toward the interior of the tube, the maximum energy it can deposit is its initial kinetic energy of 1.47 MeV. The actual alpha particle energy deposited in the gas will vary from this value down to zero as the possible location of the neutron interaction varies from the surface of the boron coating through those locations that are more than an alpha range away from the counter gas. Because all these locations are almost equally probable, the expected energy deposition distribution for alpha particles will be approximately rectangular in shape with a maximum at 1.47 MeV. This distribution is sketched in Fig. 14-4a as a dashed rectangle. A parallel argument can be made for the lithium recoil nucleus, with its maximum possible deposited energy equal to 0.84 MeV. The sum of these two individual rectangular distributions is shown as the solid line in Fig. 14-4b and is a somewhat idealized indication of the expected pulse height spectrum from a boron-lined chamber with a thick (greater than 1 mg/cm^2) boron lining. From the discussion given in Chapter 4, a differential pulse height spectrum without a "valley" structure does not lead to a counting plateau. Thus, it would be expected that boron-lined chambers would be less satisfactory than BF_3 tubes in terms of long-term counting stability. Because the average energy deposited for neutron interaction is also considerably less than for BF_3 tubes, the gamma-ray discrimination ability of boron-lined chambers will be inferior to that of BF_3 tubes.

F. Boron-Loaded Scintillators

Because the output pulse from a BF_3 tube originates with reaction products created with a more-or-less random location and direction, typical pulses will have rise times that vary by as much as 3–5 μs for tubes of average size. A further disadvantage for neutron time-of-flight applications is that the point of interaction of the neutron cannot be defined more precisely than somewhere within the volume occupied by the BF_3 fill gas. Because typical tubes are as much as 10–20 cm long to provide reasonable interaction efficiency, pathlength uncertainties can be large.

In order to circumvent both of the above limitations, other types of boron-loaded detector have been investigated. Scintillators made by fusing B_2O_3 and ZnS have found wide application in neutron time-of-flight measurements. These scintillators are usually kept quite thin (1–2 mm) because of the relative opaqueness of this material to its own scintillation light and also to minimize pathlength uncertainty. Other work has been reported[20] on combinations of boron-containing polyester plastic and zinc sulfide. Boron-based scintillators are typically less effective in discrimination against gamma-ray backgrounds compared with BF_3 tubes because most scintillators have a lower scintillation efficiency for charged particles compared with that for fast electrons.

III. DETECTORS BASED ON OTHER CONVERSION REACTIONS

A. Lithium-Containing Slow Neutron Detectors

Because a stable lithium-containing proportional gas does not exist, a lithium equivalent of the BF_3 tube is not available. Nonetheless, the larger Q-value of the lithium reaction offers some real advantage whenever discrimination against gamma-ray pile-up and other low-amplitude events is at a premium. Also, because the lithium reaction goes exclusively to the ground state of the product nucleus, the same energy is always imparted to the reaction products for all slow neutron interactions. The resulting pulse height distribution

in detectors that absorb all this energy is therefore a simple single peak. Although examples can be found[21] of the application of gas-filled detectors with solid lithium-based converters, the more common applications of this reaction employ the scintillation process to detect the products of the neutron-induced reaction.

Lithium-containing scintillators are quite common as slow neutron detectors. A logical choice, because of its chemical similarity to sodium iodide, is crystalline lithium iodide. If a small amount (less than 0.1 at. %) of europium is incorporated as an activator, light outputs of about 35% of the equivalent NaI(Tl) yield can be achieved. The scintillation mechanism is similar to that discussed earlier for sodium iodide. The scintillation decay time is approximately 0.3 μs.

Crystals of lithium iodide are generally large compared with the ranges of either of the reaction products from a neutron interaction. Therefore, the pulse height response will be free of wall effects and should be a single peak for all slow neutron interactions. The range of secondary electrons produced by gamma rays will not be large compared with typical crystal dimensions. The scintillation efficiency for lithium iodide is nearly the same for both electrons and heavy charged particles. (A 4.1 MeV electron will yield about the same light as the 4.78 MeV reaction products.) Therefore, a single gamma-ray interaction in lithium iodide is capable of producing a maximum pulse height approximately proportional to the energy of the gamma ray, whereas each neutron interaction will produce a pulse equivalent to 4.1 MeV on the same scale. The gamma-ray rejection characteristics will therefore be inferior to that of typical gas-filled neutron detectors, in which a gamma ray can deposit only a small fraction of its energy.

Similar to sodium iodide, lithium iodide is highly hygroscopic and cannot be exposed to water vapor. Commercially available crystals are hermetically sealed in a thin canning material with an optical window provided on one face. Because of the high density of the material, crystal sizes need not be large for very efficient slow neutron detection. For example, a 10 mm thick crystal prepared from highly enriched ^{6}LiI remains nearly 100% efficient for neutrons with energy from thermal through the cadmium cutoff of 0.5 eV.

Other recipes for lithium-containing scintillators have achieved some popularity. One of these reported by Stedman[22] consists of a lithium compound dispersed in a matrix of ZnS(Ag) with thickness of about 0.6 mm. These scintillators are commercially available as NE 421 (Nuclear Enterprises Limited). Their efficiency is quoted as 25–30% for 0.1 eV neutrons. Thin layer combinations of LiF and ZnS are described in Refs. 23 and 24. Because of their small thickness, gamma discrimination is very effective since a large fraction of all secondary electrons created by gamma-ray interactions will escape without depositing their full energy.

Finally, lithium-containing glass scintillators have become quite popular in neutron physics research. They are less common as slow neutron detectors, and therefore a discussion of this type of detector is postponed until Chapter 15. The same is true for combinations of lithium deposits with semiconductor detectors, and the so-called lithium sandwich spectrometer is also discussed in Chapter 15.

B. The ^{3}He Proportional Counter

With a cross section even higher than that of the boron reaction, the ^{3}He(n, p) reaction is an attractive alternative for slow neutron detection. Unfortunately, because ^{3}He is a noble gas, no solid compounds can be fabricated and the material must be used in gaseous form.

^{3}He of sufficient purity will act as an acceptable proportional gas, and detectors based on this approach have come into common use. General properties of ^{3}He propor-

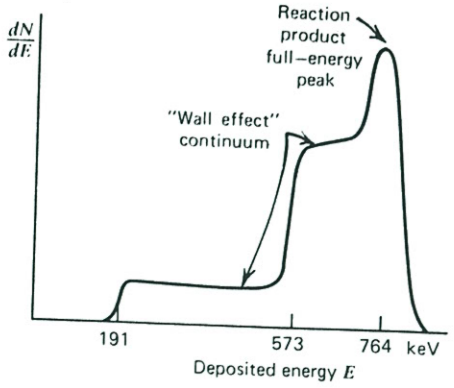

Figure 14-5 Expected pulse height spectrum from a ^{3}He tube in which the wall effect is significant.

tional tubes are surveyed in Ref. 25. In a large detector, one would expect each thermal neutron reaction to deposit 764 keV in the form of kinetic energy of the triton and proton reaction products. Because the range of these reaction products is not always small compared with the dimensions of the proportional tube, however, the wall effect discussed earlier for a BF_3 tube can also be important for ^{3}He proportional counters. The expected pulse height spectrum for a tube of typical size is illustrated in Fig. 14-5. Only a single full-energy peak should be expected for neutron energies that are small compared with 764 keV. The step structure to the left of the peak is similar to that shown in Fig. 14-3b for a BF_3 tube, except that the discontinuities will occur at energies corresponding to that of the proton (573 keV) and triton (191 keV).

The continuum in the pulse height spectrum due to the wall effect is detrimental from several standpoints. The voltage range over which an acceptable counting plateau will be observed is reduced, and the smaller pulse height for some neutron events will reduce the separation expected from low-amplitude, gamma-induced pulses. Consequently, consideration is often given in the design of ^{3}He tubes to minimize the wall effect. One obvious step is to build the counter with a diameter as large as possible so that most neutron interactions occur far away from the wall. Another is to increase the pressure of the ^{3}He gas to reduce the range of the charged particle reaction products. Because of the low atomic mass of ^{3}He, the ranges of the reaction products are unusually long and the wall effect is considerably more significant than for a BF_3 tube of the same size and fill gas pressure. One method of reducing the charged particle ranges is to add a small amount of a heavier gas to the ^{3}He to provide an enhanced stopping power. A detailed analysis of the wall effect in ^{3}He counters can be found in Ref. 26.

Compared with BF_3 tubes, ^{3}He counters can be operated at much higher pressures with acceptable gas multiplication behavior and are therefore preferred for those applications in which maximum detection efficiency is important. The lower Q-value of the ^{3}He reaction, however, makes gamma-ray discrimination more difficult than for an equivalent BF_3 tube.

The acceptable operating temperature for ^{3}He tubes has been shown[27,28] to extend as high as 200–250°C. In general, the pulse amplitude increases and the pulse height resolution decreases with increasing temperature, while the pulse rise time shows little temperature dependence.

As with all proportional counters, purity of the gas is critical, and the most typical cause of failure is leakage of air into the tube over long periods of time. Another factor is the buildup of electronegative poisons in the gas with use. As in BF_3 tubes, a layer of activated charcoal within the tube has been shown to be effective in removing these poisons and can extend the useful lifetime of a ^3He detector.[29]

C. Fission Counters

The fission reaction can also serve as a means of converting a slow neutron into ionizing reaction products that can then be detected by conventional means. One outstanding characteristic of the fission reaction is the large amount of energy (200 MeV) liberated in the reaction, about 160 MeV of which appears as kinetic energy of the fission fragments. Therefore, the neutron-induced fission reactions can be expected to be of much larger magnitude in most detectors than any other competing reaction or other event due to background or counter contamination. Under these circumstances, extremely low background rates can be achieved and neutron counting can be practically carried out at very low counting rates. In some detector types (scintillators are often an extreme example) the output pulse does not always linearly reflect the energy of the exciting particle. Nonlinearities are particularly important for densely ionizing particles such as fission fragments, and therefore the size of the neutron-induced detector pulses may not be as large as would be calculated based on simple linearity with energy. In that event, the fission fragments still may be considerably larger than competing reactions, but not by the several orders of magnitude one might ordinarily expect.

The most popular form of fission detector is an ionization chamber that has its inner surfaces coated with a fissile deposit. Because of adverse chemical and physical properties, little success has been realized in trying to incorporate the fissile material in gaseous form as part of the counter gas. In this section we stress properties of fission chambers operated in pulse mode, which is typical of nonreactor applications. Fission chambers can also function in current mode, most often as reactor flux monitors discussed later in this chapter.

The pulse height spectrum to be expected from a fission chamber depends primarily on the fissile deposit thickness and the geometric conditions under which the fission fragments are collected. For deposits that are very thin compared with fragment ranges, the familiar "double humped" fission fragment energy spectrum is observed, with the light and heavy fragment distributions peaking at about 100 and 70 MeV, respectively. If the deposit is made thicker to enhance detection efficiency, the energy loss of fragments within the deposit will reduce the average fragment energy and distort the shape of the measured distribution. Figure 14-6 illustrates the changes in spectrum shape to be expected as the thickness of a deposit of UO_2 is changed. These energy loss effects limit the practical deposit thickness to about 2–3 mg/cm^2. For a layer of highly enriched ^{235}U of this thickness, the corresponding detection efficiency in 2π counting geometry is about 0.5% at thermal energy, dropping to about 0.1% at 0.5 eV. Typical fission chambers employ a single layer, and are thus limited to an equivalent neutron detection efficiency. More complex fission chambers with higher detection efficiency can be designed[31–33] by providing multiple layers of fissile deposits, and detecting the fragments in each segment of the chamber between the layers.

The dimensions of the counter tend to be similar to that of alpha particle detectors, because the average range of a fission fragment is approximately half the range of 5 MeV alpha particles. Furthermore, because the fission fragment starts out with a very large

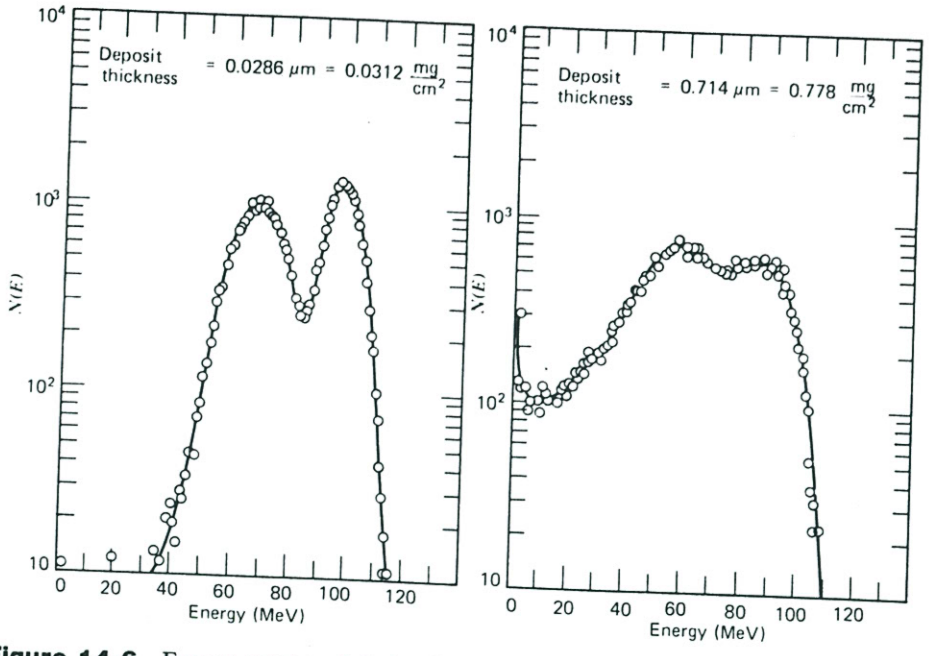

Figure 14-6 Energy spectra of fission fragments emerging from flat UO_2 deposits of two different thicknesses. A 2π detector is assumed which responds to fragments emitted in all directions from one surface of the deposit. (From Kahn et al.[30])

positive charge (on the order of 15 or 20 electronic charges) the energy loss at the beginning of the track is at its maximum, and the rate of energy loss continues to decrease as the fragment slows and additional charges are picked up. Just the reverse is true for most light charged particles, for which the rate of energy loss peaks near the end of the track. Therefore, in those detectors that do not fully stop the particle, fission fragments will yield a larger fraction of their total energy than would be expected for alpha particles or protons of the same range. For typical counter fill gases, the mean range is a few centimeters so that chambers of this dimension or larger can function reasonably as fission chambers.

The two fission fragments are always oppositely directed for slow-neutron-induced fission, and therefore detectors with a solid coating of fissionable material will respond only to the single fragment that is directed toward the active volume of the chamber. Some fission counters have been built with extremely thin backing material underneath a thin fissile deposit, so that both fragments can escape into opposite halves of a dual chamber, thereby permitting simultaneous detection of both fragments. Coincidence techniques can then discriminate against alpha particles and other background events. The very thin supports required for the fissile deposit are quite fragile, and consequently this type of fission chamber is not widely used in routine neutron detection applications.

The fissionable materials used in the construction of fission chambers are almost always alpha radioactive to some degree. As a result, typical fission chambers have an irreducible alpha-induced pulse rate that is an undesirable background. Because the average alpha particle energy is typically 5 MeV, whereas an average fission fragment energy is 10 times larger, these alpha pulses can often be simply discriminated on an amplitude basis. In those fissionable materials in which the alpha activity is relatively high (such as ^{239}Pu), problems often arise due to pile-up of alpha pulses to an amplitude that

can overlap the lowest energy fission fragments. Because the maximum amplitude expected from pulse pile-up is an inverse function of detector resolving time, it can be suppressed through the use of fast fission detectors. Small methane-filled fission chambers have been reported[34] which show pulse widths as small as 10 ns. Extremely fast fission detectors can also be built by detecting fission fragments in a gaseous scintillator or by incorporating the fissionable material as part of fast solid scintillators.[35] An extensive review of various fission chamber designs may be found in Ref. 36.

IV. REACTOR INSTRUMENTATION

A. General Considerations

In thermal nuclear reactors, most of the power is generated through fission induced by slow neutrons. Therefore, nuclear sensors that are to be part of reactor control or safety systems are generally based on detectors that respond primarily to slow neutrons. In principle, many of the detector types discussed earlier in this chapter can be adapted for application to reactor measurements. However, the extreme conditions associated with reactor operation often lead to substantial design changes, and a category of slow neutron detectors designed specifically for this application has gradually evolved. Detailed reviews of reactor instrumentation are given in Refs. 6 and 7.

It is conventional to subdivide reactor instruments into two categories: *in-core* and *out-of-core*. In-core sensors are those that are located within narrow coolant channels in the reactor core and are used to provide detailed knowledge of the flux shape within the core. These sensors can be either fixed in one location or provided with a movable drive and must obviously be of rather small size (typically on the order of 10 mm diameter). Some examples are given in Ref. 37. Out-of-core detectors are located some distance from the core and thus respond to properties of the neutron flux integrated over the entire core. The detectors may be placed either inside or outside the pressure vessel, and normally will be located in a much less severe environment compared with in-core detectors. Size restrictions are also less of a factor in their design.

The majority of neutron sensors for reactor use are of the gas-filled type. Their advantages in this application include the inherent gamma-ray discrimination properties found in any gas detector, their wide dynamic range and long-term stability, and their resistance to radiation damage. Detectors based on scintillation processes are less suitable because of the enhanced gamma-ray sensitivity of solid scintillators and the radiation-induced spurious events that occur in photomultiplier tubes. Semiconductor detectors are very sensitive to radiation damage and are never used in high radiation environments.

Nearly all the gas-filled chambers, whether they are ionization or proportional counters, can be operated in a variety of modes. In pulse mode, each neutron interaction must be separated by sufficient time so that it may be resolved as an individual pulse. This mode is therefore limited to the lower ranges of neutron flux measurement but offers the benefit of gamma discrimination through simple amplitude selection of the output pulses. Pulse mode operation of most detectors is conventionally limited to rates below about 10^5 per second, although state-of-the-art techniques in chamber design and pulse-processing electronics can raise this limit to as high as 10^7 per second (see references cited in Ref. 38).

When flux levels become high enough so that pulse mode operation is no longer possible, neutron detectors are often operated in current mode. With proper ion chamber design, the range of operation can be extended to the maximum flux level of interest in

reactors before serious nonlinear effects due to ion–electron recombination set in. Lower limits of current mode operation are usually determined by leakage currents that inevitably arise in the detector insulation and cable dielectric material. By operating the chamber in current mode, one sacrifices any chance of inherent gamma-ray discrimination because all pulses, whether large or small, add some contribution to the measured current.

One method of reducing gamma-ray sensitivity is to use the MSV mode of operation described in Chapter 4. This operational mode, commonly called the Campbelling technique, consists of deriving a signal that is proportional to the mean square of the current fluctuations from an ion chamber.[39-41] The mean square signal is seen from Eq. (4-8) to be proportional to the average pulse rate and the square of the ionization charge generated in each pulse. Because neutron-induced pulses result in much greater charge than pulses from gamma rays, the mean square signal will weight the neutron component by the square of the ratio of neutron- to gamma-ray-induced charge. This increase in neutron sensitivity is of greatest advantage in fission chambers. Although the MSV mode enhances the neutron sensitivity, it will not completely eliminate the gamma contribution. MSV mode operation has proved to be most useful in the intermediate reactor power ranges and in wide-range reactor control channels,[42-44] where one detector provides input to instrumentation that can operate in pulse mode, MSV mode, or current mode depending on the neutron flux level being measured.

A second approach for reducing the importance of the gamma-ray signal is to employ direct gamma-ray compensation in a specialized detector known as a compensated ion chamber (CIC). The CIC typically uses boron-lined ion chambers operating in current mode. Because of the much smaller Q-value of the neutron-induced reaction, neutron interactions in a boron-lined chamber result in an order of magnitude less charge than do neutron-induced events in a fission (uranium-lined) chamber. The effectiveness of the MSV mode of operation in discriminating against gamma rays is therefore reduced. The alternative approach of using a CIC is found to be more effective in reducing the gamma-ray contribution in boron-lined chambers than is the MSV mode of operation. The CIC, illustrated functionally in Fig. 14-7, employs a dual ion chamber from which two independent ion currents can be extracted separately. One chamber is boron-lined, whereas the construction of the second is nearly identical in terms of active volume and structural material, but without the boron lining. The current I_1 from the boron-lined chamber will consist of the sum of the current due to neutron interations in the boron and the gamma-ray interactions in the chamber walls and gas-filled region. The current I_2

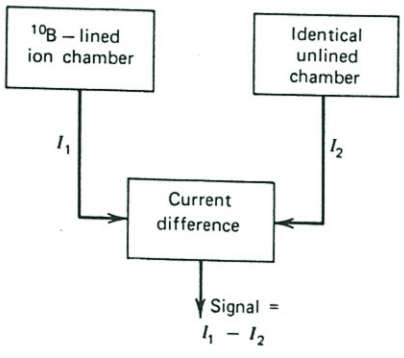

Figure 14-7 Operating principle of a compensated ion chamber (CIC).

from the unlined chamber will reflect only the gamma-ray contribution. By taking the difference between these two currents, a signal current is derived which in principle will be proportional to only the neutron contribution. The two chambers are often constructed as concentric cylinders and consequently are not identical in their response to gamma rays. Therefore, the compensation is not exact and may vary slightly with gamma-ray flux. This variation may require adjustments in the balance between the two chambers to restore exact compensation for different gamma-ray flux levels. (See Refs. 6 and 7 for further discussion of CIC design and operation.)

B. Reactor Nuclear Instrument (NI) System Overview

Before proceeding with further discussion of the specialized detectors used in reactor safety and control systems, a general discussion of the distinctly different system approaches used in pressurized water reactors (PWR) and boiling water reactors (BWR) is instructive. The reader is referred to Ref. 44 for a more detailed description of reactor NI systems.

1. PRESSURIZED WATER REACTOR NUCLEAR INSTRUMENTATION

Detectors for the routine monitoring of reactor power in a PWR are located outside the reactor pressure vessel and are characterized by the following typical environmental conditions: neutron flux up to 10^{11} n/cm^2 · s, gamma irradiation rates up to 10^6 R/h, and temperatures of approximately 100°C. Out-of-core sensors are the usual basis of reactor control and safety channels in a PWR. In choosing specific detector types, consideration must be given to the expected neutron signal level compared with noise sources, the speed of response of the detector, and the ability to discriminate against gamma-induced signals. Each of these criteria assumes different importance over various ranges of reactor power, and as a result multiple detector systems are usually provided, each designed to cover a specific subset of the power range.

Figure 14-8 illustrates a typical scheme for a PWR in which three sets of sensors with overlapping operating ranges are used to cover the entire power range of the reactor. The lowest range, usually called the source start-up range, is encountered first when bringing up reactor power from shut-down conditions. This range is characterized by conditions in which the gamma flux from the fission product inventory in the core may be large compared with the small neutron flux at these low power levels. Under these conditions, good discrimination against gamma rays is at a premium. Also, the expected neutron interaction rates will be relatively low in this range. Pulse mode operation of either fission chambers or BF_3 proportional counters is therefore possible, and the required gamma-ray

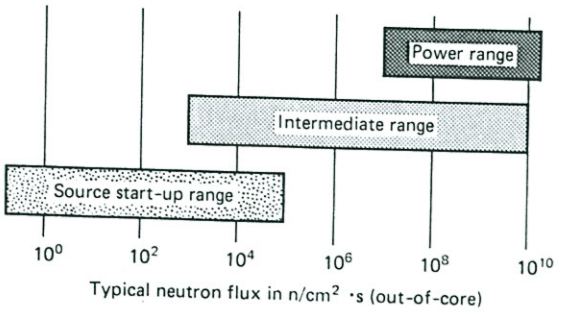

Figure 14-8 Typical ranges covered by out-of-core neutron detectors in a PWR.

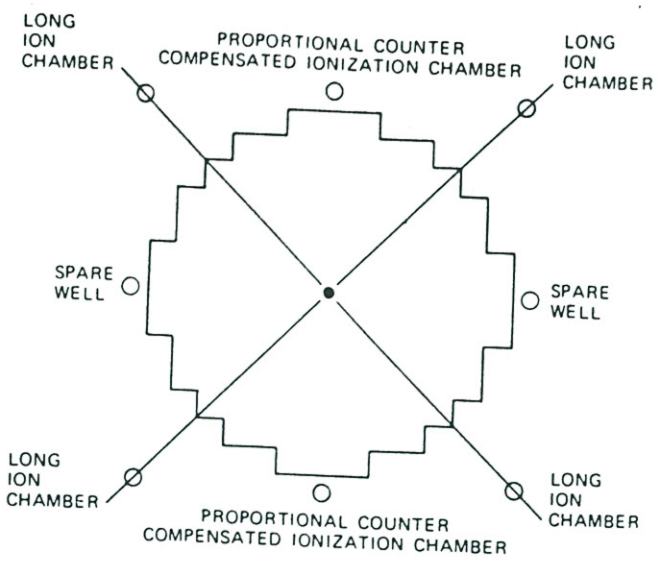

Figure 14-9 Geometric arrangement of out-of-core neutron detectors relative to the core of a PWR. (From Harrer and Beckerley.[44])

discrimination can be accomplished by accepting only the much larger amplitude neutron pulses.

As the power level is increased, an intermediate range is encountered in which pulse mode operation is no longer possible because of the excessive neutron interaction rate. In this region the gamma-ray-induced events are still significant compared with the neutron flux, and therefore simple current mode opertion is not suitable. The MSV mode of operation can reduce the importance of the gamma-ray signal in this range, but a more common method used in PWRs is to employ direct gamma-ray compensation using a CIC.

A third range of operation corresponds to the region near the full operating power of the reactor. The neutron flux here is usually so large that gamma-ray-induced currents in ion chambers are no longer significant, and simple uncompensated ion chambers are commonly used as the principal neutron sensor. Because these instruments are often part of the reactor safety system, there is a premium on simplicity which also favors uncompensated ion chamber construction.

In most PWR NI systems the geometric arrangement shown in Fig. 14-9 is employed. Two BF_3 proportional counters used in the source start-up range are placed on opposite sides of the core and two CIC detectors used in the intermediate range are placed in the same location or on the two opposing sides. Four power range monitors are then located at 90° intervals at positions between the BF_3 and CIC detectors. Each of the four power range monitors consists of two uncompensated ion chambers arranged end-to-end, resulting in a total detector length of 3–4 m. This arrangement provides both radial and axial neutron flux data for control and safety at full power as well as axial flux offset information needed for control of xenon oscillations.

Although PWR nuclear instrumentation employs out-of-core gas-filled detectors (primarily ion chambers) for control and safety channels, there remains a need for information on in-core spatial variations of the neutron flux. This information is necessary for fuel management and is provided by various types of detectors placed within the reactor core (see following descriptions).

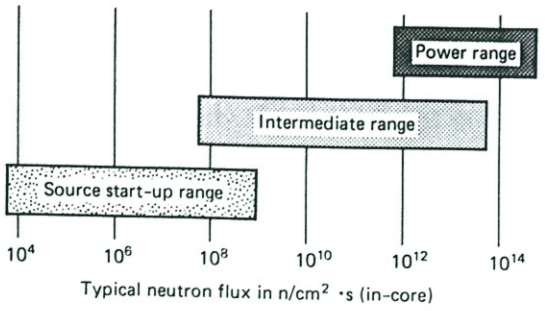

Figure 14-10 Typical ranges covered by in-core neutron detectors in a BWR.

2. BOILING WATER REACTOR NUCLEAR INSTRUMENTATION

The BWR NI system, like the PWR system, has three overlapping ranges as illustrated in Fig. 14-10. The three systems are called source, intermediate, and power range monitors. Unlike the PWR, which uses out-of-core neutron detectors, the neutron detectors are all located in-core. There are also many more detectors used in the BWR NI system than in the PWR system.

The source range monitoring system typically consists of four in-core fission chambers operating in pulse mode. Pulse mode operation provides good discrimination against gamma rays, which is necessary when measuring a relatively low neutron flux in the presence of a high gamma flux. A typical intermediate range monitoring system has eight in-core fission chambers operating in the MSV mode. The MSV mode promotes the enhanced neutron to gamma response required to provide a proper measure of neutron flux in the presence of gamma rays for both control and safety requirements. The power range monitoring system typically consists of 144–164 fission ion chambers distributed throughout the core. The fission chambers operate in current mode and are called local power range monitors (LPRM). Current mode operation provides satisfactory neutron response at the high flux levels encountered between 2 and 150% full power. In a typical system, approximately 20 LPRMs are summed to provide input to one of the seven or eight average power range monitoring (APRM) systems. The APRM system provides input for both control and reactor protection systems. Details of the neutron monitoring systems used in the BWR are described in Ref. 44.

A diagram of a typical fission chamber used in BWR NI is shown in Fig. 14-11. The physical size of the detectors used in each range are similar. The fill-gas pressures and uranium loadings are different, depending on whether the detector is designed to operate in pulse, MSV, or current mode. The LPRM system typically employs a fission chamber with a mixture of both ^{235}U and ^{234}U. The advantage of this design for extended operation in a high neutron flux is described in the next section.

C. In-Core Detectors

There is often a need to place neutron sensors within the core of a nuclear reactor to provide information on the spatial variation of the neutron flux. Because of the small size (1–7 cm) of the channel in which these instruments must be located, emphasis is placed on compactness and miniaturization in their design. They may either be left in a fixed position or provided with a motorized drive to allow traverses through the reactor core. Some may provide a continuous readout, whereas others are interrogated only at periodic intervals. Typical operating conditions are: neutron flux at full power of 5×10^{13}

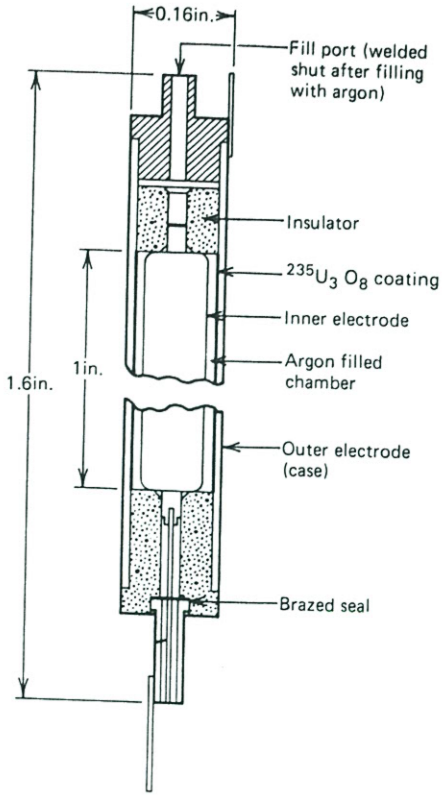

Figure 14-11 A typical in-core fission chamber used in BWR neutron monitoring systems.

$n/cm^2 \cdot s$, gamma flux up to 10^8 R/h, operating temperature up to 300°C, and operating pressure up to 2500 psi (17 MPa). In-core reactor measurements are the subject of a number of papers found in Ref. 37.

1. FISSION CHAMBERS

Miniaturized fission chambers can be tailored for in-core use over any of the power ranges likely to be encountered in reactor operation. Walls of the chamber are usually lined with highly enriched uranium to enhance the ionization current. These small ion chambers are typically made using stainless steel walls and electrodes, and operating voltage varies from about 50 to 300 V. Argon is a common choice for the chamber fill gas and is used at a pressure of several atmospheres. The elevated pressure ensures that the range of fission fragments within the gas does not exceed the small dimensions of the detector.

The gradual burn up of neutron-sensitive material is a serious problem for the long-term operation of in-core detectors. For example, a fission chamber using ^{235}U will show a sensitivity decrease of about 50% after exposure to an integrated neutron fluence of about 1.7×10^{21} n/cm^2 (Ref. 45). One method of reducing the effects of burnup in fission chambers is to combine fertile and fissile material in the neutron-sensitive lining of the chamber. Use of these *regenerative* chambers will gradually convert the fertile isotopes to fissile nuclei to help compensate for the burnup of the original fissile material

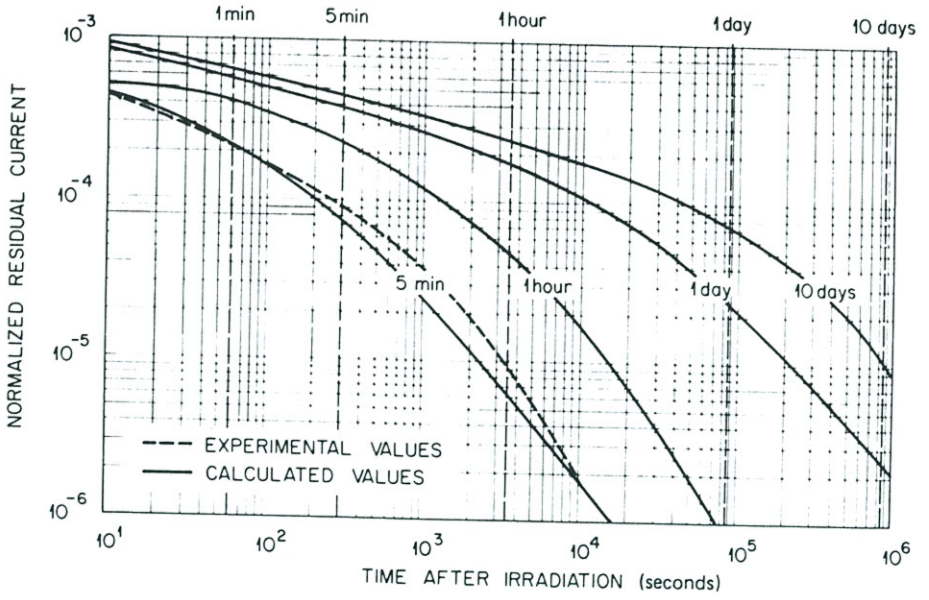

Figure 14-12 Memory effect in fission chambers corresponding to various steady-state irradiation times. (From Roux.[46])

present in the lining. The long-term response of fission chambers can greatly be improved with this method. For example, it is reported that fission chambers based on a mixture of ^{238}U and ^{239}Pu can maintain a sensitivity that does not change more than $\pm 5\%$ over an integrated neutron fluence of 4.8×10^{21} n/cm^2 (Ref. 45). Similar results have also been obtained with fission chambers based on a mixture of ^{234}U and ^{235}U.

Fission ion chambers that have been operated for long periods in high neutron fluxes will show a residual current or *memory* effect due to the buildup of fission products within the chamber. These fission products emit beta and gamma rays, which ionize the fill gas of the chamber and result in a significant ion current. Figure 14-12 shows the results to be expected if the current from a fission chamber is monitored following its removal from long-term exposure in a steady-state neutron flux. The residual current I is plotted as a fraction of the steady-state current I_0 observed during the neutron irradiation. One minute after removal about 0.1% of the signal current persists, whereas after 10 days the fission product activity has decayed sufficiently so that the residual current has dropped to about 10^{-5} of the steady-state signal.

One effect that can be important in ion chambers which must cover a wide range of irradiation rates is illustrated in Fig. 14-13. At lower rates the region of ion saturation is reached at a lower voltage than at higher rates. When the current is high, the density of ionization is correspondingly high and recombination will occur more readily than at lower currents. The electric field required to prevent recombination is therefore higher at high rates, evidenced by the increased voltage required to achieve ion saturation. It is important to select an operating voltage for these chambers at the highest irradiation rate or largest current that will be encountered. Although the change in current–voltage characteristics with increased neutron flux may be greater for in-core detectors than out of core detectors, a similar effect is observed in both the compensated and uncompensated ion chambers used in pressurized water reactors.

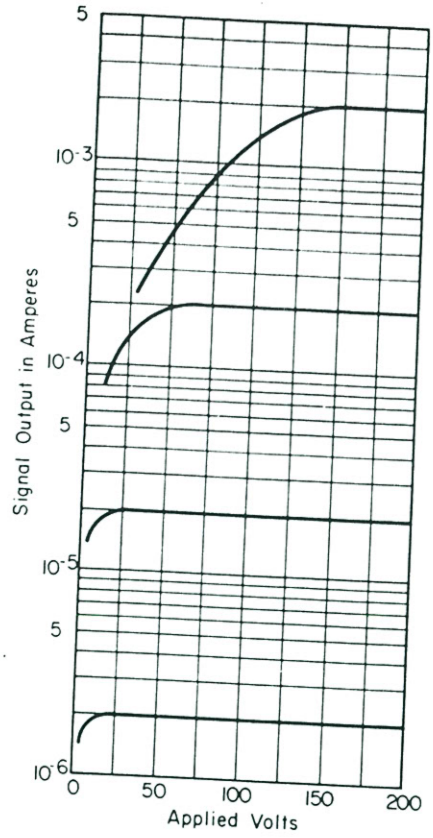

Figure 14-13 Typical current–voltage characteristics of an in-core fission chamber at different neutron irradiation levels. (Courtesy of Westinghouse Electric Corporation, Electronic Tube Division, Horseheads, NY).

2. SELF-POWERED DETECTORS

A unique type of neutron detector that is widely applied for in-core use is the *self-powered detector*. These devices incorporate a material chosen for its relatively high cross section for neutron capture leading to subsequent beta or gamma decay. In its simplest form, the detector operates on the basis of directly measuring the beta decay current following capture of the neutrons. This current should then be proportional to the rate at which neutrons are captured in the detector. Because the beta decay current is measured directly, no external bias voltage need be applied to the detector, hence the name self-powered. Another form of the self-powered detector makes use of the gamma rays emitted following neutron capture. Some fraction of these gamma rays will interact to form secondary electrons through the Compton, photoelectric, and pair production mechanisms. The current of the secondary electrons can then be used as the basic detector signal.

The self-powered detector is also known by a variety of other names. In recognition of some of the early pioneering work done by G. W. Hilborn,[47,48] they are sometimes called Hilborn detectors. Other names that can be found in the literature include beta emission detectors, collectrons, electron emission detectors, and PENA (primary emission,

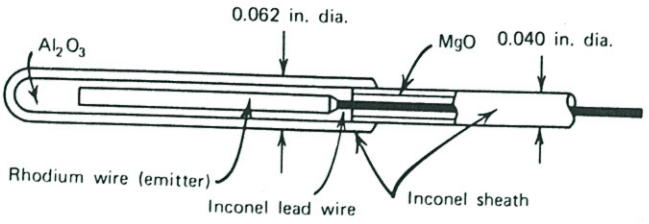

Figure 14-14 Cross-sectional view of a specific self-powered detector design. (From Stevens.[51])

neutron activation) detectors. Nonetheless, the *self-powered neutron* (SPN) detector remains the most common term applied to this family of devices.

Compared with other neutron sensors, self-powered detectors show advantages due to their small size, low cost, and the relatively simple electronics required in conjunction with their use. Disadvantages stem from the low level of output current produced by the devices, a relatively severe sensitivity of the output current to changes in the neutron energy spectrum, and, for many types, a rather slow response time. Because the signal from a single neutron interaction is at best a single electron, pulse mode operation is impractical and self-powered detectors are always operated in current mode. Various types of SPN detectors are surveyed in Ref. 49, and considerations in their application to in-core measurements in a PWR are reviewed in Ref. 50.

a. Detectors Based on Beta Decay

Figure 14-14 shows a sketch of a typical SPN detector based on beta decay. The heart of the device is the emitter, which is made from a material chosen for its relatively high cross section for neutron capture leading to a beta-active radioisotope. Ideally, the remainder of the detector does not interact strongly with the neutrons, and construction materials are chosen from those with relatively low neutron cross sections. Figure 14-15 illustrates some possible sequences which can contribute to the measured current. The principles of operation are very simple: The current corresponding primarily to the beta rays given off by the emitter is measured between the emitter and an outer shell, called the collector. The intervening space is filled with an insulator, which must be chosen to withstand the extreme temperature and radiation environment typically found in a reactor core. Various metallic oxides are often used as the insulator, with magnesium or aluminum oxide[52] most commonly used. The collector is typically high-purity stainless steel or Inconel. Great care must be taken in the fabrication of these detectors to keep the materials as clean as possible to avoid contamination by substances that might also become radioactive and add an interfering current to the measured signal. The small dimensions shown in Fig. 14-14 are necessitated by the small clearances available for instrument channels in typical reactor cores.

The key to the detector performance lies in the choice of emitter material. Factors to be considered in the selection of the emitter include its neutron capture cross section. together with the energy and half-life of the resulting beta activity. The capture cross section must be neither too high nor too low, because very low cross sections will lead to detectors with low sensitivity, whereas an excessively high cross section will result in rapid burnup of the emitter material[53] in the high neutron fluxes associated with reactor cores. The beta rays produced should be of sufficiently high energy so that excessive self-absorption in the emitter or insulator is avoided, and the half-life of the induced activity should

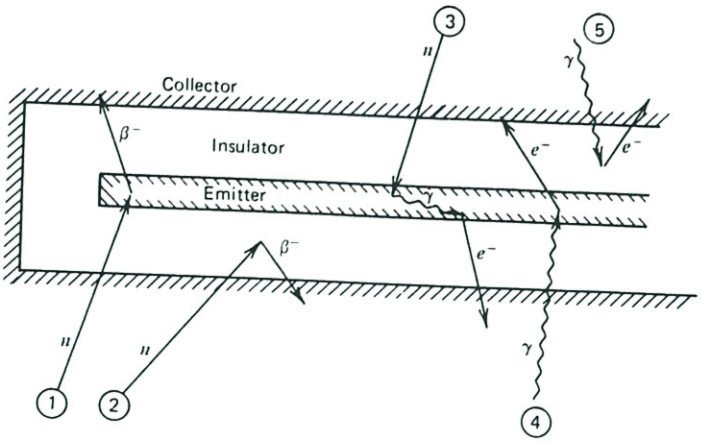

Figure 14-15 Representative events that can take place in a SPN detector. Events ① and ② are neutron capture followed by β^- decay. Event ③ shows the interaction of a prompt gamma ray emitted upon neutron capture, giving rise to a fast secondary electron. Events ④ and ⑤ show interfering fast electrons arising from interactions of external gamma rays. In standard SPN detectors, event ① is the basis of its neutron response. In those with fast response, event ③ is the preferred mode of interaction.

be as short as possible to permit the detector to respond quickly to rapid changes in neutron flux.

Based on these criteria, the two most popular choices for emitter material have been rhodium and vanadium. Table 14-1 summarizes some of the important properties of these materials when used as emitters in self-powered detectors. Vanadium produces a fairly simple beta decay with a half-life of 225 s, whereas rhodium gives rise to a more complex beta decay with an admixture of half-lives of 44 and 265 s. Figure 14-16 shows the resulting response of these materials to a step change in neutron flux level. Despite the fact that vanadium has a lower sensitivity and somewhat slower response than rhodium, vanadium emitters have become more common in reactor applications because the rate of burnup is significantly less, permitting use over periods of years in typical reactor fluxes.

In its simplest form, a self-powered detector with a single mode of induced activity and negligible burnup would behave as follows when exposed to a neutron flux for a

TABLE 14-1 Properties of Emitter Materials for SPN Detectors Based on Beta Decay

Emitter Material	Nuclide of Interest and Percent Abundance[a]	Activation Cross Section at Thermal Energy[b]	Half-Life of Induced Beta Activity[a]	Beta Endpoint Energy[a]	Typical Neutron Sensitivity[c]
Vanadium	$^{51}_{23}$V (99.750%)	4.9 barns	225 s	2.47 MeV	$5 \times 10^{-23} \frac{A}{n/cm^2 \cdot s}$
Rhodium	$^{103}_{45}$Rh (100%)	139 barns	44 s		
		11 barns	265 s	2.44 MeV	$1 \times 10^{-21} \frac{A}{n/cm^2 \cdot s}$

[a] Data from Lederer and Shirley, *Table of Isotopes*, 7th ed., Wiley & Sons, New York, 1978.
[b] Data from BNL-325, 3rd ed., Vol. 1 (1973).
[c] Sensitivity quoted for emitter of 1 cm length and typical diameter.

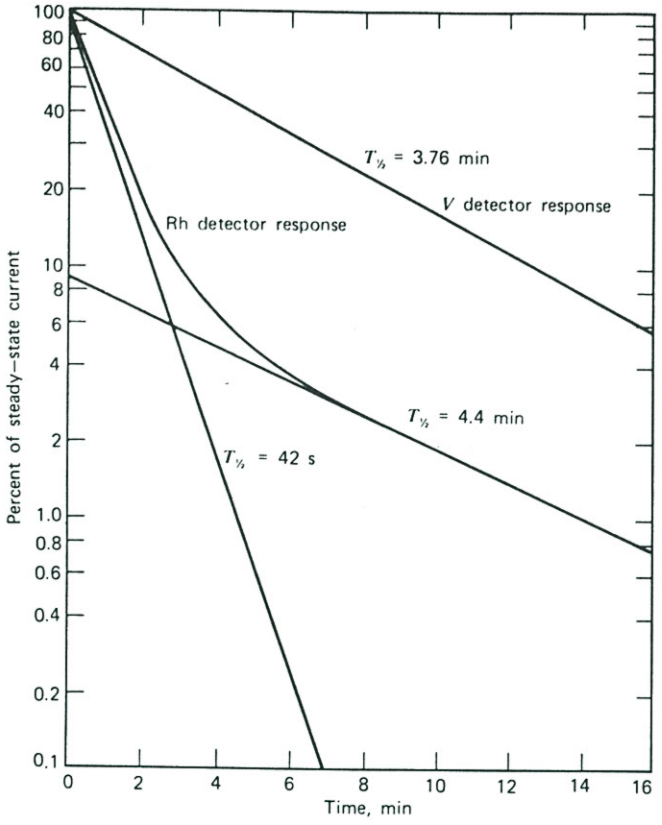

Figure 14-16 Response of rhodium and vanadium SPN detectors to an abrupt drop to zero of a steady-state neutron flux. (From Stevens.[51])

period of time t:

$$I(t) = Cq\sigma N\varphi(1 - e^{-\lambda t}) \tag{14-5}$$

where C = dimensionless constant reflecting the specific geometry and collection efficiency of the detector

q = charge liberated (number of beta particles $\times e$) per neutron absorbed

σ = activation cross section of the emitter material

N = number of emitter atoms

φ = neutron flux

λ = decay constant of activity produced in the emitter.

At saturation, or when the detector has been exposed to the flux for a period of time that is long compared with the half-life of the induced activity, the steady-state current is given simply by

$$I_{\text{sat}} = Cq\sigma N\varphi \tag{14-6}$$

The saturated current is proportional to the neutron flux and consequently can serve as a corresponding monitor of the neutron flux level.

A more complex analysis of the output of these detectors must take into account a number of other factors, including neutron flux depression due to emitter self-shielding, the Compton and photoelectrons produced from gamma rays which may accompany the beta decay process, and the self-absorption probability of the beta particles within the emitter. Some electrons are stopped in the insulator before reaching the collector, whereas others can be produced within the insulator material and travel to either the emitter or the collector. After some period of operation, an equilibrium is established in which the net amount of charge flowing into the insulator is exactly balanced by the charge flowing out. Monte Carlo calculations have shown that the current due to processes taking place within the insulator is typically less than 15%[54] and consequently is not a dominant effect in determining detector response. Fairly detailed physical models have been described[54-57] which appear to give adequate predictions[58] of the response of SPN detectors, taking into account most of these effects.

b. Self-Powered Detectors Based on Secondary Electrons from Gamma Decay

One of the primary disadvantages of self-powered detectors based on beta decay is their relatively slow response time. Some efforts have been made to remedy this situation by electronic or digital processing of the signals,[59-61] but it would be preferable to speed up the inherent response of the detector itself. One method of accomplishing this objective is to rely on the secondary electrons produced by prompt capture gamma rays which can follow neutron capture in the emitter (see Fig. 14-15). These capture gamma rays are typically emitted within a small fraction of a second, as opposed to the much slower decay of typical neutron-induced beta activities. Even in vanadium and rhodium detectors, there is a prompt component of the signal that, although much smaller than the signal due to the beta current, corresponds to the prompt capture gamma rays emitted upon neutron capture in these materials. The ratio of prompt to delayed signal in commercial vanadium detectors is reported to be about 6.5%.[59]

For fast self-powered detectors, it is more common to choose a specific emitter material that will optimize the signal arising from prompt capture gamma rays. Most experience has been gained using cobalt as a prompt emitter,[62-64] with cadmium also used in commercially available detectors. The behavior and sensitivity of other prompt emitter materials have been reported by Gebureck et al.[65] With some exceptions, the neutron sensitivity is substantially less for prompt detectors compared with those based on beta decay, but the much faster response can make them the detector of choice for certain applications.

The response to external gamma rays also can be quite significant for some emitter materials. Gamma rays incident on the detector give rise to secondary electrons, which can yield a discernible signal; the process is illustrated in Fig. 14-15. The gamma-ray-induced signal can be either positive or negative, in that the net flow of current may be either in the same or the opposite direction to the neutron-induced current. Which polarity prevails depends on whether more gamma-ray-induced electrons flow from the emitter to collector or vice versa. Either situation may exist, depending on the specific construction of the detector. The commonly used emitter materials for neutron-sensitive detectors (rhodium, vanadium, or cobalt) all have gamma-ray responses that typically are less than a few percent of the neutron response.[66] Detectors made with zirconium emitters have an almost pure gamma-ray response, whereas other materials such as platinum, osmium, or cerium will give a mixed response. Shields[66] first described the properties and application of a platinum detector for in-core flux measurements in power reactors, in which the combined gamma/neutron sensitivity provides a mix of prompt and delayed

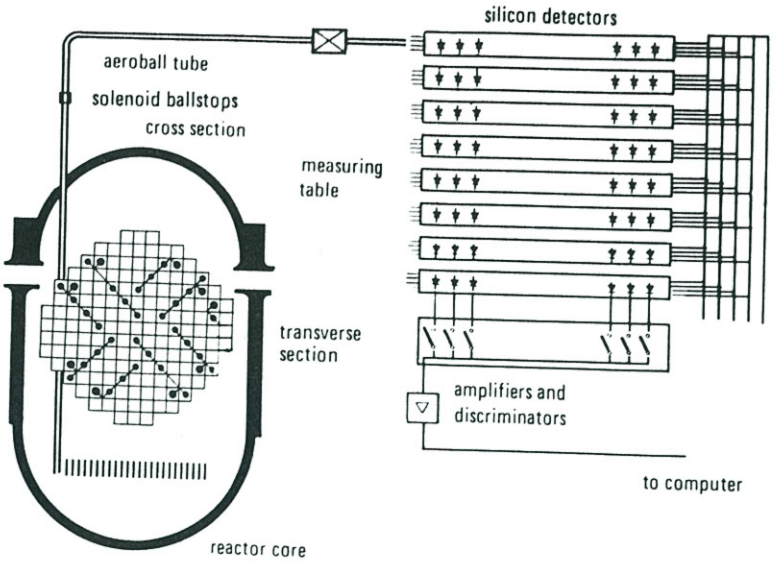

Figure 14-17 The aeroball system for continuous activation measurements of the neutron distributions in a reactor core. (From Glasow.[71])

response. Platinum detectors have gained considerable popularity, and analyses of their response have been published in Refs. 67–70.

In all types of self-powered detector, the effects of neutron and gamma-ray interactions in the connecting cable can be quite significant. As a result, considerable care must be taken in choosing the construction materials for the signal cable that lead to the detector, especially in those regions in which these cables are subjected to high radiation fields. In order to aid in the suppression of false signals arising in the connection cables, twin signal leads are often used. One lead is connected through the cable to the emitter, whereas the other is included within the same cable but is terminated without electrical contact physically near the emitter. By electronically subtracting the unconnected lead signal from the current detected from the lead connected to the emitter, effects due to cable interactions are approximately canceled out.

3. THE AEROBALL SYSTEM FOR MONITORING POWER DISTRIBUTION

A unique in-core monitoring system referred to as the computerized aeroball system[71] is used in some pressurized water reactor systems in the Federal Republic of Germany. In the aeroball system, probes containing neutron-sensitive isotopes are introduced into the reactor core and are subsequently activated. In the system shown in Fig. 14-17, the probes are columns of 1.7 mm diameter steel balls. The ball columns are piped into stainless steel tubes incorporated in selected fuel elements throughout the reactor core. The length of the columns corresponds to the height of the core. Vanadium is added to the balls as a neutron flux indicator through the 225 s half-life ^{52}V activity induced by neutron capture in ^{51}V. The activation of ^{51}V and its characteristics are summarized in Table 14-1 and the time response is shown in Fig. 14-16.

The activity of the probes is measured, following removal from the core, by using a set of silicon detectors. The count rate from each silicon detector is proportional to the relative integrated thermal neutron flux at the point where the corresponding aeroball was

located during the activation process. From many such measurements, the power density distribution throughout the reactor core can be determined.

PROBLEMS

14-1. Discuss the feasibility of operating a BF_3 or ^3He tube in the ionization or Geiger regions rather than as a proportional tube. What practical considerations dictate the latter choice?

14-2. When operated at a gas multiplication factor of 1000, estimate the pulse amplitude produced by the interaction of a thermal neutron in a ^3He tube of 100 pF capacitance.

14-3. A BF_3 tube using natural boron shows a counting efficiency of 1% for 10 eV neutrons in a given application. By what factor can the efficiency be increased by using boron enriched to 96% ^{10}B?

14-4. Calculate the detection efficiency of a BF_3 tube (96% enriched in ^{10}B) filled to 600 torr (80 kPa) for incident thermal neutrons if their pathlength through the gas is 10 cm.

14-5. In which applications might one prefer to use a ^3He tube rather than a BF_3 tube for slow neutron counting?

14-6. In BF_3 tubes of small diameter, the "step" in the pulse height spectrum of Fig. 14-3b at 1.47 MeV has a finite positive slope that is much more noticeable than that for the step at 0.84 MeV. Give a physical explanation for this observation.

14-7. Sketch the pulse height spectrum expected from a boron-lined proportional tube for thermal neutrons, if the boron thickness is small enough so that energy loss of the reaction products in the layer can be neglected.

14-8. Using the data given in Table 8-3, estimate the number of scintillation photons liberated by the interaction of a thermal neutron in $^6LiI(Eu)$ and in a typical Li glass scintillator.

14-9. Why is it not possible to increase the counting efficiency of a fission chamber indefinitely simply by increasing the thickness of the fissionable deposit?

14-10. The signal current from a typical application of a self-powered neutron detector is seldom more than a nanoampere. Find the equivalent number of beta particles transferred per second between the emitter and collector.

14-11. Find the fractional decrease in sensitivity (the "burnup") of a rhodium self-powered detector if used in a neutron flux of $3 \times 10^{13}/cm^2 \cdot s$ over a period of 6 months.

REFERENCES

1. W. D. Allen, *Neutron Detection*, George Newnes, Ltd., London, 1960.
2. W. J. Price, *Nuclear Radiation Detection*, 2nd ed., Chap. 10, McGraw-Hill, New York, 1964.
3. H. Neuert, *Kernphysikalische Messverfahren*, Chap. 9, Verlag G. Braun, Karlsruhe, 1966.
4. A. Lorenz, *A Review of Neutron Detection Methods and Instruments*, UCID-16325 (1973).
5. G. Grosshoeg, *Neutron Ionization Chambers*, North-Holland, Amsterdam, 1979.
6. J. F. Boland, *Nuclear Reactor Instrumentation (In-Core)*, Gordon & Breach, New York, 1970.
7. J. M. Harrer and J. G. Beckerley, *Nuclear Power Reactor Instrumentation Systems Handbook*, Vol. 1, Chaps. 2 and 3, TID-25952-P1 (1973).

8. I. O. Anderson and S. Malmskog, "Investigation of the Pulse Height Distribution of Boron Trifluoride Proportional Counters," AE-84 (1962).
9. R. Cervellati and A. Kazimierski, *Nucl. Instrum. Meth.* **60**, 173 (1968).
10. I. L. Fowler, *Rev. Sci. Instrum.* **34**, 731 (1973).
11. E. Sakai, S. Usui, H. Ohkado, Y. Hayashi, and H. Nakatani, *IEEE Trans. Nucl. Sci.* **NS-30** (1), 802 (1983).
12. C. W. Peters, A. L. Snyder, and A. S. Gallia, Jr., *IEEE Trans. Nucl. Sci.* **NS-13**(1), 636 (1966).
13. D. P. Brown, *IEEE Trans. Nucl. Sci.* **NS-21** (1), 763 (1974).
14. T. Tomoda and S. Fukakusa, *Nucl. Instrum. Meth.* **224**(3), 557 (1984).
15. J. Csikai and M. Buczko, *Nucl. Instrum. Meth.* **8**, 73 (1960).
16. K. Verghese, J. R. Bohannon, and A. D. Kowalczuk, *Nucl. Instrum. Meth.* **74**, 355 (1969).
17. A. J. Stokes, T. J. Meal, and J. E. Myers, Jr., *IEEE Trans. Nucl. Sci.* **NS-13**(1), 630 (1966).
18. I. L. Fowler and P. R. Tunnicliffe, *Rev. Sci. Instrum.* **21**, 734 (1950).
19. T. E. Sampson and D. H. Vincent, *Nucl. Instrum. Meth.* **95**, 563 (1971).
20. K. H. Sun, P. R. Malmberg, and F. A. Pecjak, *Nucleonics* **14**, 7, 46 (1956).
21. O. P. Joneja, R. Hecker, and A. Mohsin, *Nucl. Instrum. Meth.* **193**, 563 (1982).
22. R. Stedman, *Rev. Sci. Instrum.* **31**, 1156 (1960).
23. R. H. Bossi and A. H. Robinson, *Trans. Am. Nuc. Soc.* **22**, 153 (1975).
24. F. Mantler-Niederstatter, F. Bensch, and F. Grass, *Nucl. Instrum. Meth.* **142**, 463 (1977).
25. W. R. Mills, Jr., R. I. Caldwell, and I. L. Morgan, *Rev. Sci. Instrum.* **33**, 866 (1962).
26. S. Shalev, Z. Fishelson, and J. M. Cuttler, *Nucl. Instrum. Meth.* **71**, 292 (1969).
27. E. Sakai, K. Kubo, and H. Yoshida, *IEEE Trans. Nucl. Sci.* **NS-27**(1), 776 (1980).
28. F. L. Glesius and T. A. Kniss, *IEEE Trans. Nucl. Sci.* **NS-35**(1), 867 (1988).
29. A. E. Evans, H. O. Menlove, R. B. Walton, and D. B. Smith, *Nucl. Instrum. Meth.* **133**, 577 (1976).
30. S. Kahn, R. Harman, and V. Forgue, *Nucl. Sci. Eng.* **23**, 8 (1965).
31. H. Ries, J. Drexler, R. Fischer, W. Günther, K. Huber, U. Kneissl, H. Ströher, and W. Wilke, *Nucl. Instrum. Meth.* **185**, 373 (1981).
32. A. A. Bogdzel, A. Duka-Zólyomi, J. Kliman, V. Presperin, S. P. Avdeev, V. D. Kuznetsov, Z. Dlouhý, *Nucl. Instrum. Meth.* **200**, 407 (1982).
33. K. H. Valentine, M. K. Kopp, G. W. Allin, W. T. Clay, and V. C. Miller, *IEEE Trans. Nucl. Sci.* **NS-32** (1), 384 (1985).
34. N. W. Hill, J. T. Mihalczo, J. W. Allen, and M. M. Chiles, *IEEE Trans. Nucl. Sci.* **NS-22** (1), 686 (1975).
35. E. Catalano and J. B. Czirr, *Nucl. Instrum. Meth.* **143**, 61 (1977).
36. R. W. Lamphere, "Fission Detectors," in *Fast Neutron Physics*, Part I, p. 449 (J. B. Marion and J. L. Fowler, eds.), Interscience Publishers, New York, 1960.
37. *Proceedings of the Specialists' Meeting on In-Core Instrumentation and Reactor Assessment*, Nuclear Energy Agency (NEA), Organization for Economic Co-Operation and Development (OECD), 1984.
38. W. H. Ellis, J. L. Cooper, Jr., and G. H. Sanders, *IEEE Trans. Nucl. Sci.* **NS-20**(1), 639 (1973).
39. R. A. DuBridge, *IEEE Trans. Nucl. Sci.* **NS-14**(1), 241 (1967).
40. H. A. Thomas and A. C. McBride, *IEEE Trans. Nucl. Sci.* **NS-15**(1), 15 (1968).
41. N. R. Campbell and V. J. Francis, *JIEE* **93**, Part III (1946).
42. M. Oda, M. Wada, and S. Badono, *IEEE Trans. Nucl. Sci.* **NS-23**(1), 304 (1976).
43. S. Shirayama, T. Itok, C. C. Wimpee, and J. Sturz, Proceedings of the Specialists' Meeting on In-Core Instrumentation and Reactor Assessment, NEA/OECD, pp. 66–77 (1984).

44. J. M. Harrer and J. G. Beckerley, *Nuclear Power Reactor Instrumentation Handbook*, Vol. 2, Chaps. 15 and 16, TID-25952-P2 (1974).
45. H. Böck and E. Balcar, *Nucl. Instrum. Meth.* **124**, 563 (1975).
46. D. P. Roux, ORNL-3929 (1966).
47. J. W. Hilborn, *Nucleonics* **22**, 2, 69 (1964).
48. J. W. Hilborn, "Self-Powered Neutron Detector," U.S. Patent 3,375,370 (March 26, 1968).
49. N. P. Goldstein and W. H. Todt, *IEEE Trans. Nucl. Sci.* **NS-26**(1), 916 (1979).
50. D. P. Bozarth and H. D. Warren, *IEEE Trans. Nucl. Sci.* **NS-26**(1), 924 (1979).
51. H. H. Stevens, "Neutron Sensors—In-Core," Chap. 3 in *Nuclear Power Reactor Instrumentation Systems Handbook*, TID-25952-P1 (1973).
52. D. P. Bozarth and H. D. Warren, *Trans. Am. Nucl. Soc.* **23**, 517 (1976).
53. H. D. Warren, *Trans. Am. Nucl. Soc.* **23**, 460 (1976).
54. N. P. Goldstein, *IEEE Trans. Nucl. Sci.* **NS-20**(1), 549 (1973).
55. W. Jaschik and W. Seifritz, *Nucl. Sci. Eng.* **53**, 61 (1974).
56. H. D. Warren and N. H. Shah, *Nucl. Sci. Eng.* **54**, 395 (1974).
57. H. D. Warren, *Nucl. Sci. Eng.* **48**, 331 (1972).
58. P. S. Rao and S. C. Misra, *Nucl. Instrum. Meth. Phys. Res.* **A253**, 57 (1986).
59. W. Seifritz, *Nucl. Sci. Eng.* **49**, 358 (1972).
60. J. M. Carpenter, R. F. Fleming, and H. Bozorgmanesh, *Trans. Am. Nucl. Soc.* **22**, 606 (1975).
61. L. A. Banda and B. I. Nappi, *IEEE Trans. Nucl. Sci.* **NS-23**(1), 311 (1976).
62. H. Böck and M. Stimler, *Nucl. Instrum. Meth.* **87**, 299 (1970).
63. H. Böck, *Nucl. Instrum. Meth.* **125**, 327 (1975).
64. J. C. Kroon, F. M. Smith, and R. I. Taylor, *Trans. Am. Nucl. Soc.* **23**, 459 (1976).
65. P. Gebureck, W. Hofmann, W. Jaschik, W. Seifritz, and D. Stegemann, IAEA-SM-168/G-8, p. 783 (1973).
66. R. B. Shields, *IEEE Trans. Nucl. Sci.* **NS-20**(1), 603 (1973).
67. G. F. Lynch, R. B. Shields, and P. G. Coulter, *IEEE Trans. Nucl. Sci.* **NS-24**(1), 692 (1977).
68. N. P. Goldstein, *IEEE Trans. Nucl. Sci.* **NS-25**(1), 292 (1978).
69. N. P. Goldstein, C. L. Chen, and W. H. Todt, *IEEE Trans. Nucl. Sci.* **NS-28**(1), 752 (1981).
70. D. S. Hall, *IEEE Trans. Nucl. Sci.* **NS-29**(1), 646 (1982).
71. P. A. Glasow, *Nucl. Instrum. Meth.* **226**, 17 (1984).

RADIATION DETECTION AND MEASUREMENT 2nd ED.
GLENN F. KNOLL (1989)

CHAPTER · 15

Fast Neutron Detection and Spectroscopy

In Chapter 14 on slow neutron detection, a number of neutron-induced reactions were discussed which can serve as the basis for the conversion of neutrons to directly detectable charged particles. In principle, all these reactions could be applied to detect fast neutrons as well. As shown in the cross-section plot of Fig. 14-1, however, the probability that a neutron will interact by one of these reactions decreases rapidly with increasing neutron energy. As a result, conventional BF_3 tubes have an extremely low detection efficiency for fast neutrons and consequently are almost never used for this purpose. For reasons to be discussed later in this chapter, the ^3He proportional counter is useful both for thermal neutron detection and for fast neutron spectroscopy. As a rule, however, fast neutron devices must employ a modified or completely different detection scheme to yield an instrument with acceptable detection efficiency.

The most important additional conversion process useful for fast neutrons is elastic neutron scattering. In this interaction an incident neutron transfers a portion of its kinetic energy to the scattering nucleus, giving rise to a *recoil nucleus*. The energy that can be transferred from a slow neutron is therefore very small, and the resulting recoil nuclei are too low in energy to generate a usable detector signal. Once the neutron energy reaches the keV range, however, recoil nuclei can be detected directly and assume a large importance for fast neutron detection. By far the most popular target nucleus is hydrogen. The cross section for neutron elastic scattering from hydrogen is quite large and its energy dependence is accurately known. More important, however, is the fact that an incident neutron can transfer up to its entire energy in a single collision with a hydrogen nucleus, whereas only a small fraction can be transferred in collisions with heavy nuclei. Therefore, the resulting *recoil protons* are relatively easy to detect and serve as the basis for a wide variety of fast neutron detectors.

An important distinction in the application of fast neutron detectors is whether or not an attempt is made to measure the energy of the incoming neutron. For all the slow neutron detection methods discussed in Chapter 14, the information on initial neutron kinetic energy is hopelessly lost in the conversion process, because the neutron energy is extremely small compared with the energy liberated in the conversion reaction itself (the Q-value). Once the incoming neutron energy is no longer negligible compared with the reaction Q-value (that means at least 10–100 keV for most of the reactions discussed in

Chapter 14), the energy of the reaction products begins to change appreciably with changes in the neutron energy. An accurate measure of the reaction product energies can then, in principle, be used to deduce the incoming neutron energy. In elastic scattering the reaction Q-value is zero, so that neutron energies can begin to be measured by this technique at the point at which the resulting recoils have measurable kinetic energy. The collection of instruments and techniques applied to the measurement of fast neutron energy is conventionally included in the category of *fast neutron spectroscopy*.

In some instances, however, the purpose of the measurement is simply to record the presence of fast neutrons without a corresponding measurement of their energy. Such fast neutron counters can employ any of the methods discussed to convert neutrons to charged particles, and then simply record all pulses from the detector. Fast neutron counters of this type will have a severe variation in efficiency with neutron energy, but if the incident neutron energy is not likely to change greatly between measurements, they can provide useful information on the relative intensity of a fast neutron flux. Other applications in which the fast neutron spectrum may change considerably between measurements benefit from counters tailored to the application. We begin our discussion of fast neutron devices with counters of this type.

I. COUNTERS BASED ON NEUTRON MODERATION

A. General Considerations

The inherently low detection efficiency for fast neutrons of any slow neutron detector can be somewhat improved by surrounding the detector with a few centimeters of hydrogen-containing moderating material. The incident fast neutron can then lose a fraction of its initial kinetic energy in the moderator before reaching the detector as a lower-energy neutron, for which the detector efficiency is generally higher. By making the moderator thickness greater, the number of collisions in the moderator will tend to increase, leading to a lower value of the most probable energy when the neutron reaches the detector. One would therefore expect the detection efficiency to increase with moderator thickness if that were the only factor under consideration. A second factor, however, tends to decrease the efficiency with increasing moderator thickness: The probability that an incident fast neutron ever reaches the detector will inevitably decrease as the moderator is made thicker. Several effects are at work here, as illustrated in Fig. 15-1. As the detector becomes a smaller and smaller fraction of the total volume of the system, there will be a lower probability that a typical neutron path will intersect the detector before escaping from the surface of the moderator. Furthermore, a neutron may be absorbed within the moderator before it has a chance of reaching the detector. The absorption probability will increase rapidly with increasing moderator thickness because absorption cross sections generally are larger at lower neutron energies.

As a result of all these factors, the efficiency of a moderated slow neutron detector when used with a monoenergetic fast neutron source will show a maximum at a specific moderator thickness. Assuming that the moderator is the usual choice of a hydrogenous material such as polyethylene or paraffin, we find that the optimum thickness will range from a few centimeters for keV neutrons up to several tens of centimeters for neutrons in the MeV energy range.

If the thickness of the moderator is fixed at a fairly large value, the overall counting efficiency of the system versus incident neutron energy will also tend to show a maximum. Low-energy neutrons will not penetrate far enough into the moderator before they are

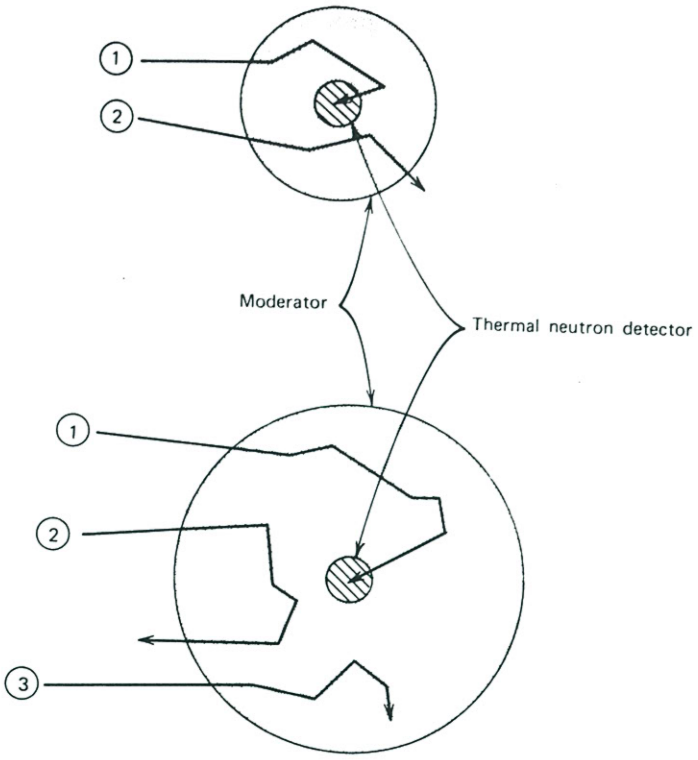

Figure 15-1 Schematic representation of neutron histories in moderated detectors. The small thermal neutron detector at the center is shown surrounded by two different thicknesses of moderator material. Histories labeled ① represent incident fast neutrons that are successfully moderated and detected. Those labeled ② are partially or fully moderated but escape without reaching the detector. History ③ represents those neutrons that are parasitically captured by the moderator. Larger moderators will tend to enhance process ③ while reducing process ②. See text for a discussion of the variation of process ①.

likely to be captured in the moderator itself, whereas high-energy neutrons will not be adequately moderated for efficient detection. By careful choice of the diameter and composition of the moderator–detector system, its overall efficiency versus energy curve can often be shaped and tailored to suit a specific application.

B. The Spherical Dosimeter

In an effort to develop a useful neutron spectrometer, Bramblett, Ewing, and Bonner[1] first investigated the properties of a small lithium iodide scintillator placed at the center of polyethylene moderating spheres of different diameters. The general behavior seen in this type of study is shown in Fig. 15-2. The difference in the shapes and position of the maxima in these response curves serves as the basis for using the set of spheres as a simple neutron spectrometer. By measuring the count rate with each sphere individually, an unfolding process can, in principle, provide some information about the energy distribution of the incident neutrons.[2–5] Because the response functions are rather broad, however, this approach to neutron spectroscopy has received only limited application.

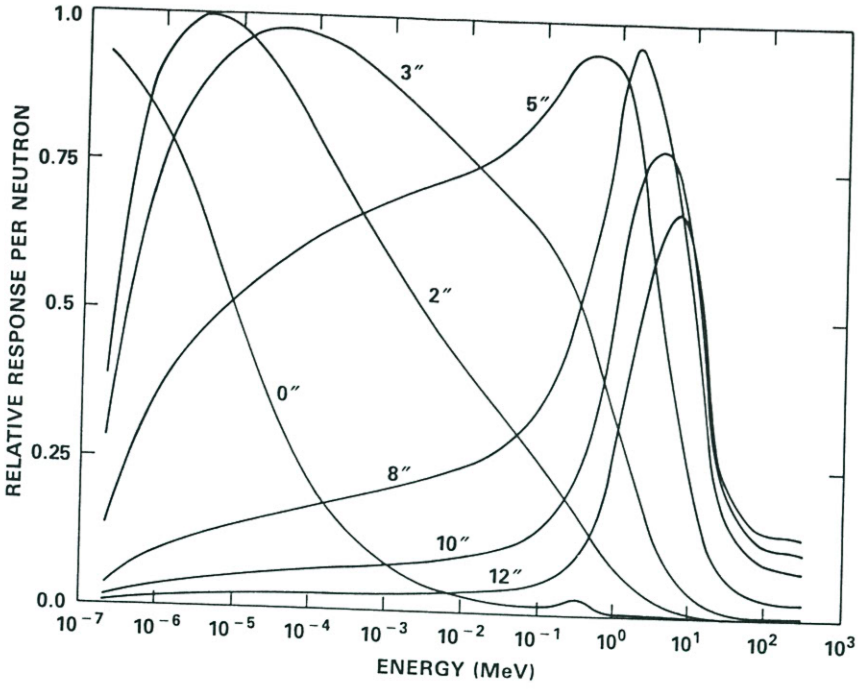

Figure 15-2 The energy dependence of the relative detection efficiencies of Bonner sphere neutron detectors of various diameters up to 12 inches. (From Johnson et al.[5])

A very useful type of counter has emerged from these studies, however. The response curve shown in Fig. 15-2 for the 12 in. sphere turns out to have a similar shape compared with the dose equivalent delivered per neutron as a function of energy. This resemblance is entirely coincidental, in that there is no fundamental relation between the probability of neutron detection at the center of the sphere and the magnitude of the dose delivered by that neutron in a biological medium. Nonetheless, this happy circumstance can be used to good advantage when it is desired to measure the dose equivalent due to neutrons with an unknown or variable energy spectrum. Because of the similarity of the two curves, the efficiency of the detector is high for those neutrons whose biological importance is high and is low for neutrons that deliver less dose. Therefore, the overall count from the detector in a polyenergetic spectrum will automatically include proper weighting factors for all energies and give a meaningful measure of the combined dose due to all the neutrons. The small size (typically 4 mm $\times$ 4 mm) of the LiI scintillator and the relatively high Q-value of the lithium capture reaction for neutrons allow for very effective discrimination against gamma rays, even in relatively large gamma-ray fields. The spherical geometry provides for a reasonably nondirectional detector response. Typical intrinsic efficiency for a 12 in. sphere, defined as the fraction of neutrons that strike the surface of the sphere which ultimately result in a count, is 2.5×10^{-4} at the peak of the 12 in. detector response. Translated into dose, the average response corresponds to about 3×10^{3} counts/mrem. It is virtually the only monitoring instrument that can provide realistic neutron dose estimates over the many decades of neutron energy ranging from thermal energies to the MeV range. However, because the detection mechanism is not fundamentally related to radiation dose, substantial errors can arise when applied to widely different source conditions.[6]

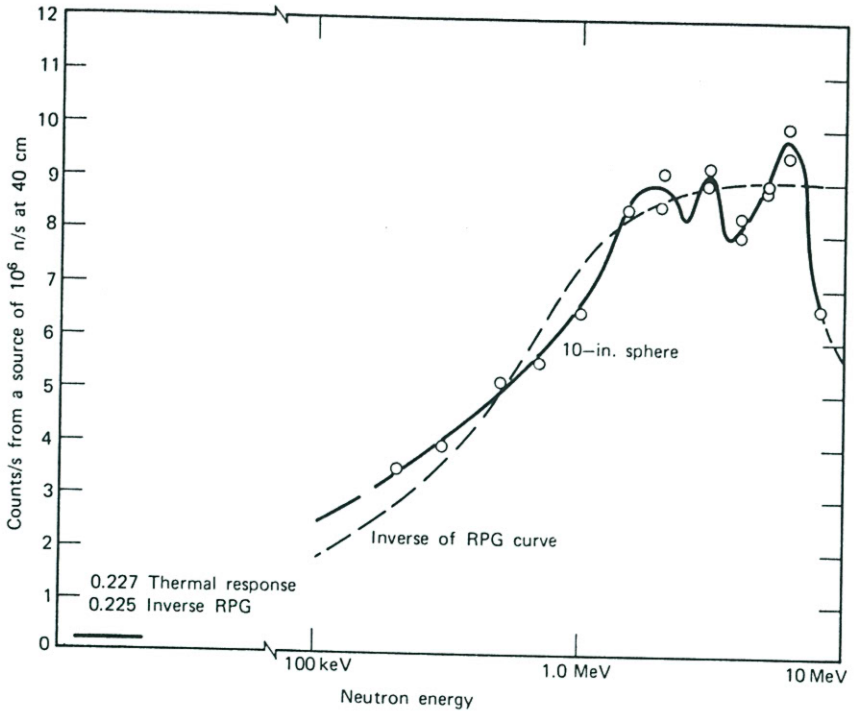

Figure 15-3 Sensitivity of a 10 in. (25.4 cm) diameter moderating sphere surrounding a 4 mm × 4 mm LiI scintillator. Also shown is the relative dose per neutron labeled "inverse of RPG curve." (From Hankins.[11])

These spherical moderator systems are generally known as Bonner spheres after one of the authors (T. W. Bonner) of the original paper describing its experimental investigation.[1] More recent work[7–10] has reexamined the response of spherical moderators used in combination with several different thermal neutron detectors, both experimentally and by neutron transport calculational techniques.

Hankins[11,12] chose to study the response of a 10 in. diameter (25.40 cm) sphere used with a 4 mm × 4 mm lithium iodide scintillator. The moderator size was selected as that likely to give the closest fit between the efficiency and the dose equivalent per incident neutron over a wide range of neutron energy. Figure 15-3 shows the estimated response of the 10 in. sphere detector together with the dose per neutron curve. Obviously, the match is quite good over several decades of neutron energy. Below 100 keV, direct measurements of the detector efficiency are difficult. Hankins[1] has applied a multigroup neutron transport code to calculate the detector response and these results are shown in Fig. 15-4. The calculations confirm the good match between the two curves above 100 keV and at thermal energy but show a sizable deviation in the intermediate energy range between 0.1 eV and 100 keV. The deviation is such as to lead to an overestimate of the neutron dose if the spectrum contains a significant component over this energy range. Although the deviation at 10 keV is as much as a factor of 5, measurements made when the neutron spectrum covers a broad range in energies will show a considerably lower average deviation. Hankins reports that, in a variety of applications, use of the 10 in. instrument leads to a maximum overestimate of the dose of 65%.

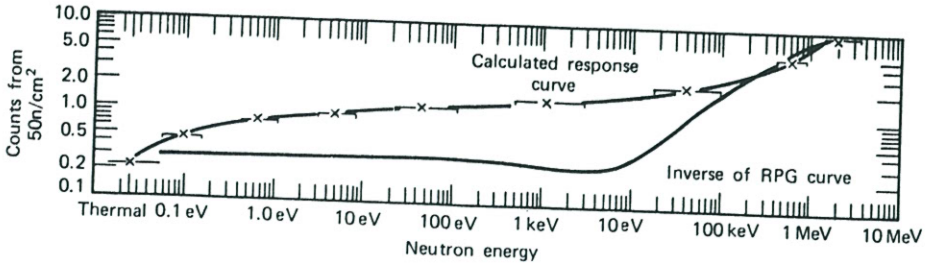

Figure 15-4 Calculated sensitivity of a 10 in. (25.4 cm) diameter moderating sphere, together with the relative dose per neutron (inverse of RPG curve). (From Hankins.[11])

An alternate version of the spherical neutron dosimeter developed by Leake[13] is shown in Fig. 15-5. This design has come to be widely implemented as the Harwell type 95/0075 neutron survey meter. A spherical ^{3}He proportional counter is substituted for the lithium iodide scintillator as the slow neutron detector. This substitution is made to minimize the response of the detector to gamma rays, and Leake reports application of the dosimeter in gamma-ray fields as high as 20 R/h. Used with a simple 20.8 cm diameter polyethylene moderator, the energy response of the system to thermal and epithermal neutrons is higher than ideal. Therefore, a spherical cadmium absorber, perforated with holes, is placed around the ^{3}He detector to shape the response curve. Although the instrument still overresponds to neutrons in the keV energy range (by a factor of 4.9 at 10 keV), the response to broad neutron spectra typical of shielded fission sources does not deviate by more than $\pm 40\%$ for a very wide range of experimental and calculated spectra.[14,15] The response at high neutron energies drops off somewhat; the instrument underestimates the dose from 14 MeV neutrons shielded by concrete by about a factor of 2 (Ref. 14).

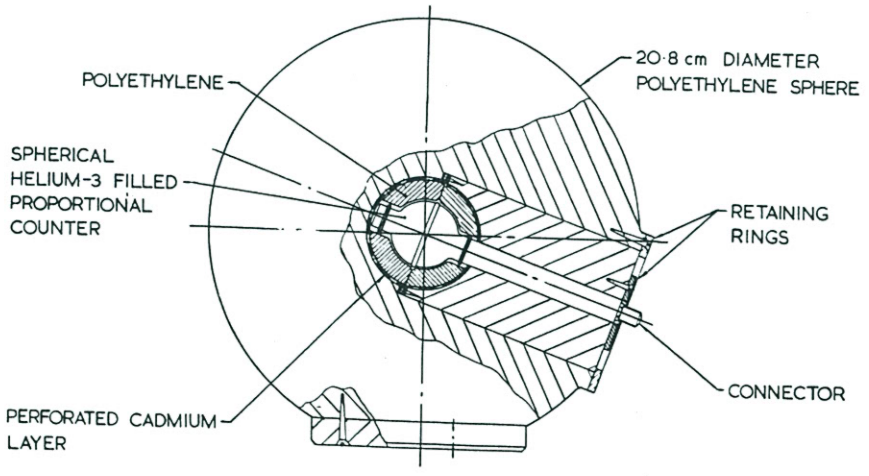

Figure 15-5 A spherical neutron dosimeter based on a ^{3}He neutron detector. (From Leake.[13])

C. The Long Counter

A detector whose counting efficiency does not depend on the neutron energy can be a very useful device in many areas of neutron physics. For an ideal detector of this type, a graph of the detection efficiency versus neutron energy is a horizontal line, which has led to the name *flat response* detectors. Although no real detector exists with a perfectly flat response over the entire range of possible neutron energies, several designs have evolved that come close to this ideal.

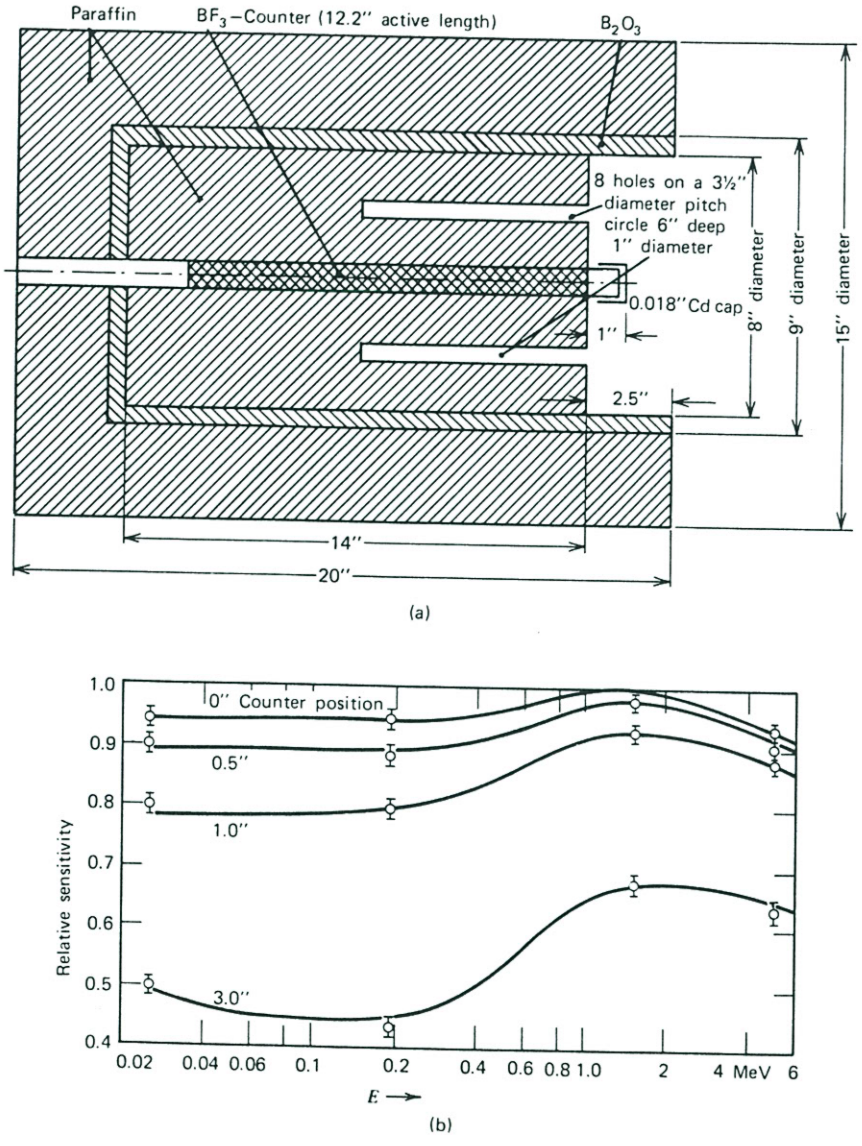

Figure 15-6 (a) Cross-section of the long counter developed by McTaggart. (b) Relative sensitivity of McTaggart long counter versus neutron energy. The parameter varied for the different curves is the distance the end of the BF_3 tube is shifted in from the front of the moderator face. The flattest response occurs when the tube is flush with the front face. (From K. H. Beckurts and K. Wirtz, *Neutron Physics*. Copyright 1964 by Springer-Verlag, Inc. Used with permission.)

Over the years, the most popular flat response neutron detectors has been the *long counter*. Like the spherical neutron dosimeter, it is based on the principle of placing a slow neutron detector at the center of a moderating medium. For the long counter, however, the slow neutron detector is a BF_3 tube, and the system is designed to respond properly to neutrons only when they are incident from a specific direction.

The combination of a BF_3 tube and cylindrical moderator was first suggested as a flat response neutron detector by Hanson and McKibben.[16] A later design by McTaggart[17] is shown in Fig. 15-6a and has achieved fairly widespread acceptance as the standard long counter. The counter is designed to be sensitive only to neutrons incident on the right-hand face of the counter within the boron oxide shell. Those incident from other directions tend to be moderated by the outer annulus of paraffin and are subsequently captured in the boron layer without giving rise to a count. Neutrons incident on the front face parallel to the cylindrical axis will penetrate some distance before undergoing moderation. The average distance of penetration will increase as the neutron energy increases. If the BF_3 tube and cylindrical moderator are sufficiently long, then a typical cross section through the cylinder at the point of moderation will not be different for various energy neutrons. Therefore, the probability that the moderated neutron will find its way to the BF_3 tube and produce a count should not depend strongly on neutron energy. It is this property that leads to the flat energy response of the detector. The holes provided in the front surface prevent a fall-off in the efficiency at neutron energies below 1 MeV by allowing lower-energy neutrons to penetrate farther into the moderator, away from the front surface from which they might otherwise escape. Figure 15-6b shows a plot of the efficiency of a McTaggart long counter versus neutron energy for various axial positions of the BF_3 tube. With the BF_3 tube flush with the front surface, the efficiency does not change by more than 10% over the neutron energy range shown. A long counter of similar design by DePangher and Nichols[18] has also achieved some recognition as a standard in health physics measurements, and documentation of its flat response between about 2 keV and 6 MeV is given in Refs. 19–21.

Long counters derive many of their operational characteristics from the BF_3 tube on which their design is based. Sensitivity to relatively high levels of gamma rays can be

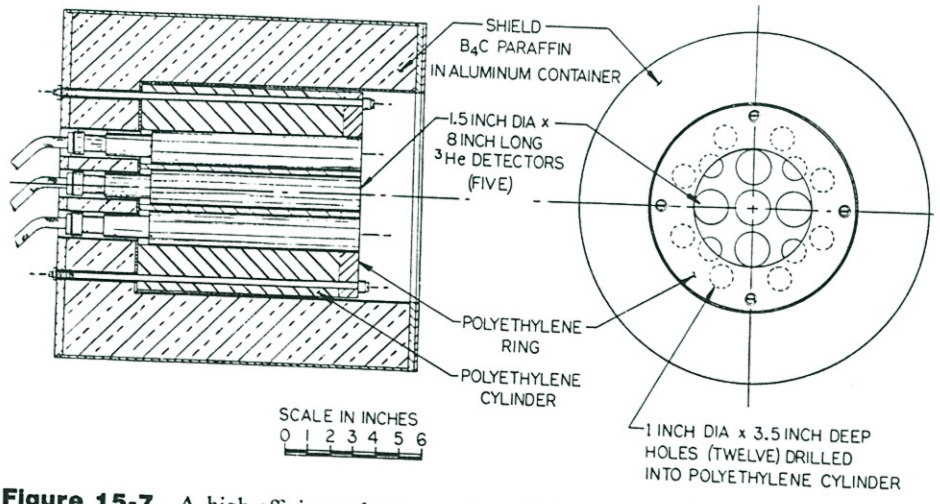

Figure 15-7 A high-efficiency long counter utilizing multiple ^3He tubes. (From East and Walton.[22])

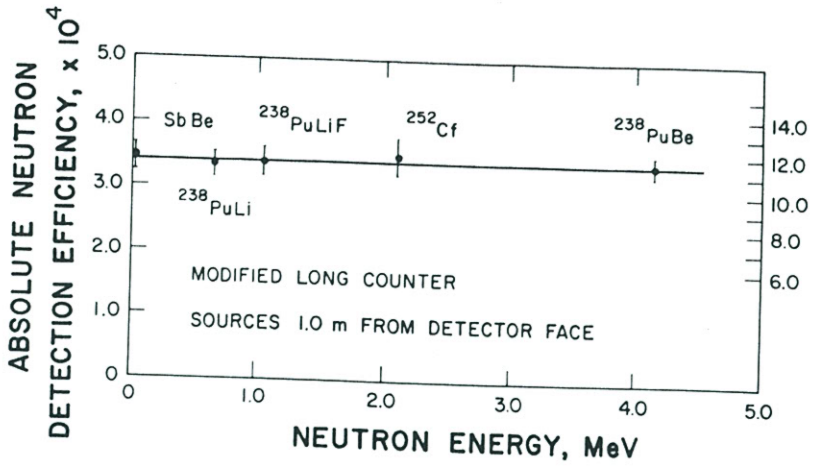

Figure 15-8 Efficiency of the long counter shown in Fig. 15-7 versus the average energy of some neutron sources. The efficiency figures are for a point source located 1 m from the detector face. (From East and Walton.[22])

eliminated by simple amplitude discrimination, while continuing to count all the neutron interactions in the tube. The long counter normally displays good long-term stability and traditionally has achieved widespread application as a neutron flux monitor in a wide variety of neutron physics experiments.

A modified long counter with some improved characteristics has been developed by East and Walton[22] and is shown in Fig. 15-7. It substitutes ^{3}He detectors for the BF_3 tube used in McTaggart design and provides five separate detectors near the center of the cylindrical moderator. By using high-pressure ^{3}He tubes, the multiple detector arrangement leads to a rather high overall neutron detection efficiency of 11.5%, compared with a standard long counter efficiency of about 0.25%. The 12 holes that penetrate the inner polyethylene cylinder are covered on the front face by a 19 mm thick ring of polyethylene to provide a geometry of moderation which best favors an overall flat response. The measured efficiency of this detector is plotted in Fig. 15-8 for a number of neutron sources with broad energy distributions. While the measured efficiency is essentially constant for these sources, greater fluctuation has been observed[23] for more nearly monoenergetic neutrons. These variations can arise because of narrow resonances in the cross sections of some of the constituent materials.

D. Other Detectors Based on Moderation

A number of detection systems have evolved which consist of a spherical assembly into which the neutron source is inserted. This approach can obviously be used for small portable neutron sources and can also be adapted for a highly collimated parallel beam of neutrons by providing a small-diameter entrance channel through which the beam can pass to reach the center of the assembly. A typical design consists of placing multiple ^{3}He or BF_3 counters in a hydrogenous moderator,[24-29] and in some sense is a spherical version of the long counter. Overall counting efficiencies on the order of 1% can be achieved with a response that is flat to within $\pm 1\%$ over a neutron energy range from 30 keV to 5 MeV.[25]

Other flat response detectors that also rely on neutron moderation have been developed. The *grey neutron detector* of Poenitz[30,31] uses a NaI(Tl) scintillator to detect the 2.2 MeV capture gamma rays produced when neutrons are thermalized in a hydrogenous sphere. To provide a faster response, the *black neutron detector* was also introduced,[32] which is based on the light produced in a hydrogenous spherical scintillator as the neutron is moderated. Both types of detector can provide a very flat efficiency curve over several decades of neutron energy.

II. DETECTORS BASED ON FAST NEUTRON-INDUCED REACTIONS

The detectors described in the previous section rely on the slowing down of a fast neutron in a moderating material before its detection as a thermal neutron. The moderating process eliminates all information on the original energy of the fast neutron and normally cannot be used if an attempt is made to extract energy information. Furthermore, the detection process is relatively slow. In most designs, the neutron must undergo multiple collisions with moderator nuclei followed by diffusion as a thermal neutron before the detection signal is generated. As a result, such detectors cannot provide a fast detection signal required in many neutron detection applications.

Both these limitations may be overcome if the fast neutron can be made to induce directly a suitable nuclear reaction without the moderation step. The reaction products will then have a total kinetic energy given by the sum of the incoming neutron kinetic energy and the Q-value of the reaction. Provided the neutron energy is not a hopelessly small fraction of the Q-value, a measurement of the reaction product energies will give the neutron energy by simple subtraction of the Q-value. Additionally, the detection process can potentially be fast because the incoming fast neutron will typically spend no more than a few nanoseconds in the active volume of the detector, and only a single reaction need occur to provide a detector signal. However, the cross sections for typical fast-neutron-induced reactions are orders of magnitude lower than the corresponding thermal neutron cross sections, and such detectors will inevitably show a much lower detection efficiency than their thermal neutron counterparts.

Excluding elastic scattering, which will be the topic of the next section, there are only two reactions of major importance in fast neutron spectroscopy: ^{3}He(n, p), and ^{6}Li(n, α). Both of these reactions were discussed at the beginning of Chapter 14. A plot of the cross-section variation with neutron energy for the fast region is shown in Fig. 15-9. We now emphasize the application of these reactions in neutron spectroscopy, where the neutron energy is inferred by measuring the energy of the reaction products. It should be clear that the same detectors can be used simply to detect the presence of fast neutrons by arranging to count all (or some fixed fraction) of the neutron-induced reactions in the detector. A third reaction, neutron-induced fission, is not of interest in spectroscopy because of the very high Q-value associated with the reaction. The fission process, however, can serve as the basis of a fast neutron counter if energy information is not required.

Finally, a class of fast neutron detectors (called *activation counters*) is based on detecting the radioactivity induced in certain materials. These detectors have proved to be useful when applied to sources producing short pulses of fast neutrons. Because these devices do not produce prompt signals, a discussion of their properties is postponed until Chapter 19.

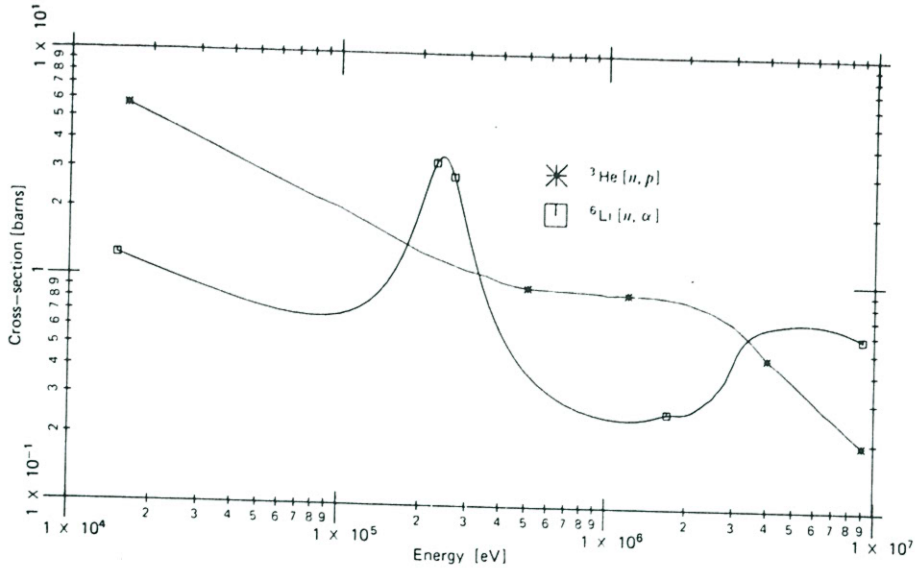

Figure 15-9 The ^{3}He(n, p) and ^{6}Li(n, α) cross sections for the fast neutron region.

A. Methods Based on the ^{6}Li(n, α) Reaction

As seen from Fig. 15-9, the cross section for the ^{6}Li(n, α) reaction drops off rather smoothly with increasing neutron energy, except for the pronounced resonance at a neutron energy of about 250 keV. The relatively large Q-value of 4.78 MeV is an advantage in thermal neutron detection but limits the application in fast neutron spectroscopy to neutrons with energy of at least several hundred keV. A competing reaction, ^{6}Li(n, n′d)^{4}He, has a Q-value of -1.47 MeV and becomes the dominant neutron-induced reaction at energies above about 2.5 MeV. Because this reaction leads to three products, one of which is a neutron that normally escapes, a continuum of deposited energy should be expected even for monoenergetic incident neutrons. Therefore, although it will contribute some neutron pulses, this additional reaction is generally an undesirable part of the response of any detector that attempts to measure the incident neutron energy.

If we neglect the continuum that may be introduced by this latter reaction, the response function of fast neutron detectors based on the lithium reaction should be a single peak located at an energy equal to the neutron energy plus the Q-value of the (n, α) reaction (4.78 MeV). In practical situations, an additional peak is often observed at 4.78 MeV from reactions induced by neutrons whose energy has been reduced to the thermal range by moderation in the laboratory walls, shielding, and any other material in the vicinity of the detector. Unless special care is taken to eliminate those low-energy neutrons, their large interaction cross section will result in many events, all of which deposit the same energy (the reaction Q-value) in the detector. The resulting peak is usually called the *epithermal peak* and can provide a convenient energy calibration point for the detector output.

1. THE LITHIUM IODIDE SCINTILLATOR

The lithium iodide (europium-activated) scintillation crystals discussed in Chapter 14 in connection with thermal neutron detection can also be applied to fast neutron spectroscopy.[33,34] However, the use of this material at room temperature is severely hampered

by its nonlinear response to the tritons and alpha particles produced from the lithium reaction. This nonlinearity results in a resolution of about 40% for the full-energy peak due to incident thermal neutrons. This very broad response function seriously limits the application of LiI(Eu) in fast neutron spectroscopy. It has been shown[35] that the nonlinearities in the crystal response can be substantially reduced by cooling the crystal to liquid nitrogen temperature, which improves the resolution of the full-energy peak to about 20%. The practical problems involved in cooling the crystal are significant, but fast neutron spectra measurements have been reported using this technique.[34]

2. LITHIUM GLASS SCINTILLATORS

Lithium can also be incorporated in other scintillation matrices and used as a fast neutron detector. Because of their relatively poor light output and nonlinearity of response, these scintillators have not been used directly for neutron spectroscopy in the manner described above for lithium iodide scintillators. In neutron time-of-flight spectroscopy, however, the detector need register only the arrival time of a neutron, and various lithium scintillators have evolved for this application. Granular scintillators consisting of mixtures of lithium fluoride and zinc sulfide have been developed[36,37] for time-of-flight use. Lithium-containing glass scintillators have become much more popular in these applications, however, because of the relatively fast response time and large areas that can easily be fabricated. Silicate glasses of various compositions, generally with cerium activation, are used as the scintillation medium.

General characteristics of glass scintillators are described in Refs. 38–42. Table 15-1 lists some properties of commercially available lithium glass scintillators and shows that lithium concentrations of up to 7.7% can be obtained. The low-background properties of NE912 are important for low-level neutron counting and are achieved through the use of materials that are low in natural thorium. In addition to the highly enriched ^{6}Li formulations shown in Table 15-1, equivalent scintillators are also available in which the lithium is present as natural lithium (7.5% ^{6}Li, 92.5% ^{7}Li) or depleted lithium (> 99.9% ^{7}Li). The latter are neutron insensitive and can be used to measure separately the gamma contribution in a mixed neutron–gamma irradiation.

TABLE 15-1 Properties of Some Commercially Available Lithium Glass Scintillators[a]

Manufacturer's Identification[b]	Type NE902	NE905	NE908	NE912
Density (g/cm^3)	2.6	2.48	2.674	2.55
Refractive index	1.58	1.55	1.57	1.55
Melting point (°C)	1200	1200	1200	1200
λ of emission maximum (nm)	395	395	395	397
Light output relative to anthracene	22–34%	20–30%	20%	25%
Decay constant (ns)	75	100	5 + 75	75
Content of Li	2.2 wt %	6.6 wt %	7.5 wt %	7.7 wt %
^{6}Li enrichment	95%	95%	95%	95%
Background α activity per 100 g of glass (/min)	100–200	100–200	100–200	20
Resolution expected for thermal neutrons (depends on glass thickness)	13–22%	15–28%	20–30%	20–30%

[a] Data from McMurray et al.[39]

[b] Commercial identification numbers are those used by Nuclear Enterprises, Ltd. Lithium glass scintillators of similar properties are also available through Koch-Light Laboratories, Ltd.

The time resolution that can be achieved from these detectors depends somewhat on the pulse amplitude distributions produced by the incident neutrons but can be as low as a few nanoseconds. Unfortunately, glass scintillators show a much reduced light output per unit energy for charged particles compared with electrons, and reaction products with 4.78 MeV energy will yield about the same light output as a 1.2 MeV gamma ray. The gamma-ray discrimination ability of these scintillators[43] is therefore not as good as other detectors in which the response is more uniform for all particles. The detection efficiency for thick lithium glasses is of considerable interest in many applications and is difficult to calculate accurately due to the influence of multiple scattering within the glass. Resonances in the scattering cross sections of various materials in the glass lead to sharp peaks in the detection efficiency at neutron energies above about 100 keV.

3. LITHIUM SANDWICH SPECTROMETER

Another way in which the lithium reaction has been widely used to measure fast neutron energies is outlined in Fig. 15-10. A thin layer of lithium fluoride or other lithium-containing material is prepared on a very thin backing and placed between two semiconductor diode detectors. When the neutron energy is low, the two reaction products are oppositely directed, and coincident pulses should be observed from the two semiconductor detectors. Neglecting energy loss of the charged particles before they reach the active volume, the sum of the energy deposited in the two detectors should be equal to the incoming neutron energy plus the Q-value of the lithium reaction.

In practice, complications arise because of the necessity to use finite thicknesses for both the lithium deposit and the backing on which it is supported. Figure 15-10 illustrates that the energy loss in the target materials, which does not contribute to the detected

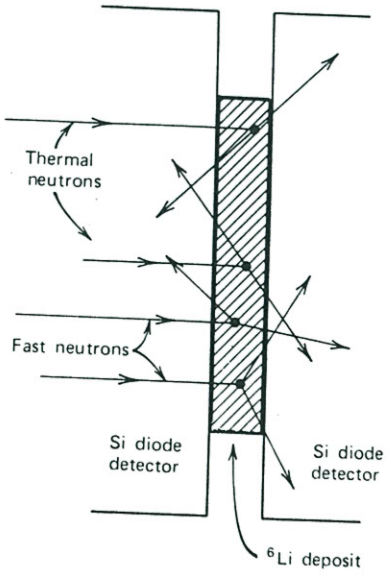

Figure 15-10 Elements of a lithium sandwich spectrometer. Reaction products from thermal neutrons are always oppositely directed, whereas fast neutron interactions will lead to some net forward momentum for the triton and alpha particle. If both are emitted in the forward direction, no coincidence will exist.

signal, will vary as the angle of the emitted reaction products changes through all possible values. Particularly troublesome are those reaction products that are emitted near the plane of the target foil, which will have long pathlengths through the deposit and backing before escaping into the detectors. These energy loss effects can be minimized by making the deposit very thin, but only at the expense of a reduced counting efficiency. Alternatively, the paths near the plane of the foil can be eliminated by geometric collimation between the deposit and detectors, but again, the counting efficiency will be reduced.

The employment of coincidence detection of the two reaction products greatly reduces the background in semiconductor sandwich spectrometers. Any background events that occur only in one detector will automatically be eliminated. If the neutron energy is significant compared with the Q-value, the reaction products must have some momentum in the direction of the incoming neutron and will not be exactly oppositely directed. Then, some fraction of all reactions will lead to two products, both of which strike the same detector and do not give rise to coincidences (see Fig. 15-10). The fraction of neutron events lost to this effect becomes more significant as the neutron energy increases.

Several methods for processing the data from semiconductor sandwich spectrometers have been described. The simplest is to record the sum signal from coincident pulses and deduce the neutron energy by subtracting the Q-value of the reaction. At neutron energies below several hundred keV, this method becomes quite sensitive to small errors and uncertainties. An alternative scheme first proposed by Maroni[44] is based on measuring the difference in energy between the triton and alpha particle. For reaction products that are collinear with the incoming neutron direction, this difference is very sensitive to small changes in neutron energy below about 100 keV. Rickard[45] discusses several other approaches to the analysis of the detector signals which can be advantageous in some applications. General discussions of the application of lithium sandwich detectors in fast neutron spectroscopy can be found in Refs. 46–52.

B. Detectors Based on the ^{3}He(n, p) Reaction

The ^{3}He(n, p) reaction discussed in Chapter 14 has also been widely applied to fast neutron detection and spectroscopy. The fast neutron cross section plotted in Fig. 15-9 falls off continuously with increasing neutron energy. Several competing reactions must be considered in any detector based on this reaction. The most significant of these is simple elastic scattering of the neutrons from helium nuclei. The cross section for elastic scattering is always larger than that for the (n, p) reaction, and this predominance becomes more pronounced as the neutron energy becomes larger. For example, the cross sections are about equal at a neutron energy of 150 keV, but elastic scattering is about three times more probable at 2 MeV. In addition, a competing (n, d) reaction on ^{3}He is possible at neutron energies exceeding 4.3 MeV, but the cross section is low for energies below about 10 MeV. The (n, p) reaction and elastic scattering therefore account for all the important features of ^{3}He detector response for all but the highest neutron energies.

The pulse height spectrum from a detector based on the ^{3}He reaction should show three distinct features. Neglecting the wall effect, the full energy of the reaction products is always totally absorbed within the detector and a spectrum similar to that shown in Fig. 15-11 should be expected. The first feature is a full-energy peak corresponding to all the (n, p) reactions induced directly by the incident neutrons. This peak occurs at an energy equal to the neutron energy plus the Q-value of the reaction. Second, a pulse height continuum results from elastic scattering of the neutron and a partial transfer of its

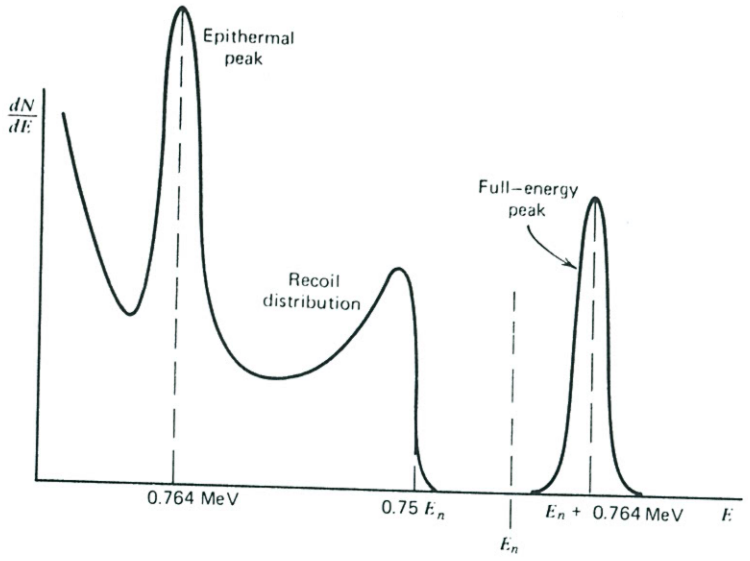

Figure 15-11 Differential energy spectrum of charged particles expected from fast neutrons incident on a ^{3}He detector.

energy to a recoiling helium nucleus. The maximum energy of the continuum can be calculated from Eq. (15-4) (given later in this chapter) and is 75% of the incoming neutron energy for ^{3}He. Third, an epithermal peak appears in virtually every spectrum taken with a ^{3}He detector (as in detectors based on the lithium reaction) and corresponds to the detection of incident neutrons which have been reduced to the thermal range by moderation in external materials. All such neutron interactions deposit an energy equal to the Q-value, or 764 keV.

Wall effects arise whenever the dimensions of the detector are not large compared with the ranges of the secondary particles produced in these reactions. As described in Chapter 14 in connection with BF_3 tubes, the effect on the pulse height spectrum is to fill in the region to the left of the peaks shown in Fig. 15-11.

1. THE ^{3}He PROPORTIONAL COUNTER

If a large ^{3}He-filled proportional counter is irradiated by fast neutrons, a spectrum similar to that shown in Fig. 15-11 will be observed. To minimize the wall effect in smaller counters, several atmospheres of pressure are usually used, and a second component consisting of a heavier gas such as krypton is often added to the ^{3}He to reduce the reaction product ranges. Specific designs and applications of ^{3}He proportional tubes are described in Refs. 53–56.

The undesirable influences of the wall effect and elastic scattering in ^{3}He proportional counters can be ameliorated considerably at the price of added complexity. The additional information carried by the rise time of the output pulses can be used to eliminate a large number of these unwanted events, while retaining virtually all the direct ^{3}He neutron capture events. In any proportional counter, the charge collection time depends on the radial distance at which the ions are formed by the original charged particle. Those tracks that are either very short or parallel to the axis of the proportional tube will generate ions, all of which are collected in about the same time. The corresponding pulse rise time will therefore be small. Tracks that cover a wide range of radii will generate ions

with widely different collection times and pulses with longer rise times. Rejection of the elastically scattered ^{3}He recoils is possible because their specific ionization is greater than protons of the same energy. As a result, recoils have a shorter range and are likely to be limited to a smaller variation in radii per track. They will therefore tend to produce pulses with a shorter rise time than the preferred proton events and can be discriminated on that basis. Because there is some overlap in these rise times, the rejection will also eliminate some true signals and will reduce the overall counting efficiency. With proper selection criteria, it has been possible to reject virtually all recoil events with no more than about a factor of 2 reduction in the (n, p) detection efficiency.[53]

There is also evidence[57] that wall effect pulses have an average rise time considerably slower than that of the full-energy pulses and can also be suppressed by eliminating long rise time events. As a bonus, long rise time rejection will also effectively eliminate gamma-ray background because fast electrons will generally travel completely across the active volume of the tube. More elaborate data recording involving two-dimensional storage of both amplitude and rise time information for each pulse[58] allows for a more selective choice of acceptance parameters but represents a considerable added complexity.

2. THE ^{3}He IONIZATION CHAMBER

Although ^{3}He filled chambers were first developed as proportional counters, there is some advantage in designing such chambers to operate instead as gridded ionization chambers of the type described beginning on p. 154. By avoiding the added fluctuations introduced by avalanche formation, gridded ion chambers can display significantly better pulse height resolution than the equivalent proportional counter. When applied to fast neutron spectroscopy, this advantage translates into superior energy resolution. Some examples of the design and application of ^{3}He ionization chambers are given in Refs. 59–65.

Based on an original design by Shalev and Cuttler,[66] a widely used version of this type of chamber uses a mixture of ^{3}He, argon, and methane at partial pressures of 3, 6, and 0.5 atm, respectively. The predominance of the heavy gas argon reduces the ranges of the reaction products and minimizes the complications of wall and end effects or partial energy loss in the gas. The FWHM of the full-energy peak identified in Fig. 15-11 ranges from about 12 keV for thermal neutrons to 20 keV for incident 1 MeV neutrons.[59] The slow charge collection time and small pulse amplitude from this type of detector create more severe problems compared with proportional tubes. Relatively long shaping times (5–10 μs) are necessary to fully develop the pulse, making such chambers susceptible to microphonic noise and pulse pileup. Sensitive low-noise preamplifiers are also needed to preserve the good energy resolution of the chamber.

3. THE ^{3}He SCINTILLATOR

As described previously in Chapter 8, the noble gases including helium can be used as scintillators. Pure helium has a rather poor light yield, but the addition of xenon with as little as a few percent concentration can enhance the light yield by as much as a factor of 5 (Ref. 67). The emitted light is relatively low in intensity compared with conventional scintillation materials, and appears mostly in the ultraviolet region of the spectrum. It is common to use additives in the gas (such as nitrogen) or wavelength shifting materials (such as *p*-terphenyl) as reflecting layers on the inner surfaces of the scintillation chamber to convert much of the ultraviolet to the visible band. Purity of the gas is very important, since trace amounts of oxygen or organic vapors are known to reduce the light yield significantly.

The decay time of the scintillation is only several nanoseconds, leading to very fast risetime of the output pulse. This advantage in timing compared with ^{3}He proportional or ion chambers is offset by a poorer pulse height resolution. One design[68] has shown a FWHM of 121 keV for the full energy peak from 2.5 MeV neutrons, limited largely by the light collection efficiency variations throughout the volume of the gas. In order to increase the neutron detection efficiency, ^{3}He scintillation chambers have been designed[67] to withstand up to 150 atm pressure.

4. THE ^{3}He SEMICONDUCTOR SANDWICH SPECTROMETER

The configuration of a neutron-sensitive target surrounded on both sides by semiconductor detectors is most commonly used with ^{6}Li as the target. This type of neutron detector was discussed earlier as the lithium semiconductor sandwich spectrometer. Less attention has been given to the use of ^{3}He as the target material, but some potential advantages have spurred efforts in this direction. These advantages can include a considerably higher detection efficiency for equivalent neutron energy resolution and a cross section that is smooth and well known. The gain in efficiency, which can be as much as a factor of 20–50 (Ref. 69) is due mostly to the lower specific energy loss of the proton and triton reaction products in helium compared with that for the alpha particle and recoil triton in lithium targets. Consequently, thicker targets can be used which also can consist of pure elemental ^{3}He. Also from Fig. 15-9, the fast neutron cross section for the ^{3}He reaction is larger than that for the ^{6}Li reaction. Disadvantages include the lower Q-value of the ^{3}He reaction which makes discrimination against gamma rays much more difficult. Furthermore, the larger volume of pressurized helium gas which must be substituted for the solid lithium target makes efficiency calculations more complicated and subject to uncertainties. Descriptions of the design and application of ^{3}He semiconductor sandwich spectrometers can be found in Refs. 69–71.

III. DETECTORS THAT UTILIZE FAST NEUTRON SCATTERING

A. General Properties

The most common method of fast neutron detection is based on elastic scattering of neutrons by light nuclei. The scattering interaction transfers some portion of the neutron kinetic energy to the target nucleus, resulting in a *recoil nucleus*. Because the targets are always light nuclei, this recoil nucleus behaves much like a proton or alpha particle as it loses its energy in the detector medium. Hydrogen, deuterium, and helium are all of interest as target nuclei, but hydrogen is by far the most popular. The recoil nuclei that result from neutron elastic scattering from ordinary hydrogen are called *recoil protons*, and devices based on this neutron interaction are often referred to as *proton recoil detectors*.

The Q-value of elastic scattering is zero because the total kinetic energy after the reaction by definition is the same as the kinetic energy before. For all practical purposes the target nuclei are at rest, and therefore the sum of the kinetic energies of the reaction products (recoil nucleus and scattered neutron) must equal that carried in by the incident neutron. For single scattering in hydrogen, the fraction of the incoming neutron energy that is transferred to the recoil proton can range anywhere between zero and the full neutron energy, so that the average recoil proton has an energy about half that of the original neutron. Therefore, it is usually possible to detect preferentially fast neutrons in the presence of gamma rays or other low-energy background, but the discrimination

becomes more difficult as the incoming neutron energy drops below a few hundred keV. By employing techniques such as pulse shape or rise time discrimination to eliminate gamma-ray-induced events, specialized proton recoil detectors can be used to a neutron energy as low as 1 keV. Recoil methods are insensitive to thermal neutrons except through any competing reactions that might be induced in the target material or other parts of the detector.

1. KINEMATICS OF NEUTRON ELASTIC SCATTERING

We first define some symbols to be used in the equations that follow:

A = mass of target nucleus/neutron mass
E_n = incoming neutron kinetic energy (laboratory system)
E_R = recoil nucleus kinetic energy (laboratory system)
Θ = scattering angle of the neutron in the center-of-mass coordinate system
θ = scattering angle of the recoil nucleus in the lab coordinate system

These definitions are illustrated graphically in Fig. 15-12.

For incoming neutrons with nonrelativistic kinetic energy ($E_n \ll 939$ MeV), conservation of momentum and energy in the center-of-mass coordinate system gives the following relation for the energy of the recoil nucleus:

$$E_R = \frac{2A}{(1+A)^2}(1 - \cos\Theta)E_n \tag{15-1}$$

To convert to the more familiar laboratory coordinate system in which the original target nucleus is at rest, we use the following transformation:

$$\cos\theta = \sqrt{\frac{1 - \cos\Theta}{2}} \tag{15-2}$$

which, when combined with Eq. (15-1), gives the following relation for the recoil nucleus

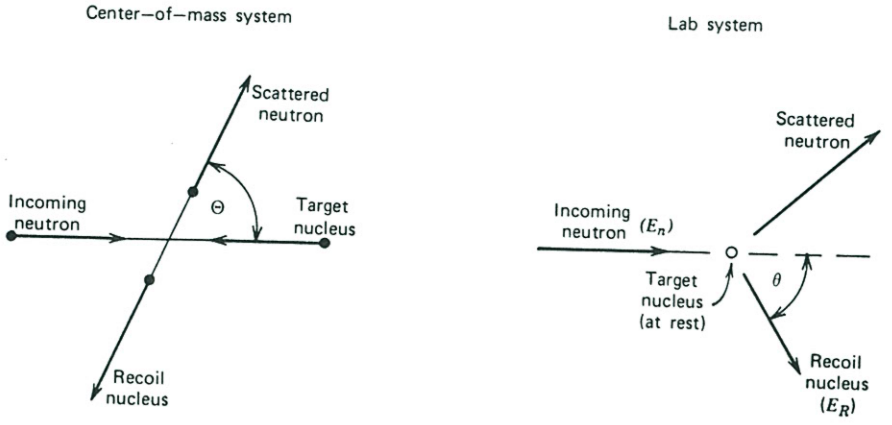

Figure 15-12 Neutron elastic scattering diagrams for the center-of-mass and laboratory coordinate systems.

TABLE 15-2 Maximum Fractional Energy Transfer in Neutron Elastic Scattering

Target Nucleus	A	$\left.\frac{E_R}{E_n}\right\|_{max} = \frac{4A}{(1+A)^2}$
$^{1}_{1}$H	1	1
$^{2}_{1}$H	2	8/9 = 0.889
$^{3}_{2}$He	3	3/4 = 0.750
$^{4}_{2}$He	4	16/25 = 0.640
$^{12}_{6}$C	12	48/169 = 0.284
$^{16}_{8}$O	16	64/289 = 0.221

energy in terms of its own angle of recoil:

$$E_R = \frac{4A}{(1+A)^2}(\cos^2\theta)\,E_n \tag{15-3}$$

From Eq. (15-3) we can see that the energy given to the recoil nucleus is uniquely determined by the scattering angle. For a grazing angle encounter in which the neutron is deflected only slightly, the recoil is emitted almost perpendicular to the incoming neutron direction ($\theta \cong 90°$), and Eq. (15-3) predicts that the recoil energy is near zero. At the other extreme, a head-on collision of the incoming neutron with the target nucleus will lead to a recoil in the same direction ($\theta \cong 0$), resulting in the maximum possible recoil energy,

$$E_R|_{max} = \frac{4A}{(1+A)^2}E_n \tag{15-4}$$

Table 15-2 lists the maximum fraction of the incoming neutron energy that can be transferred to a recoil nucleus in a single collision for a variety of target nuclei. As the target nucleus mass increases, the maximum fractional energy transfer decreases. Only in collisions with ordinary hydrogen can the neutron transfer all its energy in a single encounter. The trend shown in the table explains why only light nuclei are of primary interest in recoil detectors, with hydrogen assuming the predominant role.

2. ENERGY DISTRIBUTION OF RECOIL NUCLEI

We must also be concerned with the way in which the recoil energies are distributed between a minimum of zero and the maximum given in Table 15-2. Because all scattering angles are allowed, in principle, a continuum of possible recoil energies between these extremes should be expected. If we define $\sigma(\Theta)$ as the differential scattering cross section in the center-of-mass system, then, by definition, the probability that the neutron will be scattered into $d\Theta$ about Θ is

$$P(\Theta)\,d\Theta = 2\pi \sin\Theta\, d\Theta \frac{\sigma(\Theta)}{\sigma_s} \tag{15-5}$$

where σ_s is the total scattering cross section integrated over all angles. We are more interested in the distribution in recoil nucleus energy and will let $P(E_R)dE_R$ represent the probability of creating a recoil with energy in dE_R about E_R. Now, because $P(E_R)dE_R =$

$P(\Theta)d\Theta$, it follows that

$$P(E_R) = 2\pi \sin\Theta \frac{\sigma(\Theta)}{\sigma_s} \cdot \frac{d\Theta}{dE_R} \tag{15-6}$$

Now, evaluating $d\Theta/dE_R$ from Eq. (15-1) and substituting, we obtain

$$P(E_R) = \frac{(1+A)^2}{A} \frac{\sigma(\Theta)}{\sigma_s} \cdot \frac{\pi}{E_n} \tag{15-7}$$

Equation (15-7) shows that the shape expected for the recoil energy continuum is just the same as the shape of the differential scattering cross section $\sigma(\Theta)$ as a function of the center-of-mass scattering angle of the neutron. For most target nuclei, the shape of $\sigma(\Theta)$ will tend to be somewhat peaked to favor forward and backward scattering as shown in Fig. 15-13.

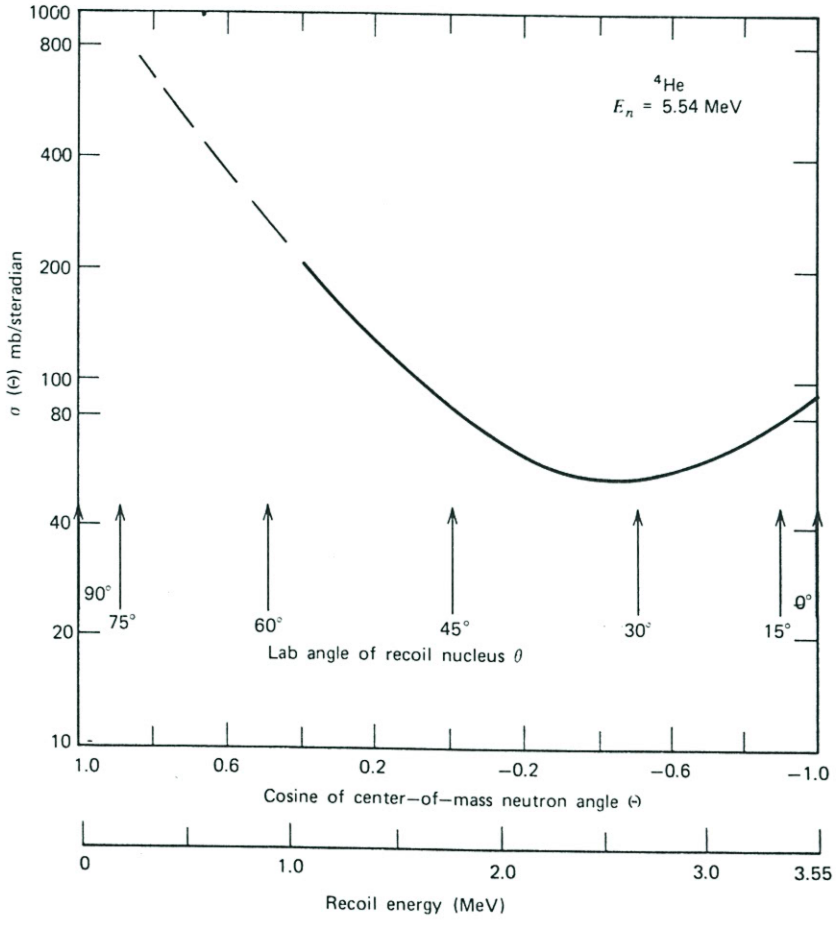

Figure 15-13 The differential scattering cross section of ^{4}He at a neutron energy of 5.54 MeV. Also indicated are the corresponding angle and energy of the helium recoil nucleus in the laboratory system.

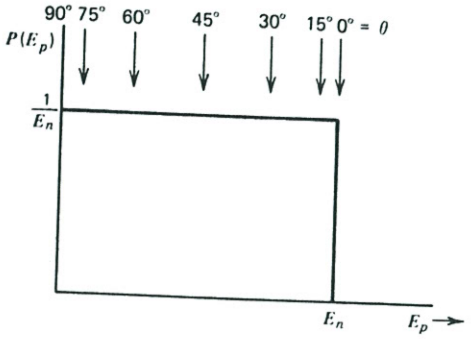

Figure 15-14 Energy distribution of recoil protons produced by monoenergetic neutrons. Recoil energies are indicated for various values of the recoil emission angle θ as given by Eq. (15-3).

A very important simplification holds if the scattering process is *isotropic in the center-of-mass-coordinate system*. Then, $\sigma(\Theta)$ does not change with Θ and is equal to a constant $\sigma_s/4\pi$. This fortunate circumstance is not generally the case but does hold for scattering from hydrogen over most of the energy range of interest ($E_n < 10$ MeV). Because hydrogen is by far the most important target nucleus, the simplifications that result are of real significance. *The expected proton recoil energy distribution is therefore a simple rectangle*, extending from zero to the full incident neutron energy, as sketched in Fig. 15-14. The response function of a detector based on simple hydrogen scattering should therefore have a correspondingly simple rectangular shape. As discussed in the following sections, however, there are a number of complicating factors that can distort this simple rectangular response.

3. DETECTION EFFICIENCY

The detection efficiency of a device based on recoil protons or other recoil nuclei can be calculated from the scattering cross section σ_s. If nuclei of only one species are present in the detector, the intrinsic efficiency is given simply by

$$\epsilon = 1 - \exp(-N\sigma_s d) \tag{15-8a}$$

where N is the number density of target nuclei, σ_s is the scattering cross section for these nuclei, and d is the pathlength through the detector for incident neutrons. Carbon often appears in combination with hydrogen in proton recoil detectors, and competing effects due to carbon scattering must then be taken into account. The counting efficiency, neglecting multiple scattering, is then given by

$$\epsilon = \frac{N_H\sigma_H}{N_H\sigma_H + N_C\sigma_C}\{1 - \exp[-(N_H\sigma_H + N_C\sigma_C)d]\} \tag{15-8b}$$

where the subscripts H and C refer to the separate hydrogen and carbon values for the quantities defined above.

Plots of the scattering cross section for several materials of interest in fast neutron detectors are given in Fig. 15-15. An empirical fit to the hydrogen scattering cross section suggested by Marion and Young[72] is

$$\sigma_s(E_n) = \frac{4.83}{\sqrt{E_n}} - 0.578 \text{ barns} \tag{15-9}$$

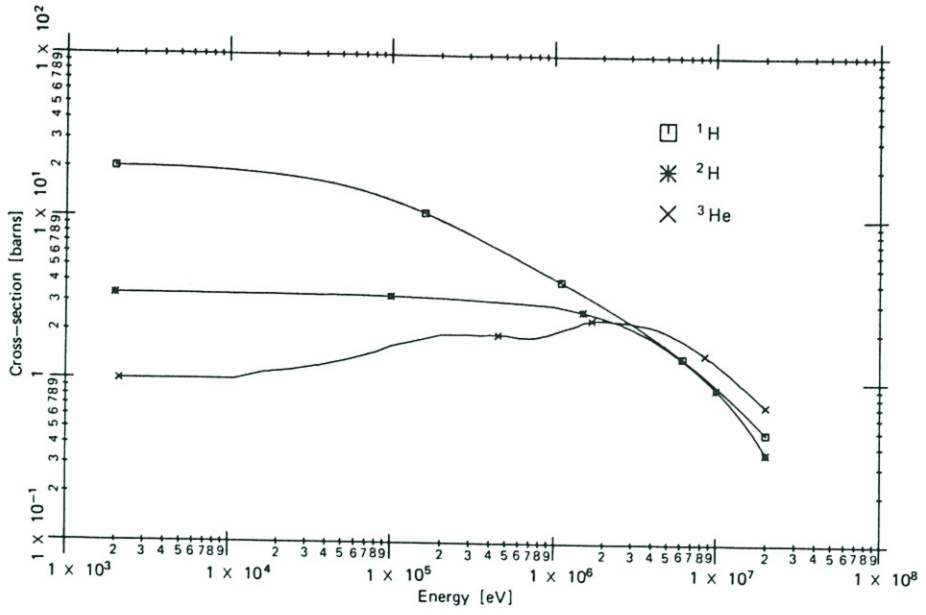

(a)

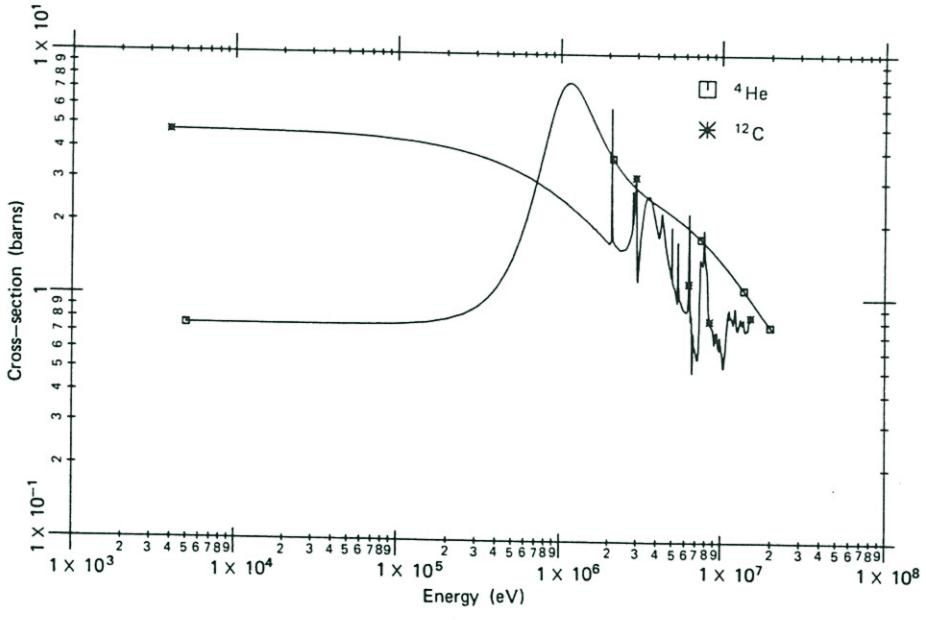

(b)

Figure 15-15 (a) Elastic scattering cross sections for ^{1}H, ^{2}H, and ^{3}He. (b) Elastic scattering cross sections for ^{4}He and ^{12}C.

where E_n is in MeV. This approximation is accurate to within about 3% over the neutron energy range of $0.3 < E_n < 30$ MeV.

B. Proton Recoil Scintillators

One of the easiest ways to use proton recoil in the detection of fast neutrons is through the application of hydrogen-containing scintillators. Fast neutrons incident on the scintillator give rise to recoil protons whose energy distribution should be approximately rectangular, ranging from zero to the full neutron energy. Because the range of the recoil protons is usually small compared with the dimensions of the scintillator, their full energy is deposited in the scintillator and the expected pulse height distribution is also approximately rectangular. Hydrogen-containing scintillation detectors are widely applied in many areas of fast neutron physics research, as indicated in the extensive review by Harvey.[73]

1. SCINTILLATION MATERIALS

Because scintillation materials that contain hydrogen are quite common, there is no shortage of candidates for use as fast neutron scintillators. Successful applications have been reported using organic crystals such as anthracene or stilbene, liquid scintillators that combine an organic scintillant dissolved in a hydrogen-containing organic solvent, and plastic scintillators in which an organic scintillant is incorporated in a bulk matrix of polymerized hydrocarbon. A general discussion of the basic properties of these scintillators can be found in Chapter 8.

Much of the early work in developing proton recoil scintillators was done using crystals of anthracene or stilbene. Anthracene has the largest light output of any organic scintillator, but attention gradually shifted to stilbene because of its superior gamma-ray rejection characteristics. However, both crystals are difficult and expensive to obtain in large sizes (greater than a few centimeters in dimension) and are also subject to damage from thermal and mechanical shock. A further disadvantage stems from the directional variation of the light output from such crystals, which depends on the orientation of the path of the charged particles with respect to the crystal axis. It is not unusual to observe variations as large as 25% as the charged particle orientation is varied. This effect, although not serious if the detector is used only to count neutrons, greatly complicates the job of unfolding an observed pulse height spectrum to derive the incident fast neutron energy spectrum.

Consequently, emphasis has shifted toward the use of liquid and plastic organic scintillators for fast neutron spectroscopy. These materials are relatively inexpensive, can be tailored to a wide variety of sizes and shapes, and are totally nondirectional in their scintillation response. Table 15-3 lists some properties of representative liquid and plastic scintillators that are commercially available and are formulated specifically for use in fast neutron spectroscopy.

For specialized purposes, liquid scintillators are also available with deuterium substituted for the normal hydrogen content. Other formulations based on hexafluorobenzene are totally free of hydrogen and can be used to measure separately the gamma-ray contribution in a mixed fast neutron–gamma-ray field.

2. SCINTILLATOR SIZE

In choosing a size for a recoil proton scintillator, several compromises must be struck. The first involves a trade-off of counting efficiency versus energy resolution. By making the scintillator thick, the efficiency calculated from Eq. (15-8) is obviously enhanced. For

TABLE 15-3 Some Representative Plastic and Liquid Scintillators of Interest as Fast Neutron Detectors[a]

Manufacturer	Identification	Light Output	Decay Constant (ns)	Wavelength of Maximum Emission (nm)	H/C Atomic Ratio	Comments
			PLASTIC			
Nuclear Enterprises, Ltd.	NE 102 A	65% of anthracene	2.4	425	1.104	General applications
Nuclear Enterprises, Ltd.	NE 104	68%	1.8	405	1.099	Fast timing
Nuclear Enterprises, Ltd.	NE 111	55%	1.7	375	1.093	Ultrafast timing (cannot be used in large sizes due to light self-absorption)
Nuclear Enterprises, Ltd.	Pilot B	68%	1.8	408	1.100	General applications
Nuclear Enterprises, Ltd.	Pilot U	67%	1.36	391	1.100	Ultrafast timing
Amperex Electronic Corp.	SPF	55–65%	4	430	1.0	
Koch–Light Laboratories, Ltd.	KL 211	60%	2.2	420	0.992	General applications
Koch–Light Laboratories, Ltd.	KL 236	65%	1.87	410	0.992	Ultrafast timing
			LIQUID			
Nuclear Enterprises, Ltd.	NE 211	78% of anthracene	2.6	425	1.248	General use
Nuclear Enterprises, Ltd.	NE 213	78%	3.7	425	1.213	For pulse shape discrimination against gamma rays
Nuclear Enterprises, Ltd.	NE 228	45%	—	385	2.11	High H/C ratio

[a] For all the plastic scintillators shown, density = 1.03–1.06 g/cm^3; refractive index = 1.58–1.59; and softening temperature = 75–85°C.

example, if the scintillator is made about 5 cm thick in the direction of the neutron path, interaction probabilities of at least 40% will hold for neutrons whose energy is less than 2 or 3 MeV. As the neutron energy increases, the detection efficiency will decrease, and consequently there will be strong motivation to make the scintillator larger. However, it is more difficult to achieve uniform light collection from a large-volume scintillator, and the energy resolution will worsen. Another factor that often limits scintillator size is the pulse rate due to gamma rays interacting within the detector. In many applications, this rate exceeds that from fast neutrons, and the scintillator must be kept sufficiently small so that the pileup of gamma-ray events is not a problem.

If the scintillator is used as a fast neutron spectrometer, other factors enter into the choice of size. In small crystals, a typical neutron is likely to scatter only once, and the energy spectrum of proton recoils will closely approximate the rectangular distribution discussed earlier. As long as the scintillator dimensions are larger than a few millimeters, escape of protons from the surface is unlikely, and the response function of the detector is simple and easily calculated. As the detector dimensions are increased, multiple scattering of the neutrons becomes more likely and the response function is more complicated and harder to predict. Because an accurate knowledge of the response function is critical for the unfolding process, one would like to keep the scintillator small so that these complicating effects do not introduce large uncertainties.

3. RESPONSE FUNCTION

For that subset of detectors for which the rectangular response function is a reasonable approximation, the task of deriving the incident neutron energy spectrum is particularly simple. Because the derivative with respect to energy of a rectangular distribution is zero everywhere except at the maximum, the derivative of the recoil proton spectrum will give a narrow peak located at the incident neutron energy. The derivative of the spectrum recorded from a complex source therefore gives an easily calculated representation of the incident neutron spectrum.

For response functions that are more complex, the general techniques of deconvolution or unfolding, discussed in Chapter 18, must be applied. Representative examples of the application of unfolding methods to the neutron response of organic scintillators are given in Refs. 74–77. Because of their complexity, unfolding calculations of this type are inevitably cast in the form of large computer codes.[78,79] An accurate knowledge of the detector response function is a necessary input to all these unfolding methods. We therefore list some of the factors that distort the simple rectangular distribution in organic scintillators and show the qualitative effect on the response function.

a. Nonlinear Light Output with Energy

As discussed in Chapter 8, the light output from most organic scintillators does not increase linearly as the deposited energy increases. This nonlinear behavior distorts the expected rectangular proton energy distribution of Fig. 15-16c into the pulse height distribution shape sketched in Fig. 15-16d. For many organic scintillators, the light output H is approximately proportional to $E^{3/2}$, in which case

$$H = kE^{3/2} \tag{15-10}$$

and the pulse height distribution shape is given by

$$\frac{dN}{dH} = \frac{dN/dE}{dH/dE} = \frac{\text{constant}}{\frac{3}{2}kE^{1/2}} = k'H^{-1/3} \tag{15-11}$$

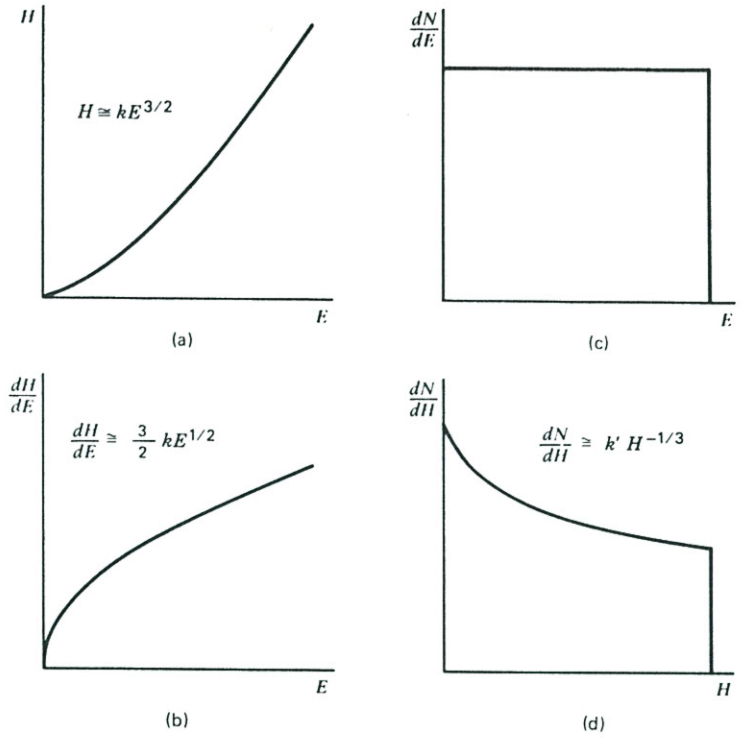

Figure 15-16 Part (a) shows a plot of pulse height versus energy for a typical organic scintillator. This nonlinear response leads to a distortion of the rectangular proton recoil spectrum of part (c) into the spectrum shown in part (d).

where k and k' are proportionality constants. This relation is only an approximation to the actual distortion caused by the nonlinearity, and a more detailed description of the light output versus energy is required as a basis for accurate spectrum unfolding.[80]

b. Edge Effect

If the scintillator is sufficiently small or the neutron energy very high so that the range of the recoil protons is not small compared with detector dimensions, some effects can be expected due to escape of protons from the surface of the scintillator. The event is not lost but simply shifted to an energy lower than would normally have been observed. The effect on the response function will be to shift events from high pulse height to low pulse height, further increasing the slope of Fig. 15-16d.

c. Multiple Scattering from Hydrogen

For detectors that are not small, it is possible for an incident neutron to scatter more than once from hydrogen nuclei before escaping from the scintillator. Because all such events normally occur within a very short period of time compared with the scintillation decay time, the light from all recoil protons is summed and a pulse produced whose amplitude is proportional to the total light output. Multiple scattering will therefore increase the average pulse height and change the expected response function by adding events at large pulse heights at the expense of those at lower amplitudes.

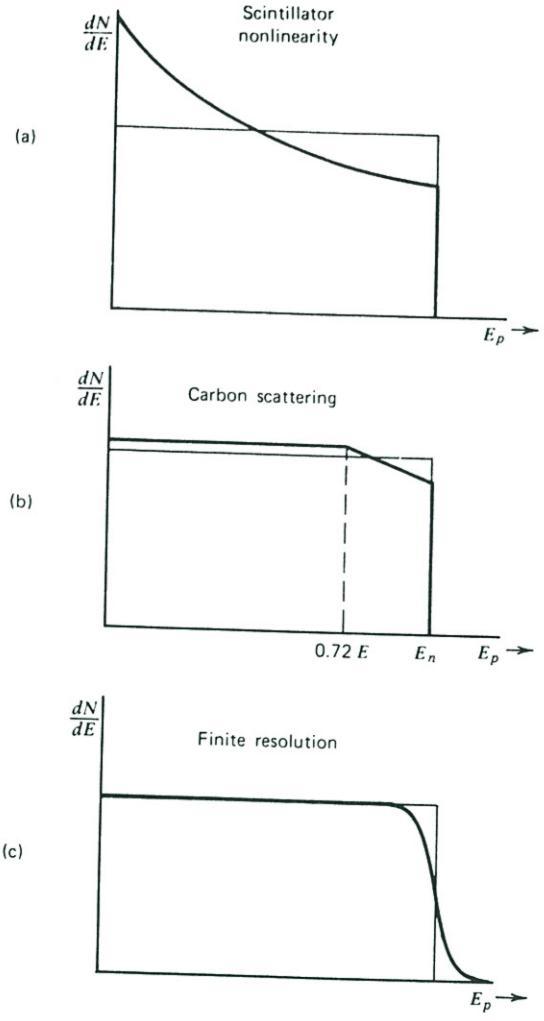

Figure 15-17 Distortions to the rectangular recoil proton energy spectrum due to three separate factors.

d. Scattering from Carbon

All organic scintillators contain carbon as well as hydrogen. Because of the decreased scintillation efficiency for high dE/dx particles, carbon recoils produced by neutron elastic scattering do not contribute much to the detector output. However, scattering from carbon does affect the detector response function indirectly in that the scattered neutrons may still undergo a hydrogen scattering before escaping from the scintillator. Because the neutron energy has been decreased in the initial carbon scatter, the proton recoil spectrum produced from carbon-scattered neutrons will not extend to as high an energy as that from unscattered neutrons. Because the incident neutron can lose between 0 and 28% of its initial energy in a carbon scattering, the maximum energy of a subsequent recoil proton will vary between 100 and 72% of the original energy. The corresponding effect on the detector response function is shown in Fig. 15-17b.

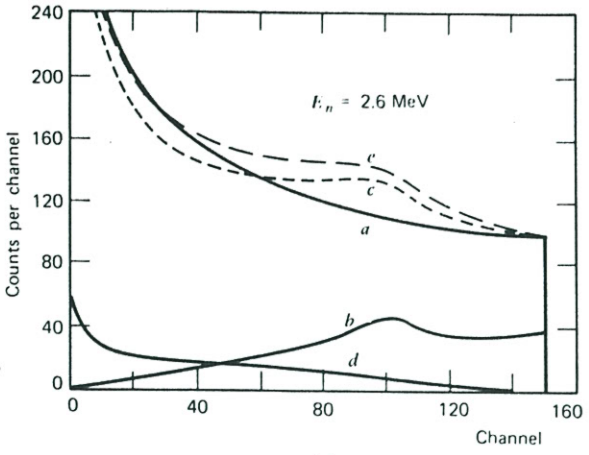

(a)

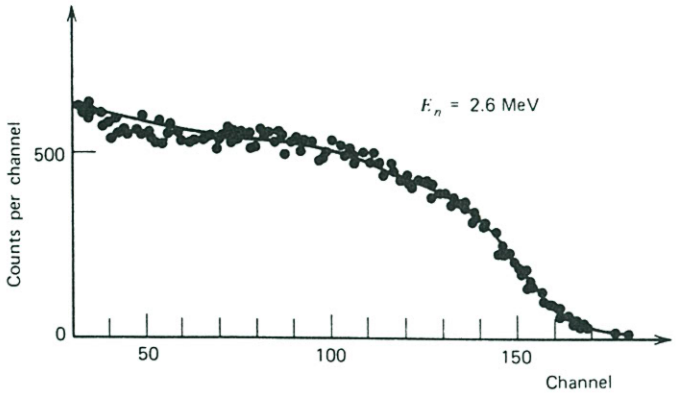

(b)

Figure 15-18 (a) Calculated response function at 2.6 MeV (for perfect detector resolution) for a 2.54 cm × 2.54 cm cylindrical stilbene crystal. Separate components shown are: *a*—single scattering with detector nonlinearity and edge effects; *b*—double scattering from hydrogen; *c*—single plus double scattering from hydrogen; *d*—proton recoils from carbon-scattered neutrons; *e*—composite spectrum. (b) Measured pulse height spectrum at 2.6 MeV for the same crystal included in the calculation of part (a). The added influence of imperfect detector resolution is evident. (From Bormann et al.[81])

e. Detector Resolution

The discussion to this point has dealt with ideal detector response without considering the spread introduced by nonuniform light collection, photoelectron statistics, and other sources of noise. These sources of dispersion will tend to wash out some of the distinct structure expected in the response function, as illustrated in Fig. 15-17c.

f. Overall Response Function

The manner in which all these distorting effects combine to give the overall detector response function is illustrated in Fig. 15-18, for a 2.54 × 2.54 cm cylindrical stilbene crystal at a neutron energy of 2.6 MeV. This example is fairly typical of any organic or

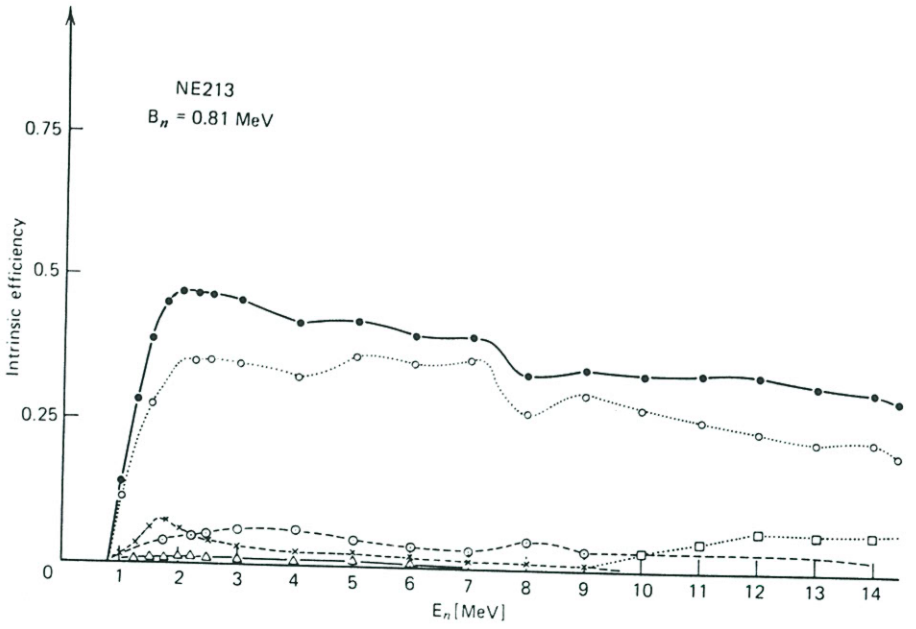

Figure 15-19 The calculated efficiency of a NE213 liquid scintillator (1.9 cm radius, 10 cm length) for a discrimination level of 0.81 MeV. Identification of the symbols is as follows: ● combined efficiency from all processes; ○ single hydrogen scattering; × n-H, n-H double scattering; ⊙ n-C, n-H double scattering; △ n-C, n-H, n-H triple scattering; □ (n, α) and (n, n′)3α reactions. (From Hermsdorf et al.[82])

plastic scintillator response to neutrons whose energy lies below the threshold of competing reactions discussed in the following section.

g. Competing Reactions at High Neutron Energies

Once the neutron energy exceeds 8 or 9 MeV, two competing reactions must be considered in the overall response of organic scintillators:

	Neutron Energy at Threshold
$^{12}C(n, \alpha)^{9}Be$	6.17 MeV
$^{12}C(n, n')3\alpha$	7.98 MeV

The combined effects of multiple scattering and the competing reactions can be seen in Fig. 15-19, which plots the counting efficiency of a liquid organic scintillator versus neutron energy. In the figure, the competing reactions $^{12}C(n, \alpha)$ and $^{12}C(n, n')3\alpha$ are seen to contribute to the detection efficiency at high neutron energies. The threshold energies for these reactions are 6.17 and 7.98 MeV, but they become significant only above about 9 MeV. An inhibiting factor is the lower light output per unit energy that most organic scintillators exhibit for alpha particles compared to recoil protons.

4. DETECTOR COUNTING EFFICIENCY VERSUS DISCRIMINATOR BIAS LEVEL

A common mode of application of proton recoil detectors is to set a fixed discrimination level to eliminate all pulse amplitudes below a given size. Some finite discrimination level is always required to eliminate inevitable noise pulses that arise spontaneously in the

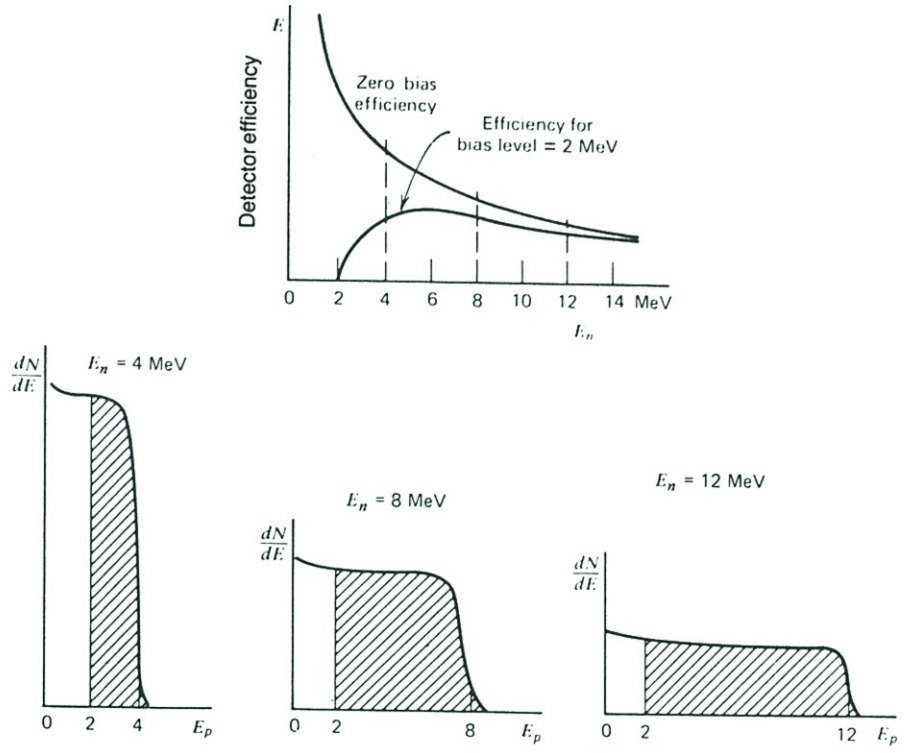

Figure 15-20 The effect of discrimination level on proton recoil detector efficiency. The upper graph gives both the zero bias efficiency and the reduced efficiency when a discrimination level corresponding to a proton energy of 2 MeV is used. See text for further elaboration.

counting system, but gamma rays and other background events may dictate discrimination at a substantially higher level. Because the proton recoil energy distribution extends all the way to zero, some recoil events will inevitably be eliminated in the discrimination process. Therefore, the efficiency assuming that all pulses are counted is sometimes called the *zero bias* efficiency, and a real detector with a finite discrimination level will always have a somewhat lower efficiency, particularly at lower neutron energies.

The effect of discrimination level on counting efficiency is shown graphically in Fig. 15-20. Sketched along the bottom of the figure are three differential pulse height spectra representing the response of a scintillator to three different neutron energies. Neglecting more complex interactions, the total area under each of these curves is proportional to the number of neutron–hydrogen scattering events in the detector at that energy. This number is proportional to the zero bias efficiency, shown plotted versus neutron energy at the top of the figure.

When a discriminator is used, that area under the differential spectrum which lies to the right of the discrimination level is proportional to the number of recorded counts. For the example shown, this reduced efficiency is also plotted versus neutron energy on the upper graph. This efficiency obviously drops to zero for neutron energies below the discrimination level and approaches the zero bias efficiency at neutron energies that are large by comparison. More detailed analyses of detection efficiency of organic scintillators can be found in Refs. 83–91.

5. ENERGY CALIBRATION WITH GAMMA RAYS

The light output of organic scintillators for electrons is always higher per unit energy than for heavy charged particles. Therefore, the problem of gamma discrimination is made more severe because it may require a neutron with energy of 2 or 3 MeV to give the same light output as a 1 MeV gamma ray. The low Z value of the constituents of organic scintillators (hydrogen, carbon, and perhaps oxygen) results in a very low photoelectric cross section, so that virtually all gamma-ray interactions are Compton scatterings. A gamma-ray spectrum taken with an organic scintillator will therefore show no photopeaks, and Compton edges are the only distinguishable features. Because the scintillation response to electrons is fairly linear, a gamma-ray source is often used to calibrate the energy scale of the detector output. Because there are no photopeaks, some point on the Compton edge must be selected and associated with the maximum energy of a Compton recoil electron. Details of the shape of the Compton continuum and the effects of detector resolution have led Flynn[92] to suggest a standard procedure in which the channel number at which the Compton continuum has fallen to half its plateau value is associated with an energy equal to 104% of the maximum Compton electron energy. A more detailed procedure that takes into account variability of the detector resolution is described in Ref. 93.

6. PULSE SHAPE DISCRIMINATION AGAINST GAMMA RAYS

As discussed in Chapter 8, the relative intensity of the fast and slow components of the light yield of some organic scintillators depends on the specific ionization of the ionizing particle (see Fig. 8-5). Therefore, particles of different mass or charge will produce signal pulses with different time characteristics. Specifically, gamma-ray-induced fast electrons generate a larger fraction of their scintillation light in the prompt component as compared with recoil protons. The methods of pulse shape discrimination discussed in Chapter 17 can be very effective in rejecting gamma-ray pulses from organic scintillators, while retaining reasonable fast neutron efficiency.[94–100]

If the gamma-ray pulses are not simply rejected but instead are analyzed in a separate spectrum, simultaneous spectroscopy on both neutrons and gamma rays can be carried out. Because of the lack of full-energy gamma-ray peaks, the gamma-ray spectra must be unfolded using the same type of computation as is applied to the neutron spectrum. Both calculated[101,102] and measured[103] response functions to gamma rays for NE213 liquid scintillator have been published and can be used as input to the unfolding codes.

C. Gas Recoil Proportional Counters

1. GENERAL

As an alternative to the organic scintillator, gas proportional counters can also be used to measure fast neutrons through the recoil process. In these applications, the fill gas is usually hydrogen, a hydrogen-containing gas such as methane, or some other low-Z gas such as helium. In the case of hydrogen, the expected proton recoil spectrum should again be the simple rectangular shape described earlier. As in the case of organic scintillators, however, complicating effects often arise which distort this simple response function and make the task of unfolding observed pulse height spectra a great deal more complicated.

Because the detection medium is a gas, recoil proportional counters inevitably have a lower counting efficiency than typical organic scintillators. Equation (15-8) can again be used to estimate the neutron detection efficiency for simple hydrogen-filled counters, and typical values for neutrons in the MeV energy range will be less than 1%. This reduced

interaction probability is not entirely lacking some compensating advantages. For example, the interaction probability for scattered neutrons will also be quite low, and thus the response function of gas detectors will be largely free of the multiple scattering complications discussed earlier for scintillators.

Recoil proportional counters are undoubtedly more sensitive detectors than organic scintillators. As discussed in Chapter 6, purity of the fill gas is of utmost importance and microscopic air leaks will ultimately lead to detector failure. Although recoil proportional counters are commercially available, there is a common tendency for experimenters to design their own counters specifically tailored to the application required. The reader should note that considerable attention to construction details such as surface preparation, high vacuum pumping before gas filling, and high voltage insulator design are necessary to have a successful detector. By comparison, scintillators are relatively easy to assemble and operate. The fact that recoil proportional counters are not large compared with the range of recoil nuclei in a gas means that the correction for wall and end effects, usually quite small in scintillators, becomes an important consideration in determining the response of these detectors. An extensive review of response functions for recoil proportional counters of different designs is given in Ref. 104.

2. GAMMA-RAY SENSITIVITY AND PULSE SHAPE DISCRIMINATION

Another consequence of the low-density gas detection medium is the behavior of the detector in the presence of gamma rays. Typical recoil scintillators will have dimensions that are large with respect to both the recoil nuclei produced by neutron interactions as well as to fast electrons created in gamma-ray interactions. Therefore, the full energy of each is almost always deposited within the detector active volume. Gas proportional counters, on the other hand, are often of a size that is not extremely large compared with recoil nuclei ranges, and usually they are much smaller than the range of gamma-ray-produced electrons. Therefore, it is likely that neutron-induced events deposit all their energy in the gas, whereas gamma rays will deposit only a small part of their energy. Furthermore, the inherent response of organic scintillators is such that the light output may be as much as a factor of 2 or 3 times greater for electrons than for charged particles of the same energy. This extreme variation in response does not exist in proportional counters, in which the energy expended to create one ion pair changes only slightly with the nature of the ionizing particle.

A difference that works to the disfavor of the proportional counter is the nature of gamma-ray interactions in the detector.[105] For the organic scintillator, both neutrons and gamma rays must interact within the scintillator volume in order to give rise to detected pulses. In the gas counter, neutrons must interact within the fill gas, but gamma rays may interact either in the gas or, more likely, in the walls and other construction materials of the counter, leading to secondary electrons that can escape into the gas volume. Therefore, if the fill gas of a recoil proportional counter with the same elemental composition as that for an organic scintillator is chosen, one would expect a considerably larger ratio in the number of gamma rays to neutron pulses in the proportional counter compared with the organic scintillator. In the proportional counter, however, the average gamma-ray pulse amplitude would be considerably smaller.

As in all proportional counters, the rise time of observed signal pulses depends primarily on the radial distribution of the ionization track that gives rise to that signal pulse. As discussed for ^{3}He tubes, this property can be used to count preferentially neutron-induced events in the presence of potentially interfering gamma radiation. Provided the neutron energy is fairly low, proton recoil tracks will tend to be rather short

and consequently will be confined to a limited range in radius. Gamma-ray-induced fast electrons will almost always pass completely through the gas and, on the average, involve a much greater range of radii in the tube. As a result, neutron-induced pulses will tend to have shorter rise times than those induced by gamma rays, and pulse shape discrimination methods will serve to differentiate between the two. Extension of the proton recoil technique in proportional counters down to a neutron energy as low as 1 keV, as pioneered by Bennett,[106] is critically dependent on elimination of the majority of the gamma-ray pulses by this method.

3. COUNTER DESIGN AND CHOICE OF FILL GAS

Although some results have been reported for spherically shaped chambers,[107,108] the majority of recoil proportional counter designs incorporate cylindrical geometry similar to that discussed in Chapter 6 and illustrated in Fig. 6-5. As in all proportional counters, the axial anode wire must be of very uniform and small diameter to ensure uniform gas multiplication along its length. The field tubes at either end of the anode wire are common devices used to abruptly terminate the region in which gas multiplication can occur, so that the active volume of the counter is well defined. Nonetheless, there remains some nonuniformity (sometimes called the *tip effect*) due to the curvature of the electric field lines at the point of discontinuity between the field tube and anode wire. Bennett and Yule[109,110] report that the electric field distortions can be minimized by reducing the outer diameter of the cathode in these regions. Nonetheless, the distortion of the electric field in the end regions of the tube remains one of the important complicating factors that must be considered in analyzing the efficiency and response function of the detector.

By far the majority of all recoil detectors utilize hydrogen or some compound of hydrogen to make use of recoil protons produced by neutron elastic scattering. The simple rectangular energy distribution for proton recoils illustrated in Fig. 15-14 is distorted by several important effects in proportional counters. The most important of these is the effect of the finite size of the active volume of the chamber which leads to proton tracks that are truncated either in the walls or end of the tube. There are several approaches to this problem. One is simply to live with these losses and either attempt to calculate or measure their effects on the overall detector response function. Reasonably good success has been achieved with this approach under some circumstances,[111–113] but it would clearly be preferable to eliminate these events as much as possible. If those proton tracks that leave the active volume can be identified and discarded, a much simpler response function will result. A track that leaves the active volume at the cylindrical cathode can be recognized if a somewhat more complex chamber is constructed, in which the cathode consists of a cage of fine wire so that the proton can pass through and continue to produce ionization outside the cathode. A ring of counters around the central region can be used to detect this leaked ionization and thus to reject the original event by anticoincidence. Such a chamber has been described by Heiberg,[114] in which losses to the ends of the tubes were also eliminated through the use of signals derived from the field tubes. Tracks that overlap the active volume and end region of the tube will give coincident pulses on both the anode and field tubes and therefore can also be rejected through anticoincidence.

Although hydrogen is in many ways the ideal target for neutron scattering, its use as a fill gas in proportional counters is limited by its low density and relatively low stopping power for recoil protons. Methane is a more common choice, but complicating effects introduced by the carbon nuclei must then be taken into account. It has been estimated[109] that carbon ions will create approximately 75% as much ionization in the gas as the

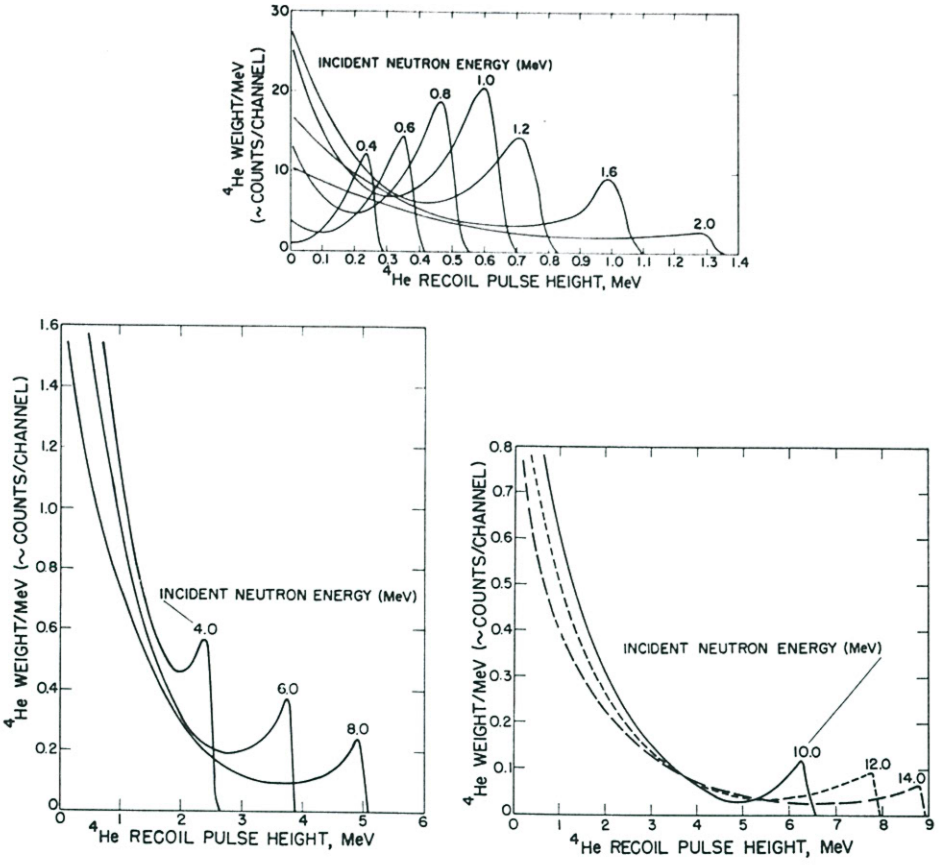

Figure 15-21 Calculated pulse height spectra for a recoil proportional counter filled with ^{4}He at 8 atm pressure. (From Atwater.[115])

equivalent energy proton. Because the maximum energy of a carbon ion is 28% of the neutron energy, we would then expect that all carbon recoil pulses should lie below about 21% of the maximum proton recoil pulse amplitude. Helium is also widely used as a fill gas, and typical recoil spectra are shown in Fig. 15-21. Because elastic scattering from helium is not isotropic in the center-of-mass system (see Fig. 15-13), these distributions will not be rectangular even in the absence of complicating effects.

4. ENERGY CALIBRATION AND LINEARITY

Because sources of monoenergetic neutrons are not commonly available, the energy calibration of a proton recoil proportional counter is not a straightforward process. Gamma rays cannot be used as previously described in the calibration of proton recoil scintillators because the secondary electrons created in gamma ray interactions generally cannot be stopped in the fill gas. One possible method is to incorporate a small amount of ^{3}He into the fill gas so that, when irradiated with thermal neutrons, proton and triton pairs sharing 764 keV kinetic energy (see p. 485) are generated internally. The corresponding peak in the recorded spectrum then provides an energy marker. Although this technique has proven very useful, errors in the calibration can result[116] because one of these particles is not a proton. Differences then can arise that are related to differences in

the energy required to form an ion pair or due to disparities in the particle ranges. At low energies, the addition of a small amount of radioactive ^{37}Ar will result in a peak from the 2.82 keV X-rays that are emitted in its decay.[112] This approach has the disadvantage that the calibration peak is present in all measurements and may interfere with an interesting region of the spectrum. The calibration is also sensitive to potentially large differences in the energy loss behavior of the low energy photoelectrons generated by the X-rays compared with the recoil protons of interest.

Above about 10 keV, there seems to be little doubt that the ionization produced by recoil protons in standard proportional counters is essentially linear with the proton recoil energy. Stated another way, the W-value (defined as the energy expended per ion pair produced) in hydrogen is a constant for protons above 10 keV. Below this energy, however, there is evidence[117] that the value of W falls off and may be as low as about 70% of its high-energy value at a proton energy of 1 keV. These nonlinearities in the relation between energy and ionization must obviously be taken into account when unfolding the detector response to low-energy neutrons.

D. Proton Recoil Telescopes

In conventional organic scintillators or recoil proportional counters, one has little choice but to accept all angles of neutron scattering as they occur. Therefore, the response function of these detectors to monoenergetic neutrons incorporates all recoil proton energies up to the neutron energy and has the approximately rectangular shape discussed earlier. For spectroscopy purposes, however, it would be preferable if the response function were a simple narrow peak to avoid the problems of spectrum unfolding otherwise required. If only those proton recoils that occur at a fixed angle with respect to the neutron direction can be singled out, the recoil proton energy will be fixed for monoenergetic neutrons and the response function will approach the ideal narrow peak. Devices based on a narrow selection of recoil directions are generally known as *proton recoil telescopes* and have been applied to a wide variety of fast neutron measurements.

From Eq. (15-3), the energy of recoil protons observed at an angle θ with respect to the incoming neutron direction is given simply by

$$E_p = E_n \cos^2 \theta \tag{15-12}$$

Recoil proton telescopes can be applied only to situations in which the incoming neutron direction has been defined by collimation or other means.

A schematic diagram of a common form of recoil telescope is shown in Fig. 15-22. Neutrons are incident on a thin film, usually made from an organic polymer, whose thickness is kept small compared with the range of the lowest energy recoil proton to be measured. The angle θ at which recoil protons are observed is defined by positioning a detector some distance from the radiator, with the intervening space evacuated to prevent proton energy loss. Because of the $\cos^2 \theta$ fall-off of recoil proton energy, the detector is usually positioned at a small angle with respect to the neutron direction. Many designs put the proton detector at $\theta = 0$, but others choose a finite observation angle to avoid neutron-induced background events in the detector from the primary beam.

Although a single detector can, in principle, be used to measure the proton energy and hence the neutron energy through Eq. (15-12), multiple detectors are often used in coincidence to reduce backgrounds from competing reactions and other unwanted events. The arrangement shown in Fig. 15-22 is a common one in which a very thin ΔE detector is placed in front of a thicker E detector, which fully stops the recoil protons. By

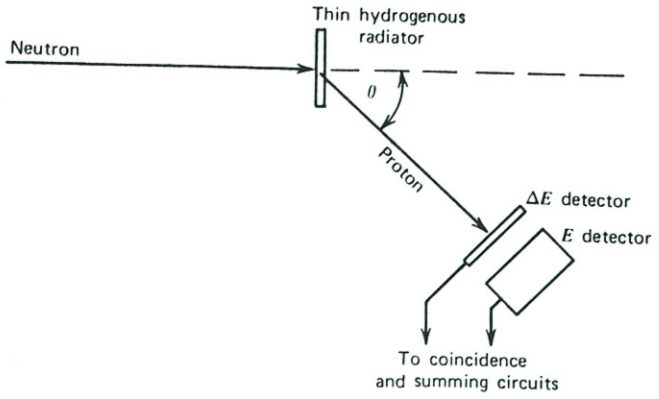

Figure 15-22 A proton recoil telescope.

operating the two detectors in coincidence, only particles incident from the direction of the radiator are recorded. If both detector responses are linear, the sum of the two signals will be proportional to the total proton energy. More elaborate particle identification schemes (see p. 380) can be applied to this arrangement by demanding that the ΔE signal be of proper size relative to the E signal to correspond to the energy loss expected from protons. This requirement will then effectively eliminate other charged particle events such as alpha particles produced in (n, α) reactions in the radiator or other structural components. Proton recoil telescopes of this design, which use semiconductor diode detectors to measure recoil proton energy, are described in Refs. 118 and 119. Other detector types, including gas proportional counters and scintillation detectors, also have been incorporated as the proton detector.

The dominant disadvantage of the proton recoil telescope is its extremely low detection efficiency (typically one count per 10^5 incident neutrons.) This low efficiency stems from two factors, neither of which can be improved without sacrificing energy resolution of the device. First, the radiator thickness must be kept small to avoid appreciable energy loss of the recoil protons before they leave the radiator. Usable radiator thicknesses lead to a probability of about 10^{-3} or 10^{-4} that the incident neutron undergoes a scattering event within the radiator. Second, the solid angle subtended by the recoil proton detectors must be kept relatively small to avoid including too large a spread in recoil angles, and consequently smearing the peak response function.

One of the attractive features of proton recoil telescopes is the fact that their detection efficiency can be calculated quite accurately. Because complications such as multiple scattering or wall effects are largely avoided, the probabilities of neutron scattering and subsequent proton recoil detection are quite easily calculated from the accurately known hydrogen scattering cross section and geometric evaluation of the detector solid angle. Useful analyses of these factors can be found in Refs. 120–123.

One way to improve the detection efficiency is to make the radiator thick and to record separately the energy loss of the protons before they escape. Then the radiator takes the form of a hydrogenous detector such as an organic scintillator[124] or methane-filled proportional counter.[125] Protons that originate at any depth up to their range can deposit part of their energy in the radiator-detector, and then leave its surface to deposit the remainder in a second detector located some distance away to define the recoil angle. By analyzing the coincident pulses observed from the two detectors, the neutron energy that gave rise to the recoil proton can be inferred.

PROBLEMS

15-1. Calculate the efficiency of a 4 mm thick ^{6}LiI scintillator for incident 1 MeV neutrons. Repeat for thermal neutrons.

15-2. A thermal neutron detector is placed at the center of a spherical moderator that is exposed to a source of 5 MeV neutrons. If the moderator diameter is varied while holding all other conditions constant, sketch the corresponding expected variation of the counting rate. Offer physical explanations for the behavior of this curve at both large and small diameters.

15-3. A lithium iodide scintillator is often used as the central detector in the neutron spherical dosimeter. Sketch the expected pulse height spectrum from the scintillator in this application.

15-4. An incident fast neutron is moderated and then diffuses a total pathlength of 10 cm before being captured in the BF_3 tube of a long counter. Estimate the time delay between the time of neutron incidence and the leading edge of the output pulse.

15-5. Incident 3 MeV neutrons interact in a lithium sandwich spectrometer. Calculate the reaction product energies for the case in which the alpha particle is emitted in the forward direction at 0° and the triton at 180°.

15-6. Calculate the maximum proton energy from the ^{3}He(n, p) reaction when induced by 1.5 MeV neutrons.

15-7. Explain the physical origin of the epithermal peak observed in most pulse height spectra from ^{3}He proportional tubes when used with fast neutron sources.

15-8. Calculate the detection efficiency of a methane-filled proportional counter for incident 100 keV neutrons if the gas pressure is 1 atm and the neutron pathlength through the gas is 5 cm.

15-9. A 1 MeV neutron enters a plastic scintillator and undergoes two sequential scatterings from hydrogen nuclei before escaping. If the first scattering deflects the neutron at an angle of 40° with respect to its original direction and the scattering sites are 3 cm apart, calculate the time that separates the two events. If the PM anode time constant is 20 ns, will the two events be resolved?

15-10. Sketch the differential pulse height spectrum you would expect from a proton recoil detector if the incident neutron energy spectrum is known to have three very prominent and narrow peaks at 75, 150, and 300 keV.

15-11. Show that the angle (in the laboratory frame) between a recoil proton and the corresponding scattered neutron is always 90°.

15-12. Using the parameters listed in Table 6-1, estimate the maximum pulse amplitude expected if a methane-filled proportional counter with the following properties is irradiated by 1 MeV neutrons: gas pressure, 0.75 atm; applied voltage, 2000 V; anode radius, 0.005 cm; cathode radius, 2 cm; tube capacitance, 60 pF.

15-13. A silicon detector is irradiated by 1 MeV neutrons. Find the minimum and maximum energies expected for the silicon recoil nuclei produced in elastic scattering of the incident neutrons.

15-14. What basic physical difference leads to the observation that the recoil energy distribution from 5 MeV neutron scattering from hydrogen is uniform or rectangular shaped, while it is highly nonuniform for scattering from helium?

15-15. What factor limits increasing the detection efficiency of a proton recoil telescope by simply increasing the thickness of the hydrogenous radiator?

REFERENCES

1. R. L. Bramblett, R. I. Ewing, and T. W. Bonner, *Nucl. Instrum. Meth.* **9**, 1 (1960).
2. G. J. H. Jacobs and R. L. P. van den Bosch, *Nucl. Instrum. Meth.* **175**, 483 (1980).
3. L. W. Brackenbush and R. I. Scherpelz, PNL-SA-11645, CONF-840202-13 (1983).
4. W. H. Miller and R. M. Brugger, *Nucl. Instrum. Meth.* **A236**, 333 (1985).
5. T. L. Johnson, Y. Lee, K. A. Lowry, and S. C. Gorbics, *Proceedings of the American Nuclear Society Topical Meeting on Theory and Practices in Radiation Protection and Shielding*, April 1987.
6. D. W. O. Rogers, *Health Phys.* **37**, 735 (1979).
7. M. A. Gomaa and E. Moustafa, *Nucl. Instrum. Meth.* **136**, 379 (1976).
8. M. P. Dhairyawan, P. S. Nagarajan, and G. Venkataraman, *Nucl. Instrum. Meth.* **169**, 115 (1980).
9. P. M. Thomas, K. G. Harrison, and M. C. Scott, *Nucl. Instrum. Meth.* **224**, 225 (1984).
10. N. E. Hertel and J. W. Davidson, *Nucl. Instrum. Meth.* **A238**, 509 (1985).
11. D. E. Hankins, LA-2717 (1962).
12. D. E. Hankins and R. A. Pederson, LAMS-2977 (1964).
13. J. W. Leake, *Nucl. Instrum. Meth.* **63**, 329 (1968).
14. K. G. Harrison, *Nucl. Instrum. Meth.* **166**, 197 (1979).
15. J. W. Leake, *Nucl. Instrum. Meth.* **178**, 287 (1980).
16. A. O. Hanson and M. L. McKibben, *Phys. Rev.* **72**, 673 (1947).
17. M. H. McTaggart, AWRE NR/Al/59 (1958).
18. J. De Pangher and L. L. Nichols, BNWL-260 (1966).
19. J. B. Hunt and J. C. Robertson, *Proceedings of the First Symposium on Neutron Dosimetry in Biology and Medicine*, EUR 4896 d-f-e, 935 (1972).
20. D. R. Slaughter and D. W. Rueppel, *Nucl. Instrum. Meth.* **145**, 315 (1977).
21. J. B. Hunt and R. A. Mercer, *Nucl. Instrum. Meth.* **156**, 451 (1978).
22. L. V. East and R. B. Walton, *Nucl. Instrum. Meth.* **72**, 161 (1969).
23. A. E. Evans, *Nucl. Instrum. Meth.* **199**, 643 (1982).
24. H. H. Thies and K. J. Böttcher, *Nucl. Instrum. Meth.* **75**, 231 (1969).
25. R. F. Barrett, J. R. Birkelund and H. H. Thies, *Nucl. Instrum. Meth.* **68**, 277 (1969).
26. B. K. Kamboj, M. G. Shahani, U. V. Phadnis, and D. Sharma, *Nucl. Instrum. Meth.* **148**, 57 (1978).
27. E. Hochhäuser and E. Schönfeld, *Nucl. Instrum. Meth.* **80**, 347 (1970).
28. K. K. Sekharan, H. Laumer, B. D. Kern, and F. Gabbard, *Nucl. Instrum. Meth.* **133**, 253 (1976).
29. E. A. Sokol et al., *Nucl. Instrum. Meth.* **219**, 336 (1984).
30. W. P. Poenitz, *Nucl. Instrum. Meth.* **58**, 39 (1968).
31. W. P. Poenitz, *Nucl. Instrum. Meth.* **72**, 120 (1969).
32. W. P. Poenitz, ANL-7915 (1972).
33. J. R. P. Eaton and J. Walker, *Proc. Phys. Soc. (London)* **83**, 301 (1964).
34. D. R. Johnson, J. H. Thorngate and P. T. Perdue, *Nucl. Instrum. Meth.* **75**, 61 (1969).
35. R. B. Murray, *Nucl. Instrum. Meth.* **2**, 237 (1958).

36. A. R. Spowart, *Nucl. Instrum. Meth.* **75**, 35 (1969).
37. A. R. Spowart, *Nucl. Instrum. Meth.* **82**, 1 (1970).
38. J. M. Neill, D. Huffman, C. A. Preskitt, and J. C. Young, *Nucl. Instrum. Meth.* **82**, 162 (1970).
39. W. R. McMurray, N. J. Pattenden, and G. S. Valail, *Nucl. Instrum. Meth.* **114**, 429 (1974).
40. A. R. Spowart, *Nucl. Instrum. Meth.* **135**, 441 (1976).
41. A. R. Spowart, *Nucl. Instrum. Meth.* **140**, 19 (1977).
42. E. J. Fairley and A. R. Spowart, *Nucl. Instrum. Meth.* **150**, 159 (1978).
43. G. L. Jensen and J. B. Czirr, *Nucl. Instrum. Meth.* **205**, 461 (1983).
44. C. Maroni, F. Russo, and E. Verondini, *Nucl. Instrum. Meth.* **74**, 256 (1969).
45. I. C. Rickard, *Nucl. Instrum. Meth.* **113**, 169 (1973).
46. M. G. Silk, *Nucl. Instrum. Meth.* **66**, 93 (1968).
47. G. B. Bishop, *Nucl. Instrum. Meth.* **62**, 247 (1968).
48. R. A. Wolfe and W. F. Stubbins, *Nucl. Instrum. Meth.* **60**, 246 (1968).
49. H. Bluhm and D. Stegemann, *Nucl. Instrum. Meth.* **70**, 141 (1969).
50. G. Koutzoukos and C. B. Besant, *J. Br. Nucl. Energy Soc.* **14**, 83 (1975).
51. P. J. Clements, *Nucl. Instrum. Meth.* **127**, 61 (1975).
52. T. Pinelli et al., *Nucl. Instrum. Meth.* **150**, 497 (1978).
53. A. Sayres and M. Coppola, *Rev. Sci. Instrum.* **35**, 431 (1964).
54. J. L. Friedes and R. E. Chrien, *Rev. Sci. Instrum.* **35**, 469 (1964).
55. T. Fuse, T. Miura, A. Yamaji, and T. Yoshimura, *Nucl. Instrum. Meth.* **74**, 322 (1969).
56. S. Nishino, T. Nakamura, and T. Hyodo, *Mem. Fac. Eng. (Kyoto Univ.)* **35**(3), 309 (1973).
57. S. Izumi and Y. Murata, *Nucl. Instrum. Meth.* **94**, 141 (1971).
58. J. M. Cuttler, S. Greenberger, and S. Shalev, *Nucl. Instrum. Meth.* **75**, 309 (1969).
59. H. Franz, W. Rudolph, H. Ohm, K.-L. Kratz, G. Herrmann, F. M. Nuh, D. R. Slaughter, and S. G. Prussin, *Nucl. Instrum. Meth.* **144**, 253 (1977).
60. J. G. Owen, D. R. Weaver, and J. Walker, *Nucl. Instrum. Meth.* **188**, 579 (1981).
61. W. A. Fisher, S. H. Chen, D. Gwinn, and R. R. Parker, *Nucl. Instrum. Meth. Phys. Res.* **219**, 179 (1984).
62. A. E. Evans, *IEEE Trans. Nucl. Sci.* **NS-32**(1), 54 (1985).
63. K.-H. Beimer, G. Nyman, and O. Tengblad, *Nucl. Instrum. Meth. Phys. Res.* **A245**, 402 (1986).
64. H. Ohm, K.-L. Kratz, and S. G. Prussin, *Nucl. Instrum. Meth. Phys. Res.* **A256**, 76 (1987).
65. F. Hoenen and W. Bieger, *Nucl. Instrum. Meth. Phys. Res.* **A259**, 529 (1987).
66. S. Shalev and J. Cuttler, *Nucl. Sci. Eng.* **51**, 52 (1973).
67. A. E. Evans, Jr., "Development of a High-Pressure ^{3}He Neutron Scintillator Spectrometer," Los Alamos National Laboratory Program Technical Note, LA-Q2TN-82-109, Apr. 29, 1982.
68. M. S. Derzon, D. R. Slaughter, S. G. Prussin, *IEEE Trans. Nucl. Sci.* **NS-33**(1), 247 (1986).
69. H. Bluhm, *Nucl. Instrum. Meth.* **115**, 325 (1974).
70. M. G. Silk, "The Determination of the Fast Neutron Spectrum in Thermal Reactors Using ^{6}Li and ^{3}He Semiconductor Spectrometers," AERE-R-5183 (1966).
71. T. R. Jeter and M. C. Kennison, *IEEE Trans. Nucl. Sci.* **NS-14**(1), 422 (1967).
72. J. B. Marion and F. C. Young, *Nuclear Reaction Analysis*, North-Holland, Amsterdam, 1968.
73. J. A. Harvey and N. W. Hill, *Nucl. Instrum. Meth.* **162**, 507 (1979).
74. N. R. Stanton, COO-1545-92 (1971).
75. J. Devos et al., *Nucl. Instrum. Meth.* **135**, 395 (1976).
76. R. H. Johnson et al., *Nucl. Instrum. Meth.* **145**, 337 (1977).

77. D. Slaughter and R. Strout II, *Nucl. Instrum. Meth.* **198**, 349 (1982).
78. M. J. Coolbaugh, R. E. Faw, and W. Meyer, "Fast Neutron Spectroscopy in Aqueous Media Using an NE213 Proton Recoil Spectrometer System," COO-2049-7 (1971).
79. M. E. Toms, *Nucl. Instrum. Meth.* **92**, 61 (1971).
80. N. Sasamoto and S. Tanaka, *Nucl. Instrum. Meth.* **148**, 395 (1978).
81. M. Bormann, R. Kühl, K. Schäfer, and U. Seebeck, *Nucl. Instrum. Meth.* **88**, 245 (1970).
82. D. Hermsdorf, K. Pasieka, and D. Seeliger, *Nucl. Instrum. Meth.* **107**, 259 (1973).
83. M. Reier, *Nucl. Instrum. Meth.* **65**, 119 (1968).
84. S. Mubarakmand and M. Anwar, *Nucl. Instrum. Meth.* **93**, 515 (1971).
85. S. T. Thornton and J. R. Smith, *Nucl. Instrum. Meth.* **96**, 551 (1971).
86. R. Plasek, D. Miljanic, V. Valkovic, R. B. Liebert, and G. C. Phillips, *Nucl. Instrum. Meth.* **111**, 251 (1973).
87. R. De. Leo, G. D'Erasmo, A. Pantaleo, and G. Russo, *Nucl. Instrum. Meth.* **119**, 559 (1974).
88. P. Leleux, P. C. Macq, J. P. Meulders, and C. Pirart, *Nucl. Instrum. Meth.* **116**, 41 (1974).
89. R. A. Cecil, B. D. Anderson, and R. Madey, *Improved Predictions of Neutron Detection Efficiency for Hydrocarbon Scintillators from* 1 *MeV to About* 300 *MeV*, North-Holland, Amsterdam, 1979.
90. J. L. Fowler, J. A. Cookson, M. Hussain, R. B. Schwartz, M. T. Swinhoe, C. Wise, and C. A. Uttley, *Nucl. Instrum. Meth.* **175**, 449 (1980).
91. M. Drosg, D. M. Drake, and P. Lisowski, *Nucl. Instrum. Meth.* **176**, 477 (1980).
92. K. F. Flynn, L. E. Glendenin, E. P. Steinberg, and P. M. Wright, *Nucl. Instrum. Meth.* **27**, 13 (1964).
93. G. Dietze and H. Klein, *Nucl. Instrum. Meth.* **193**, 549 (1982).
94. Y. Furuta, S. Kinbara and K. Kaieda, *Nucl. Instrum. Meth.* **84**, 269 (1970).
95. R. St. Onge, A. Galonsky, R. K. Jolly, and T. M. Amos, *Nucl. Instrum. Meth.* **126**, 391 (1975).
96. J. B. Dance and P. E. Francois, *IEEE Trans. Nucl. Sci.* **NS-23**(4), 1433 (1976).
97. A. Chalupka, G. Stengl, M. R. Maier, and P. Sperr, *Nucl. Instrum. Meth.* **150**, 209 (1978).
98. L. J. Perkins and M. C. Scott, *Nucl. Instrum. Meth.* **166**, 451 (1979).
99. R. E. Howe, *Nucl. Instrum. Meth.* **190**, 309 (1981).
100. A. G. Da Silva, L. T. Auler, J. C. Suita, L. J. Antunes, and A. A. Da Silva, *Nucl. Instrum. Meth. Phys. Res.* **A264**, 381 (1988).
101. N. A. Lurie, L. Harris, Jr., and J. C. Young, *Nucl. Instrum. Meth.* **129**, 543 (1975).
102. C. Chen, J. A. Lockwood, and L. Hsieh, *Nucl. Instrum. Meth.* **138**, 363 (1976).
103. D. T. Ingersoll and B. W. Wehring, *Nucl. Instrum. Meth.* **147**, 551 (1977).
104. V. V. Verbinski and R. Giovannini, *Nucl. Instrum. Meth.* **114**, 205 (1974).
105. P. K. Ray and E. S. Kenney, *Nucl. Instrum. Meth.* **144**, 579 (1977).
106. E. F. Bennett, *Nucl. Sci. Eng.* **27**, 16 (1967).
107. P. W. Benjamin, C. D. Kemshall, and J. Redfearn, *Nucl. Instrum. Meth.* **59**, 77 (1968).
108. E. Korthaus, EURFNR-1197; KFK-1994 (1974).
109. E. F. Bennett and T. J. Yule, ANL-7763 (1971).
110. E. F. Bennett and T. J. Yule, *Nucl. Instrum. Meth.* **98**, 393 (1972).
111. N. L. Snidow and H. D. Warren, *Nucl. Instrum. Meth.* **51**, 109 (1967).
112. R. Gold and E. F. Bennett, *Nucl. Instrum. Meth.* **63**, 285 (1968).
113. D. W. Vehar and F. M. Clikeman, *Nucl. Instrum. Meth.* **190**, 351 (1981).
114. S. A. Heiberg, *Nucl. Instrum. Meth.* **63**, 71 (1968).
115. H. F. Atwater, *Nucl. Instrum. Meth.* **100**, 453 (1972).

116. I. R. Brearley, A. Bore, N. Evans, and M. C. Scott, *Nucl. Instrum. Meth.* **192**, 439 (1982).
117. H. Werle, G. Fieg, H. Seufert, and D. Stegemann, *Nucl. Instrum. Meth.* **72**, 111 (1969).
118. T. B. Ryves, *Nucl. Instrum. Meth.* **135**, 455 (1976).
119. M. Cambiaghi, F. Fossati, and T. Pinelli, *Nucl. Instrum. Meth.* **82**, 106 (1970).
120. H. Gotoh and H. Yagi, *Nucl. Instrum. Meth.* **97**, 419 (1971).
121. H. Gotoh and H. Yagi, *Nucl. Instrum. Meth.* **101**, 395 (1972).
122. D. Sloan and J. C. Robertson, *Nucl. Instrum. Meth.* **198**, 365 (1982).
123. B. R. L. Siebert, H. J. Brede, and H. Lesiecki, *Nucl. Instrum. Meth. Phys. Res.* **A235**, 542 (1985).
124. K. N. Geller, D. Eccleshall, and T. T. Bardin, *Nucl. Instrum. Meth.* **69**, 141 (1969).
125. H. Borst, *Nucl. Instrum. Meth.* **169**, 69 (1980).